March 1996

EUROPEAN ORGANIZATION FOR EXPERIMENTAL PHOTOGRAMMETRIC RESEARCH

THE OEEPE GEOSAR TEST OF GEOCODING ERS-1 SAR DATA

Report by I. Dowman
University College London

Official Publication No 32

March 1996

EUROPEAN ORGANIZATION FOR EXPERIMENTAL PHOTOGRAMMETRIC RESEARCH

THE OEEPE GEOSAR TEST OF GEOCODING ERS-1 SAR DATA

Report by I. Dowman
University College London

Official Publication No 32

ISSN 0257-0505

Printed and published by the Institut für Angewandte Geodäsie, Frankfurt am Main

EUROPEAN ORGANIZATION
for
EXPERIMENTAL PHOTOGRAMMETRIC RESEARCH

STEERING COMMITTEE

(composed of Representatives of the Governments of the Member Countries)

President:	Dipl.-Ing. R. KILGA Bundesamt für Eich- und Vermessungswesen Krotenthallergasse 3 A-1080 Wien	Austria
Members:	Administrateur-Général J. DE SMET Institut Géographique National 13, Abbaye de la Cambre B-1050 Bruxelles	Belgium
	Mr. J. VANOMMES LAEGHE Dept. of Photogrammetry Institut Géographique National 13, Abbaye de la Cambre B-1050 Bruxelles	
	Mr. O. JACOBI Institut for Surveying and Photogrammetry Technical University of Denmark Landmaalervej 7 DK-2800 Lyngby	Denmark
	Abt. Dir. Dr.-Ing. H. BAUER Niedersächsisches Landesverwaltungsamt – Landesvermessung – Warmbüchenkamp 2 D-30159 Hannover	Federal Republic of Germany
	Präsident und Prof. Dr.-Ing. H. SEEGER Institut für Angewandte Geodäsie Richard-Strauss-Allee 11 D-60598 Frankfurt am Main	
	Prof. Dr. B. WROBEL Technische Hochschule Darmstadt Institut für Photogrammetrie und Kartographie Petersenstraße 13 D-64287 Darmstadt	
	Mrs. P. NOUKKA National Land Survey of Finland Box 84 SF-00521 Helsinki 52	Finland
	Prof. Dr. R. KUITTINEN Department of Photogrammetry and Remote Sensing Finnish Geodetic Institut Geodeetinrinne 2 SF-02430 Masala	

Mr. P. DENIS — France
Ecole Nationale des Sciences Geographiques
2, Avenue Pasteur
F-94160 Saint-Mande

Mr. A. BAUDOIN
Centre National
d'Etudes Spatiales
2, Place Maurice-Quentin
F-75039 Paris Cedex 01

Dr. Eng. L. SURACE — Italy
Geographical Military Institute
Via Cesare Battista 8–10
I-50100 Firence

Prof. R. GALETTO
University of Pavia
Dept. di Ingegneria del Territorio
Via Abbiategrasso 209
I-27100 Pavia

Prof. Dr. M. G. VOSSELMAN — Netherlands
Delft University of Technology
Thijsseweg 11
NL-2629 JA Delft

Ir. P. VAN DER MOLEN
Dienst Kadaster en de Openbare Registers
Waltersingel 1
NL-7314 NK Apeldoorn

Mr. I. INDSET — Norway
Statens Kartverk
N-3500 Hønefoss

Prof. Ø. ANDERSEN
Norges Landbrukshøgskole
Institutt for Landmåling
P. O. Box 5034
N-1432 Ås

Prof. J. TALTS — Sweden
National Land Survey of Sweden
S-80112 Gävle

Prof. K. TORLEGÅRD
Royal Institute of Technology
Dept. of Photogrammetry
S-10044 Stockholm 70

Prof. Dr. O. KÖLBL — Switzerland
Institut de Photogrammétrie, EPFL
GR-Ecublens
CH-1015 Lausanne

Mr. F. JEANRICHARD
Bundesamt für Landestopographie
Seftigenstrasse 264
CH-3084 Wabern

Lt. Col. M. ÖNDER — Turkey
Ministry of National Defence
General Command of Mapping
TR-06100 Ankara

Col. S. FOÇALIGIL — Turkey
Ministry of National Defence
General Command of Mapping
TR-06100 Ankara

MR. N. S. SMITH — United Kingdom
Ordnance Survey
Romsey Road
Maybush
Southampton S016 4GU

Prof. Dr. I. J. DOWMAN
Dept. of Photogrammetry and Surveying
University College London
Gower Street 6
London WC 1E 6BT

SCIENCE COMMITTEE

Prof. Dr. I. J. DOWMAN — United Kingdom
Dept. of Photogrammetry and Surveying
University College London
Gower Street 6
London WC 1E 6BT

EXECUTIVE BUREAU

Mr. C. PARESI
Secretary General of the OEEPE
International Institute for Aerospace Survey
and Earth Sciences
350 Boulevard 1945, P. O. Box 6
NL-7500 AA Enschede (Netherlands)

Ir. J. TIMMERMAN
Smaragdstraat 20
NL-7314 HG Apeldoorn

SCIENTIFIC COMMISSIONS

Commission A – **Aerotriangulation**

President:
Prof. Dr. T. SARJAKOSKI
Finnish Geodetic Institute
Geodeetinrinne 2
SF-02430 Masala

Commission B – **Digital Elevation Models**

President:
Dr. G. ROBINSON
NUTIS
University of Reading
White Knights
GB-Reading

Commission C – **Large Scale Restitution**

President:
Prof. Eng. S. DEQUAL
Dipartimento Georisorse e Territorio
Polytecnico di Torino
Corso Duca Degli Abbruzzi 24
I-10129 Torino

Commission D – **Photogrammetry and Cartography**

President:
see Commission I

Commission E – **Topographic Interpretation**

President:
Prof. Dr. B.-S. SCHULZ
Institut für Angewandte Geodäsie
Richard-Strauss-Allee 11
D-60598 Frankfurt am Main

Commission F – **Fundamental Problems of Photogrammetry**

President:
Prof. Dr. W. FÖRSTNER
Institut für Photogrammetrie
Universität Bonn
Nußallee 15
D-53115 Bonn

APPLICATION COMMISSIONS

Commission I – **Topographic Mapping**

President:

Mr. M. J. D. BRAND
Director
Ordnance Survey of N. Ireland
Colby House, Stranmillis Court
Belfast BT 9 5BJ
United Kingdom

Commission II – **Cadastral Mapping**

President:

Ir. L. A. KOEN
Dienst
v. h. Kadaster en de Openbare Registers
Waltersingel 1
NL-7314 GH Apeldoorn

Commission III – **Engineering Surveys**

Commission V – **Land Information Systems**

THE OEEPE GEOSAR TEST OF GEOCODING ERS-1 SAR DATA

(with 5 Figures, 2 Tables and 2 Appendices)

Report by I. Dowman
University College London

Table of Contents

Abstract

The OEEPE (Organisation Européenne d'Etudes Photogrammétriques Expérimentales) has collaborated with the GeoSAR working group[1] to prepare and carry out a test to compare different methods of geocoding ERS-1 SAR data and of the application of geocoded SAR data to topographic mapping. ESA has supported the test by providing the data and The German Aerospace Research Establishment (DLR) has copied and distributed the data. IfAG provided additional data for the phase 2 work, this included KFA-1000 photography, Thematic Mapper data and a digital elevation model (DEM).

The test site is around Frankfurt am Main in Germany and 4 ERS-1 images have been provided together with two DEMs and ground control information.

20 organisations from Europe and North America expressed an interest in the test and data was sent to 14 of them. Reports from some of these were presented at the 4th GeoSAR workshop.

This report sets out the objectives of the test and describes the data which was provided. The methods and results of the participants are summarised and papers are included in the appendices which give more detail. The test concludes that high accuracy can be achieved from geocoding when compared to maps but that the information content for mapping is limited.

[1]The GeoSAR working group was set up in 1987 with support from ESA to bring together scientists from around the world with an interest in geocoding SAR data.

1. Background

1.1 Organisation

This report covers the work carried out in a test organised by OEEPE and the GeoSAR Working group on the accuracy of geocoding of ERS-1 SAR data and the application of the data to mapping. The GeoSAR working group comprises scientists and engineers from the international community involved in the definition, development and operation of processing facilities for geocoding of Synthetic Aperture Radar image data from air and spaceborne sensors. The group has held 4 workshops since 1987. The latest was in May 1993 and at that meeting the work done on the OEEPE/GeoSAR test was presented and discussed. The proceedings of that meeting are published by Earth Observation Sciences Ltd (1994). A Seminar was also held by OEEPE at Institut für Angewandte Geodäsie (IfAG) in Frankfurt am Main which brought together the geocoding test and the OEEPE project in a Digital Landscape Model for Europe. The Proceedings of that meeting have been published by University College London (1994).

1.2 Characteristics of SAR Data

A radar image is created from the backscattered energy received at the sensor from a point on the ground recorded at a particular time at a measured distance or range. The energy is transmitted in the microwave portion of the energy spectrum. Radar data is based on the following operations:

- A radar transmitter sends a pulse of electromagnetic energy towards the Earth at an incident angle θ.
- The waves scatter from the surfaces which they strike.
- The back scattered radiation is detected by the radar system which defines the slant range by the time delay between transmission and reflection.

Figure 1.1 illustrates the local geometry of a radar beam interacting with an undulating surface.

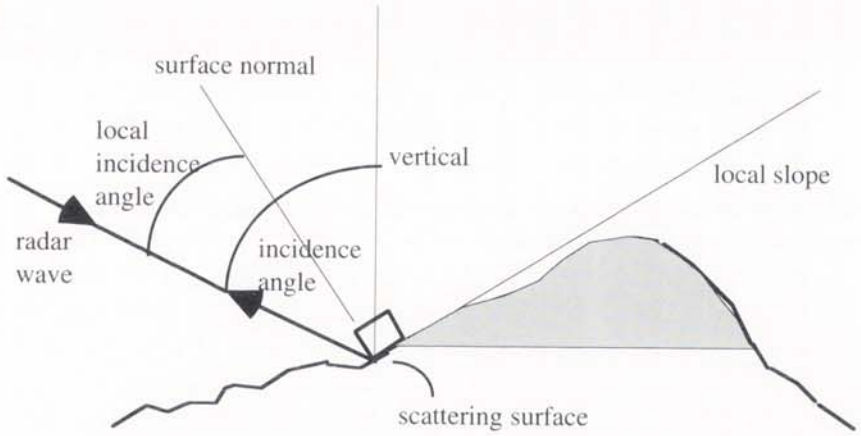

Figure 1.1 – Local radar beam incidence geometry.

Radar data have several advantages over traditional types of remotely sensed imagery such as thermal and infrared/ visible scanner data or aerial photography. The main advantage over visible and infrared sensors, is that radar sensors can provide imagery on a regular basis, independent of weather or conditions of luminance. The radar wavelengths are not scattered or absorbed by the clouds and can be used to detect surface features. Radar sensors can provide imagery day or night even in haze, light rain, snow clouds or smoke. There are however disadvantages with SAR data, the main one is the difficulty is interpreting the data because of the image formation process. There is also significant geometric distortion which make interpretation more difficult and also makes geometric correction essential in hilly areas.

The radar signal does not detect colour information (which is gained from optical wavelength sensors) or temperature information (derived from thermal infrared sensors) but the backscatter is related to surface roughness, slope and electrical conductivity. Detail of the the characteristics of SAR and a guide to interpretation can be found in Lillesand and Kiefer (1994).

There are two types of radar sensors.

- SLAR (Sideways-Looking Airborne Radar) which point to the side to transmit and receive the signal.

SAR (Synthetic Aperture Radar) which is modified especially for use from a spacecraft, Lillesand and Kiefer (1994). This utilises the motion of the space vehicle during transmission of the ranging pulses to synthesise an effectively long antenna. This is the major difference between an aircraft-borne side-looking radar and the space-borne synthetic aperture radar which lies in the fact that, to achieve a reasonable spatial resolution from orbital altitudes, a very large antenna would be needed. The SAR uses a simulated large antenna, hence the name synthetic aperture radar.

Both SLAR and SAR have the same geometric theory (see fig. 1.1).

Radar image resolution is given separately for range and azimuth and it is determined by the pulse length and antenna beam width. The pulse length controls the dimensions of the ground sampling element away from the aircraft track in the range direction and the antenna beam width controls the dimension of the ground sampling element along the track of the aircraft in the azimuth direction. The spatial resolution in the slant range R_r is equal to half of the transmitted pulse length:

$$R_r = \frac{rc}{2}$$

where r is the pulse rate and c the propagation speed of the radar wave.

The width of the antenna beam determines the spatial resolution in the azimuth direction. As the beam fans out from the antenna the spatial resolution decreases with ground distances, from minimum directly below the aircraft. The spatial resolution in the azimuth direction R_α is given by:

$$R_\alpha = \frac{\lambda R}{D}$$

where λ is the wavelength of the signal, R the slant range and D the width of the antenna.

To improve spatial resolution the beam width must be increased or there must be a large decrease in the wave length used, which is impractical as it would make the microwaves sensitive to atmospheric effects like rain clouds, or a large increase in the antenna length, that constitute aviation hazard. Therefore, the real antenna (SLAR) is modified to synthetic antenna (SAR).

The geometric properties of a radar image bear very little relationship to those of an aerial photograph or of an image from a push broom sensor such as SPOT. In a radar system the measured range is projected onto a plane (Fig 1.2 a). The roll of the sensor has no effect on the range in the way tilt affects aerial and pushbroom images however the effect of the terrain on the position of the objects is considerable.

There are three types of distortions due to terrain relief:

- Foreshortening of the slant range of SAR to the earth's surface, has the effect of object displacement (Fig. 1.2 b). Tall features on a SAR image are displaced from their proper positions so that the top of the object appears to be closer than the bottom.

- Layover is an extreme case of foreshortening, where the slope angle a is bigger than the off-nadir angle θ (Fig. 1.2 c). Then, features are reversed.

- Shadow is the hidden information on the SAR imagery. Shadowed areas occur on the radar imagery when the slope of the terrain is steeper than the incidence of the radar beam and therefore the terrain is not "seen" by the radar (Fig. 1.2 d).

SAR geometry allows topographic information to be extracted from the image, but it also requires that careful corrections be undertaken in extracting cartographic information. Errors due to ground relief, platform's velocity and altitude variations, and drift are corrected by geocoding. The objective of geocoding SAR imagery is to transform the uncorrected slant range data to a standard map projection with the errors caused by relief removed, rotated so that north is aligned with standard map system boundaries, in a standard pixel spacing. Geocoding techniques allow a sub-pixel accuracy for the geocoded product. The areas effected by layover and shadow can be predicted from the DEM and orbit information during geocoding and can be provided with the geocoded image to assist the user interpretation.

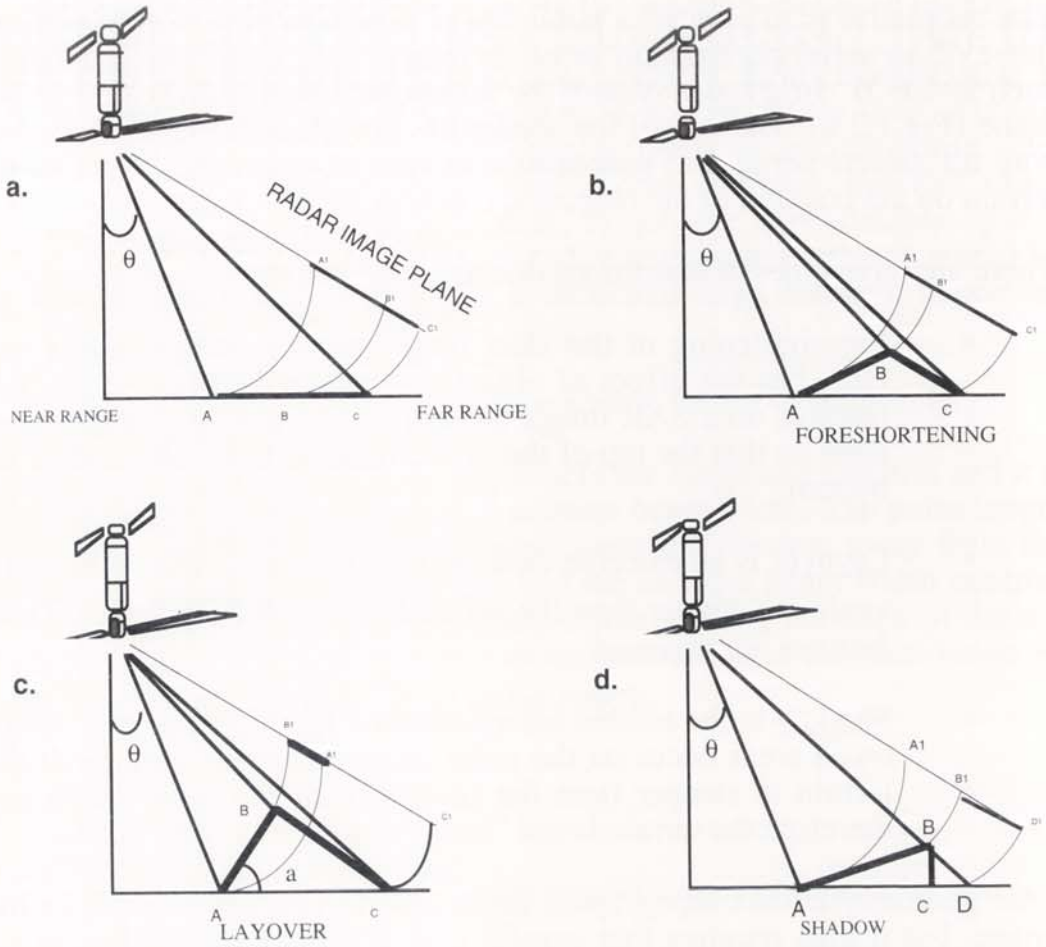

Figure 1.2 – Relief effects on image geometry of SAR imagery in range.

1.3 Characteristics of the ERS-1 Satellite

The Earth Resources Satellite 1 (ERS-1) was launched by the European Space Agency (ESA) on 17 July 1991. The satellite was launched into a sun-synchronous orbit at a mean altitude of 780 km with a repeat cycle of 3 days although the repeat cycle has been changed at stages during the life of the satellite.

ERS-1 carries an imaging sensor, the Active Microwave Instrument (AMI), operating in C-band either as Synthetic Aperture Radar or as a Wave-Scatterometer and simultaneously as Wind-Scatterometer, to be used primarily for ocean observation and ice monitoring. This operational instrument was activated on 27 July 1991 and since then is working in a routine operational manner, producing a substantial amount of data for

subsequent analysis and post-processing. ESA has launched a second satellite system, ERS-2, in April 1995 thus ensuring continuity to the remote sensing community.

With a spatial resolution of 30 x 30 m in imaging mode, the SAR scans a swath of 100 km width, 250 km to the right side of the orbital track and at an incident angle (θ) of 23° at mid-swath (fig. 1.3).

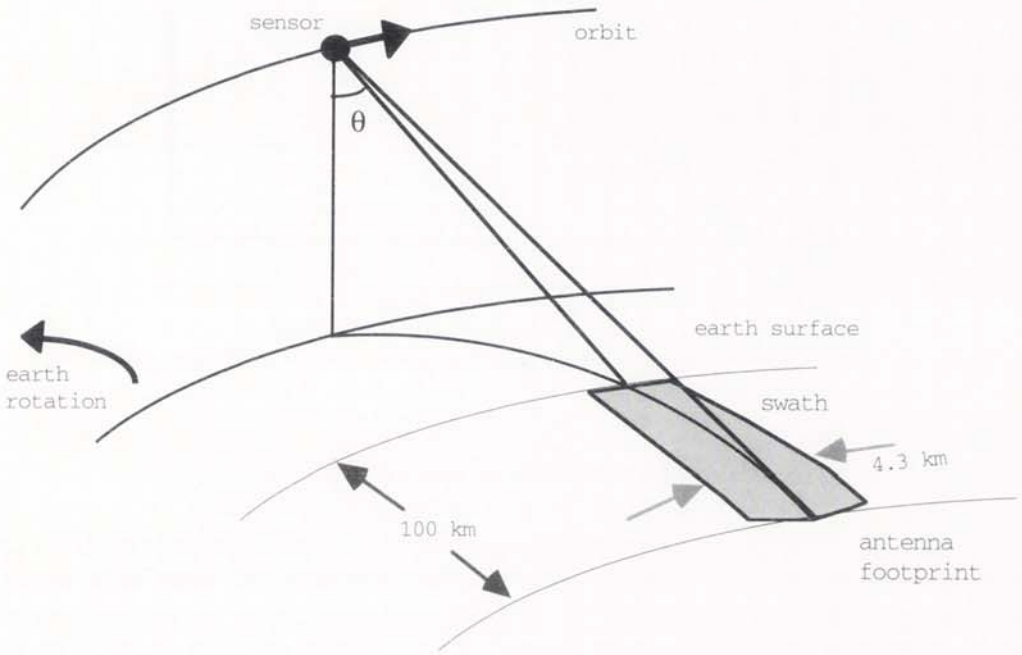

Figure 1.3. – Typical imaging geometry of the ERS-1 SAR.

The radar senses in the microwave portion of the electromagnetic spectrum with a frequency of 5.3 GHz (approximately 5.6 cm wavelength) which is the C-band. The characteristics of the ERS-1 Active Microwave Instrument are given in table 1.1.

Technical parameters of ERS-1	
flight altitude	783 km
orbital inclination	98°
wavelength	5.6 cm in C-band
incident angle	23°
spatial resolution	
range	<33 m
azimuth	<30 m
radiometric resolution	16 bits per pixel
scene size	100 x 100 km
geographic limitation	poles
coverage cycle	3, 35, 176 days

Table 1.1. – Characteristics of ERS-1

2. Objectives and organisation of the test

The geocoding test has two objectives – first to assess the potential to produce geocoded data and second to assess the accuracy of that data and the usefulness of the data in terms of content for mapping, map revision and the creation and revision of data bases.

The test is divided into two parts. Phase 1 involves geocoding of the SAR data and organisations who have the capability to carry out either terrain geocoding (correction of relief effects with a digital elevation model) or ellipsoid geocoding (correction only of earth curvature effects), were invited to take part in the test. The geocoding system to be used should have the capability to validate the resulting geocoded image.

Phase 2 involves testing the accuracy of the geocoded image and its application for mapping. Organisations involved in mapping were invited to take part in this phase of the test.

The test has been carried out with extensive assistance from ESA who agreed to release data and by DLR in Oberpfaffenhofen who has assembled the data and distributed it and also taken part in the test.

20 organisations originally expressed an interest and 18 agreed to participate, with 2 wishing to observe; 2 originally wished to participate in phase 2 only. This report contains the results from 10 organisations who contributed to the final report. A list of these 10 is given in appendix 1.

3. Description of the test

3.1 Phase 1 - geocoding

A precision image in slant range was distributed to centres which could demonstrate a capacity for geocoding; this capacity did not need to include terrain geocoding as ellipsoid geocoding should also be assessed and would allow more centres to participate. The centres were also provided with a DEM, topographic maps of the test area and a number of ground control points derived from ground survey.

Each participating centre was asked to produce a geocoded image of the test scene and to validate this image with their own test procedures but using a consistent set of parameters.

The results were reported at the 4th GeoSAR workshop and at the OEEPE Seminar on integrating data for a Digital Landscape Model (See University College London, 1994) and compiled in this report. Detailed reports from the participants are included in appendix 2.

3.2 Phase 2 – Assessment of geocoding and content

It was planned that the geocoded images would be passed on to organisations involved in mapping for further evaluation. The mapping organisations would also be provided with the DEM and ground control points but only with maps of part of the area. The mapping centres would test the accuracy of the geocoded images and use the images to produce and revise topographic maps.

Phase 2 was not fully completed by any of the participants because of lack of resources or suitable equipment. Three did carry out work to evaluate the content of the geocoded images and a report of their work is included in section 6.

3.3 Test Data

The test area is in the Frankfurt region . The area covers the 1:50.000 map sheet "Frankfurt am Main West" (Topographische Karte 1:50.000 (TK50), sheet L 5916 of Frankfurt am Main West in Hessen Region) compiled in 1989. The Gauss-Krüger projection is used, (Transverse Mercator) based on Bessel ellipsoid and Potsdam Datum). The corners of the area in geographical and Gauss-Krüger coordinates of the are:

Upper left (NW):	$08^0 20'$ E;	x = 3452407.40 m	Upper right (NE):	$08^0 40'$ E;	x = 3476203.63 m
	$50^0 12'$ N;	y = 5562735.94 m		$50^0 12'$ N;	y = 5562576.39 m
Lower left (SW):	$08^0 20'$ E;	x = 3452208.84 m	Lower right (SE):	$08^0 40'$ E;	x = 3476104.35 m
	$50^0 00'$ N;	y = 5540492.54 m		$50^0 00'$ N;	y = 5540332.79 m

The area is shown in Figure 3.1 which is an abstract from the 1:200.000 map and Figure 3.2 is the SAR.PRI image of the area.

The following data was provided:

ERS-1 images: ESA SAR.PRI ground range image;
ESA SAR.GEC ellipsoid geocoded image;
ESA SAR.GTC terrain geocoded image;
DLR slant range image;

Orbit data. This was the preliminary orbit determined by the satellite operating centre for ESA.

DEMs area in Gauss from: 20 km x 20 km elevation data set of the Frankfurt Krüger projection, with 40m grid. This was derived photogrammetrically measured profiles of the area.

ETOPO5 global elevation data provided by NOAA.

Ellipsoid parameters for WGS 84.

1:200.000 map of the area of the full scene;
1:50.000 topographic map of the area of the 40m DEM..

Ground control points.

The test site has variations in the terrain morphology which contains a variety of land-uses such as:

- rough terrain, mountains, plain,
- forests and parks,
- water features (rivers, canals),
- densely build-up inner city areas,
- loosely built-up suburban areas with residential housing,
- industrial and manufacturing areas,
- airport area,
- major, minor roads.

The terrain in that area is not flat. The altitude variations are from 85m to 570m.

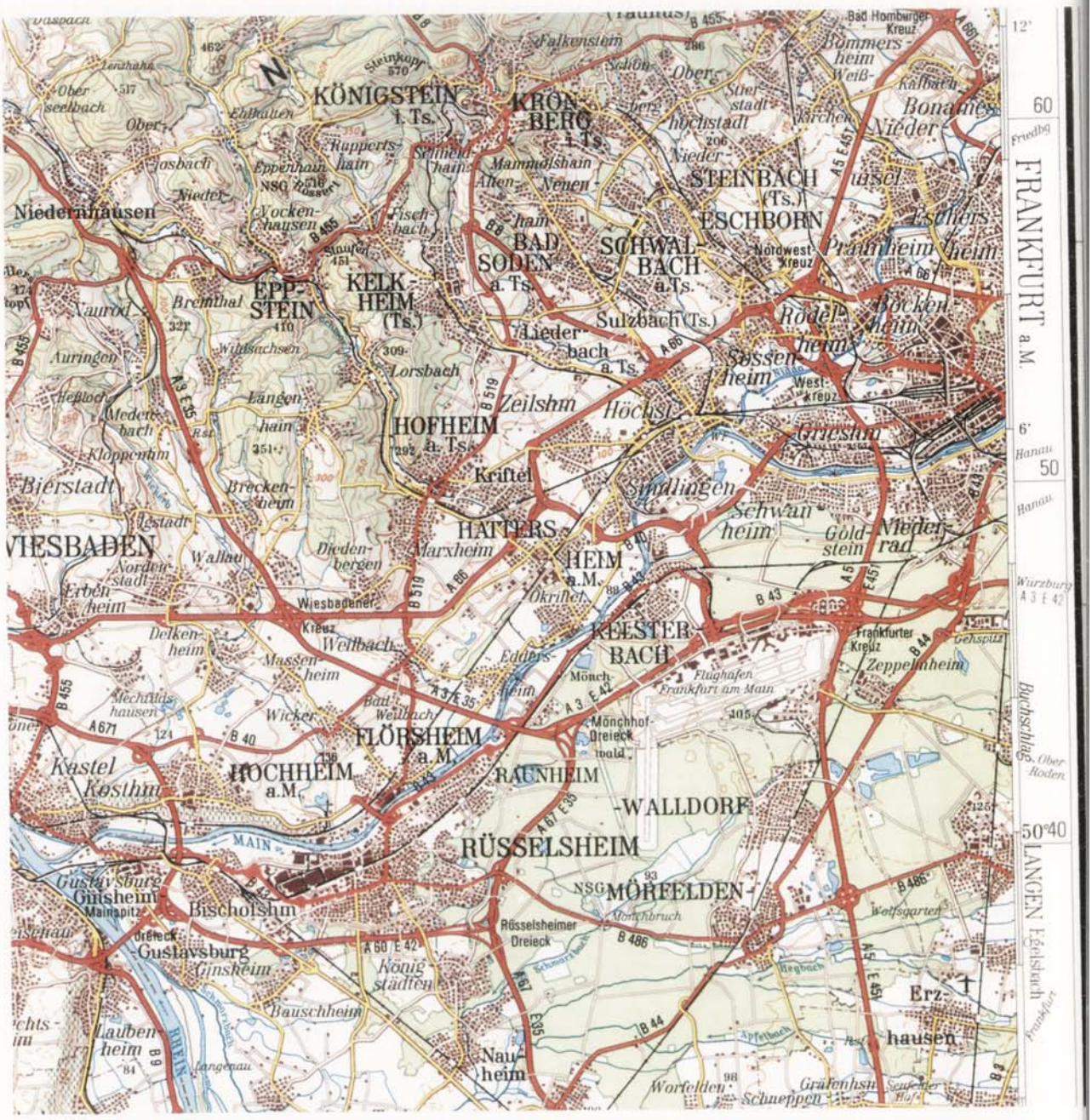

Figure 3.1. – 1:200.000 map of the test area.

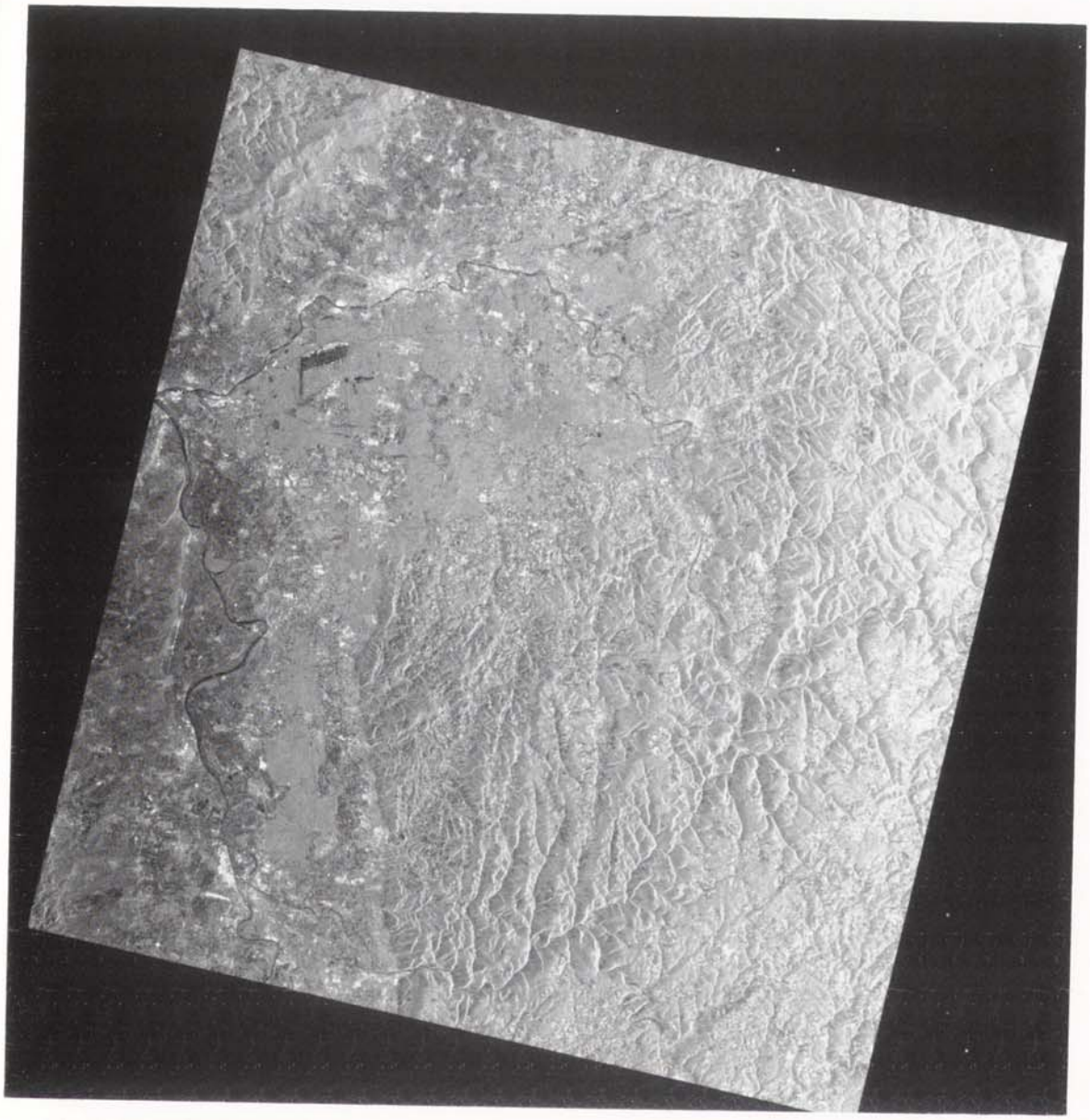

Figure 3.2. – Full SAR image showing the test area in the North West corner.

4. Methods of geocoding

4.1 General principles of geocoding

A full description of the geometry of SAR and methods of geocoding and processing is given in Schreier (1993). However a brief introduction is given here.

A real aperture side looking radar transmits a pulse which is reflected from the ground and received back at the sensor. The time taken for the double journey is used to compute the range from the sensor to the ground. The time of transmitting the pulse, with reference to a starting time, gives the azimuth position. In order to increase the resolution a chirp is added to the pulse and matched filtering carried out in the processor with a reference function. A slant range image can be constructed from the range and azimuth, and the value of the signal received back at the sensor after backscattering at the ground. The image will be distorted, when compared to a map, because the range will not be the distance to the map datum, but to a point a height h above the datum. This distortion gives rise to the well known layover effects and the relief also causes shadow as shown in figure. 1.2. Additional distortion will be caused by the movement of the platform.

A synthetic aperture radar has a similar geometry but the azimuth position is now calculated by processing the signals received over a period of time, first by performing matched filtering on each pulse return and second by considering the Doppler history and hence determining the zero Doppler. The zero Doppler will give the time at which the target is perpendicular to the satellite track represented by the sensor velocity vector. Image position is then given as slant range and azimuth time.

The process of geocoding involves the determination of corresponding points on the image p, with coordinates (i, j) and on the ground P with coordinates (X_p, Y_p, Z_p) and the transformation of the radiometric value in the image into the corresponding ground position. The basic relationship between the sensor position S and the ground position P both given in the rectangular X, Y, Z co-ordinate system is shown in figure 4.1.

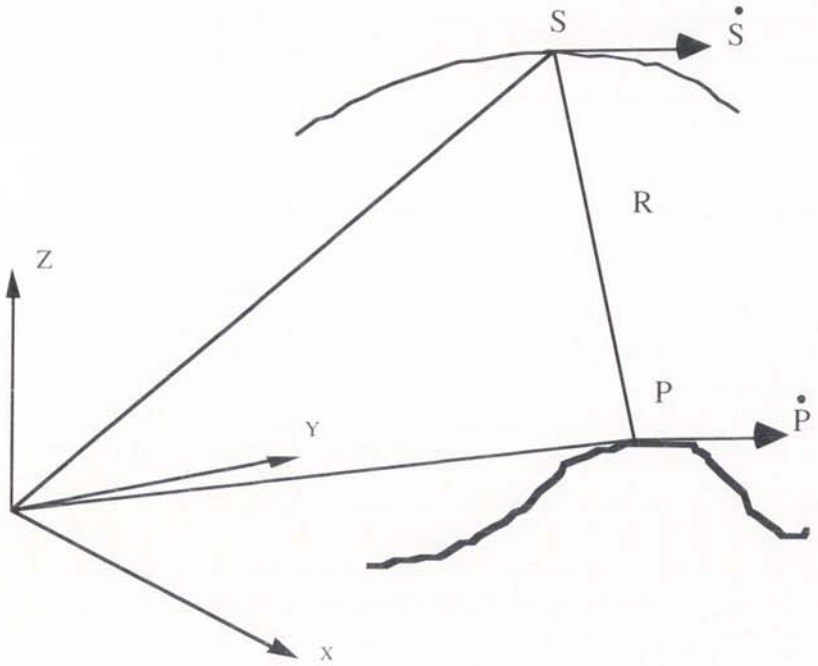

Figure 4.1. – Basic geometrical relationships of SAR.

The relationship between these points is given by the following equations:

$$R = |\underline{S} - \underline{P}| \qquad [1] \text{ the range equation}$$

$$f_D = \frac{2}{\lambda . R} (\dot{\underline{S}} - \dot{\underline{P}}) \cdot (\underline{S} - \underline{P}) \qquad [2] \text{ the Doppler equation}$$

where at a given time t:

R	is slant range
$\underline{S}$	is sensor position vector $(X_S\ Y_S\ Z_S)$
$\dot{\underline{S}}$	is sensor velocity vector
$\underline{P}$	is point position vector $(X_p\ Y_p\ Z_p)$
$\dot{\underline{P}}$	is point velocity vector
f_D	is Doppler frequency
λ	is radar wavelength

For each point in the image, defined by pixel co-ordinates, i, j, a range is known relative to some fixed points in the image, for example the first and last pixel. The time is also known relative to the same fixed points. The orbit of a satellite will be known to some degree of accuracy but this will vary according to the satellite.

For geocoding, an object to image transformation is normally used. With this method the coordinates of P are defined in the output image. The height will be derived from a digital elevation model (DEM). If a DEM is not available then an earth model such as an ellipsoid must be used but then the accuracy of the geocoding is reduced because relief effects are not corrected. The ellipsoid may be modified in order to reduce the effect of terrain displacement by taking the mean height of the terrain. In equation [1] and [2] $\underline{P}$ is therefore known and $\dot{\underline{P}}$ is the velocity vector of the earth at that point which can be determined. The problem is then to find the image coordinates of p (i, j). It is necessary to know the orbit of the satellite and this is usually given with the data. The Doppler frequency must also be known and with ERS-1 images this is normally zero. It is then necessary to find the orbit position, $\underline{S}$, and corresponding velocity, $\dot{\underline{S}}$ which gives a range which satisfies the equation. This is done by iteration. Having found the correct position on the orbit this can be translated into the time at which that point was determined and the time and range can then be converted into line and sample coordinates in the image. To carry out this conversion a point of correspondence between the image and the satellite must be known, this is also given in the image header data in the form of the time and range of the first and last pixel in the image.

This process can be carried out without ground control if the orbit and the relationship between image and orbit position is given to sufficient accuracy. If sufficient accuracy is not available then ground control points will have to be used.

A typical computation process based on the above method is given in Figure 4.2.

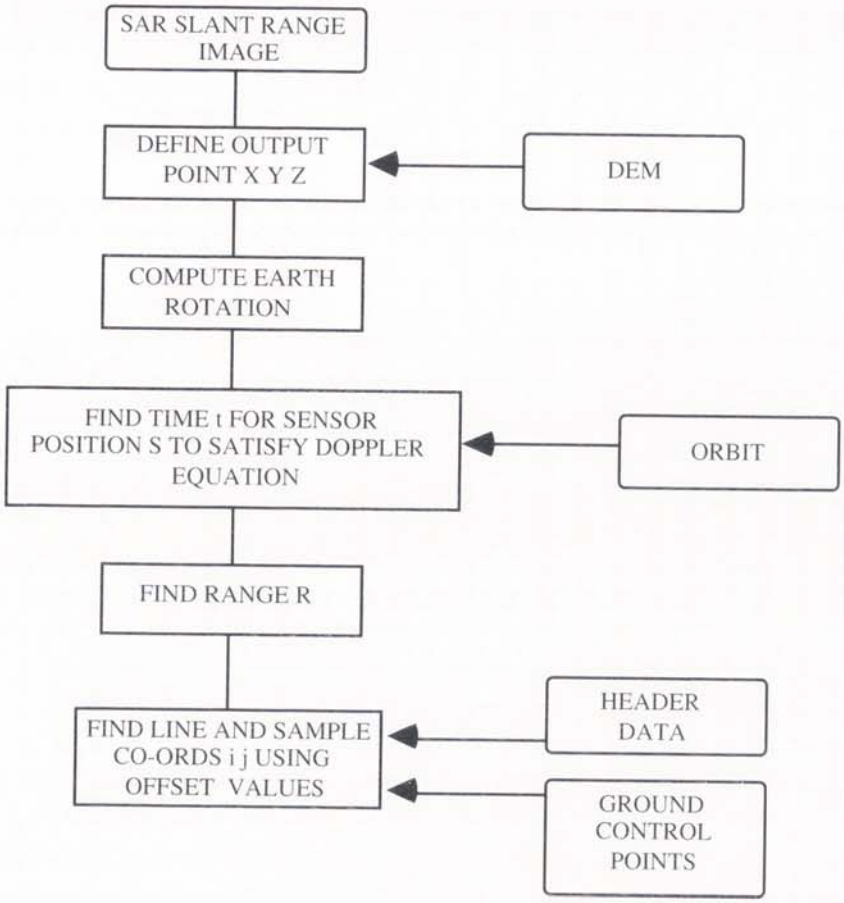

Figure 4.2. – Geocoding stages for a slant range image.

ERS-1 SAR data can be obtained as a slant range complex image (SAR.SLC) which is a one look image, or as a multi look ground range image (SAR.PRI). SAR geocoders are usually designed to input one or the other of these products. If the ground range image is used then an additional step of converting the computed slant range, to the ground range recorded in the image, is necessary.

The participants in the geocoding test all used variations on this method. A summary of all the methods together with comments received are summarised in section 4.3. Papers which describe the methods and results in more detail are included in appendix 2.

4.2 Ancillary products

As a by-product of geocoding it is possible to produce ancillary products which assist in the evaluation and use of the geocoded image. The main products are masks which show areas of shadow and layover and an image which can be calculated from the DEM and used to show which areas of the original image or the geocoded image are expected to be in layover or shadow. Another product is an incidence angle mask which shows the actual incidence angle taking into account the slope of the terrain and the position in the swath. A refinement of this is an 'energy map' which also determines the area covered on the ground of a pixel and its orientation with respect to the sensor.

These products are described in more detail in Meier et al (1993) and Dowman et al (1993).

4.3 Methods and results of participants

4.3.1 Introduction

In this section a brief summary is given of the method of the participants. More details of the methods are given in appendix 2 in papers written by the participants. A summary and discussion of results is given in section 5.

4.3.2 DLR

The German Processing and Archiving Facility (PAF) are responsible for producing geocoded products for ESA. The principle products are a geocoded ellipsoid product (SAR.GEC) and an geocoded terrain product (SAR.GTC). Both of these products were provided by DLR for the test.

The geocoding algorithm used by DLR follows the process set out in figure 3.2 and described by Roth et al (1993) and Meier et al (1993). First sensor positions and sensor velocity vectors ($\underline{S}$ and $\dot{\underline{S}}$) are calculated and stored for each azimuth position in the SAR image. A Doppler frequency shift f_D is calculated for each point and compared to the Doppler centroid which was used in the SAR processor, a comparison of these two values allows a new estimate of the satellite position and a new iteration to be performed. Ground control points (GCPs) are used in the product generation and are also used to assess the quality of the product.

DLR reports that the critical item in the production of the terrain corrected geocoded product for this test is the manual measurement of tiepoints. More generally the problems are the acquisition and handling of DEMs when different projections and datum's are involved.

4.3.3 Dornier

Dornier used a warping method which involved the calculation of a linear two dimensional polynomial and made no correction for the relief.

4.3.4 Institut Cartogràfic de Catalunya and Universitat de Barcelona

The paper describing the method is included in appendix 2. The method is also that described in figure 3.2 and no ground control points are needed for a slant range image but if a ground range image is used (the PRI image used for the test), then GCPs are needed to transform from slant range to ground range. GCPs can also be used to refine the header information given for the time of the first and last row.

4.3.5 ISTAR

ISTAR used a method of 'data geometric fusion' developed for SPOT and aerial imagery and adapted for SAR. The method uses a geometric model and different weights can be introduced for the control. The solution is quite sensitive to the weights.

ISTAR also used the ETOPO5 data and showed that it gave better results than obtained with only the ellipsoid.

4.3.6 Thomson-CSF

The paper describing the work carried out by Thomson-CSF (Pikeroen and Tannous, 1994) is attached in appendix 2. Thomson use the same basic process but incorporate GCPs into their solution. A so called 'geometric fusion kernel' which solves for the unknown parameters of the sensor model and corrections to initial values of tie points is used . (The model can also be used for SPOT and other sensors and can be adapted to register images and to determine a DEM from SAR.) It is concluded that it is essential to adjust the tie point positions when the measurement errors are significant. The method is particularly useful if SAR is to be fused with data from other sensors.

4.3.7 Telespazio

Telespazio runs the Italian Processing and Archiving Facility (PAF) and the method used for the test is that used by the PAF. Both ellipsoid and terrain geocoded images can be produced. The transformation is carried out for points on a grid superimposed on the image and the parameters are calculated for each point on the grid, points within a grid square are inter-

polated. The method is described by Tarantino and Pasquali (1993) but no transformation formulae are given. A full listing of results is given in appendix 2.

4.3.8 University College London and GEC Marconi Research Laboratory

UCL used a geocoder developed with GEC Marconi for the UK Defence research establishment, the method is described in Dowman et al (1993) and a report on the geocoding for the OEEPE test are given in appendix 2. The method also uses the process described in figure 5.2. A 'tie pointing' scheme has been adopted which introduces GCPs after the object to image transformation and compares the computed image coordinates with measured coordinates and then applies a correction to the image in the form:

$$ds = c + b.l + a.l^2$$

where:

ds	is range or azimuth error
l	is range or azimuth co-ordinate
a,b,c	coefficients.

Tests showed that in most cases a shift in both range and azimuth were sufficient to correct the image. In some cases a linear term in azimuth gave a slight improvement.

In regions that are near layover, a small change in image positions can correspond a large change in map position. This leads to a spreading out of such regions in the geocoded image. For this reason the comparison in image space of the layover map against the image is a better check on spatial accuracy than the same comparison in map space.

4.3.9 Technical University of Vienna

The method of Vienna differed from the previous methods in that it uses a modified photogrammetric bundle adjustment program and does not use orbit data as input but determines the co-efficients of a polynomial describing the orbit by using ground control points. The bundle adjustment program is called ORIENT and uses a 9 parameter cubic polynomial to describe the orbit and imaging parameters for scale and offset in the range direction. The method is described when used with aircraft scanner data (Ecker et al, 1991).

5. Results of geocoding

The results obtained from the participants are summarised in table 5.1

Organisation	Tie points			Check points			Map points		
	No	E(m)	N(m)	No	E(m)	N(m)	No	E(m)	N(m)
Dornier (2D transformation only)	16	30	57						
DLR	35	12.3	10.3	9	9.2	4.8			
ICC	25	18.4	13.4	23	17.4	18.9	16	18.6	21.0
ISTAR	31	8.7	8.0	27	11.4	8.0			
Telespazio									
GEC				17	60.5	36.0			
GTC							30	17.9	18.5
Thomson CSF									
Adj without tie points	35	12.0	10.8						
Adj with tie points	35	1.6	0.5						
TU Vienna	35	5.0						25.0	
University College London	7	4.0	8.5						

Table 5.1. – Results from the centres from geocoding.

It can be seen that the results are quite consistent in that they generally show residuals on control points of less than 20m, demonstrating that SAR geocoding is possible with this accuracy and that this standard can be achieved with a variety of algorithms. Not all of the participants used check points to verify their results. This was for a number of reasons. Thomson-CSF felt that the available check points were not accurate enough to check their results. Other participants reported difficulty in finding control points particularly in the hilly areas.

It is likely that some of the differences in accuracy are due to the methods used. Clearly the 2D transformation of Dornier does not correct for the effect of relief and the results from Vienna indicating a good fit to control but slightly poorer results on the map points is a result of the use of the photogrammetric bundle adjustment and the introduction of additional

errors from the map. Apart from these comments the results can be left to speak for themselves.

A number of problems have been highlighted. A major problem is obtaining suitable DEMs and if they are available, converting them to the required projection and datum. It was noted that the deterioration of geocoding accuracy with DEM spacing is slow up to a limit of 200m, Although some algorithms are designed to work without tie points, control is necessary to check and, in many cases, correct a systematic shift. As noted above the selection of tie points is a manual process and is time consuming. A similar problem exists when check results as the selection of a large number of points is required. TU Vienna experimented with the use of features extracted from maps but similar problems resulted, particularly in upland areas where there were few cultural features and woodland was not easy to delimit.

6. Application of SAR to mapping

6.1 Overview

Three organisations took part in phase 2 of the test and assessed the application of the geocoded SAR data to mapping. The three organisations were University College London, The Agricultural University of Norway and the Technical University of Vienna. The work done by each was different and is reported separately. The following three sections summarises the work of each participant and longer reports from University College London and The Agricultural University of Norway are included in appendix 2. An overall summary of conclusions is included in section 6.5.

6.2 University College London

A study was carried out at UCL to determine the utility of SAR data for mapping by itself or with other satellite data. Two geocoded images from phase 1 of the geocoding test were available as well as other data from the OEEPE Digital Landscape Model project. The following data was used:

ERS-1 SAR geocoded scene by DLR
ERS-1 SAR geocoded scene by TU Vienna
Landsat-TM 7 bands of the Thematic Mapper
KFA-1000 spaceborne camera orthophoto

The images were registered geomtrically and fused using different band combinations and an assessment made of the image content. The geometric accuracy of the resulting images was also made. The following paragraphs summarise the main conclusions on feature identification.

The shoreline of the Main River of Frankfurt area is the most easy plotted feature of the test site. It is the dominant characteristic of the scene which clearly visible on all types of imagery including the SAR scenes. Apart from that river, minor rivers proved to be difficult to identify and in many cases were misidentified with other linear features such as second-order roads, because of their spatial pattern similarity. Other areal waterbodies such as lakes, were easily plotted only from the fused Landsat-TM scenes with the SAR data, and vaguely seen on the merged SAR/ KFA-1000 scene

Buildings, due to their small dimensions, are the most misidentified features on SAR imagery. Only the boundaries of an urban area can be recognised on a radar image. Large buildings at the industrial and airport zones, were indicated very vaguely and houses in residential areas were not recognised. Again the colour image-composites helped identification a lot, especially for individual buildings discrimination in open country.

Main roads could be identified easily without the use of a map in every data set except the single SAR scenes. Some difficulties arose with the major roads interpretation within the urban area, as the signal from the buildings tend to dominate the image.

The relative accuracy of the registration was verified by superimposing the reference map on the resampled images, and was considered quite good in flat areas, where were most of the GCPs were located. The image fitting is very good along the river where the location of GCPs at the bridges was easy. In the hilly area of the SAR images showed great contradictions due to difficulties of GCPs selection.

The use of ERS-1 SAR data for the purpose of topographic mapping can cause difficulties because of its nature. Optical spaceborne data from other sources proved to be much more useful in direct plotting. Results from the visual interpretation showed that SAR data can be better used in conjunction with a map of the area for map revision purposes, or in combination with multispectral data. When data is merged in this way an accurate registration is the most important stage of the pre-processing and the goecoding test has shown that this can be done effectively.

6.3 *Agricultural University of Norway*

The Agricultural University of Norway adopted a qualtative approach to assessing the data for mapping. Five sub areas, each of 400 lines by 500 pixels were selevted from the data set provided by the Technical University of Vienna. For each area a visual interpretation was carried out directly from the screen display on the ERDAS image processing system. Each area was interpreted by a different person and was recorded as a vector file along with comments from the interpreter. The detailed interpretation and the comments are presented in appendix 2.

All the interpreters find that the noisy appearance of the ERS-1 SAR images compared to images from the ptical sensors in Landat and SPOT, represents a problem for the interpretation. The strong influence of the terrain surface on the reflection of radar signal is also considered to be a problem as is the smearing out of data in layover areas which have been corrected by the geocoding. Satellite images from optical sensors are generally preferred for mapping purposes by the interpreters taking part in the test. For some applications however, ERS-1 SAR images can be useful and in general this type of satellite data map represent a valuable supplement to the Landsat and SPOT images.

6.4 *Technical University of Vienna*

Killiany (1991) has developed a method of registration of images using features and this was tried on the SAR data of Frankfurt. 16 ground control features were identified and digitised from the 1:50.000 scale map and an affine transformation used to relate them to the corresponding feature on the image. 12 of the 16 features were successfully matched and yielded residuals of 11.5 ± 12.5m in X and 0.2 ± 20.0m in Y. This showed that when linear or areal features, as opposed to point features, are used a good correspondence can be obtained. This however does not help the identification of point features. This method has the potential of automation.

Other results from Vienna showed large differences at the edges of the geocoded image between the two geocoded products produced by DLR and the product from Vienna.

6.5 *General comments*

The evaluation of potential of ERS-1 SAR data for topographic mapping was under investigation in phase 2 of the test. UCL assessed the data after fusion with other image data and shown that cultural features can be recognised from the radar data as well as the Thematic Mapper scanning system and KFA-1000 space borne camera. These have been compared to

an existing map. Results for the potential use of space borne microwave image data, indicate that the level of information which can be extracted is low without supporting map data. The accuracies were not satisfactory, compared to those obtained by Landsat-TM data or optical data coming from KFA-1000. If existing data is used then new features can be identified and mapped.

The detectability of features in the ERS-1 geocoded SAR imagery depends upon the 12.5 m ground pixel resolution. The nature of the spaceborne backscattering mechanism of the radar controls the response of a target, and thus introduces significant speckle and geometric distortions. Pointing accuracies in ERS-1 SAR data, especially those involved the location of GCPs in the stage of rectification, are essentially determining the geometric quality of the geocoded image.

Merging the ERS-1 SAR data with KFA-1000 orthophoto and especially with Landsat-TM bands, proved to be a very sophisticated technique in order to increase the spatial information. Certain features were much easier to interpret in these colour image products without the aid of a map.

The interpreters at The Agricultural University of Norway found the SAR images difficult to interpret and preferred optical imagery. It was felt that enhancement would improve the quality of the output.

7. Conclusions

This two phase project has involved a number of participants and allowed the properties of ERS-1 SAR data to be investigated. It has been clearly shown that the methodology exists to accurately geocode SAR data and that if an accurate DEM is available the resulting orthoimage can be registered with a 1:50.000 map. It is clear that the rigorous methods of geocoding such as those developed by DLR for the ESA Processing and Archiving Facility (PAF) are the most effective and that although methods derived from photogrammetric bundle adjustments can produce equal results, they must include specific provision for the use of SAR data. Ellipsoid geocoding of less rigorous methods can be used effectively in areas with little relief.

In phase 2 the problems of interpreting SAR data have been identified and some proposals made for improving the quality of the image for this purpose. The techniques and benefits of merging SAR with other data have also been demonstrated.

As well as involving a number of organisations in the project itself, there has been interaction with the OEEPE project on the Digital Landscape Model for Europe (DLME) and a joint workshop was held with that group which resulted in useful discussion. A number of applications of SAR data were identified: Flood monitoring (multi temporal), geology, coastal, lake surfaces, land cover (can detect change but not quantify it). The all weather capability is an important advantage and can be particularly useful when applied to snow and flood mapping. These applications can be enhanced with the use of Interferomtric SAR for coherence maps and change detection. It was thought that there is a potential for SAR and optical to be mixed for classification. It was also expected that the use of multi polarisation, multi incidence data from SIR-B and X SAR would extend the use of SAR but much work is still required.

A useful data set has been built up in the Frankfurt area from the two projects and this could be made available to scientists. The existing SAR data has been augmented with multitemporal scenes and will be distributed by DLR. IfAG has provided the DLME data to DLR and this has all been compiled onto an exabyte for distribution. This includes Thematic Mapper data from 1984 and 1987, digitised KFA1000 data and raster products from the DLME project.

A number of recommendations can be drawn from the project:

- Automation of ground control points is required. This is a major bottleneck in SAR geocoding and subsequent data merging.

- Work is required on validating products derived from a number of sources, each with different error characteristics. This includes image data, DEMs and map data. Methods of quantifying and presenting these errors are needed.

- More work is required on merging optical data with SAR to develop techniques and also identify applications of SAR data.

- Data from future SAR missions: Radarsat, SIR-C and Envisat with a variety of observing parameters must be investigated.

Despite the problems of interpreting the radar imagery in mapping applications, it has been established within the wider scientific community as an extremely effective sensor for Earth observation. The fact that it has several advantages over other sensors, like providing a unique view of the terrain and continuity of the data supply, as well as the data availability in terms of spatial coverage of Earth and the all-weather sensing capability,

has led researchers to concentrate on the development of more sophisticated techniques in order to yield better results. These include the use of multi temporal SAR data and multi sensor data fusion. The latter techniques has been shown to be useful in this study. Image processing methods such as filtering and edge detection can improve the quality of the image and provide map-relevant linear information.

This project has shown that SAR data can be corrected geometrically to a high dgree of accuracy but that there are significant problems in identifying ground control points and interpreting features. However there are applications when the all weather capability of SAR can provide invaluable information, unobtainable by any other means. In these cases the correction and registration of the data is essential.

ACKNOWLEDGEMENTS

OEEPE is very grateful to ESA who provided the ERS-1 SAR data, to IfAG who provided additional DEM data and data from other sensors, and to DLR who processed the data for ESA and distributed it to the participants.

REFERENCES

Dowman ,I.; Laycock ,J.; Whalley, J. (1993): Geocoding in the UK. – SAR Geocoding: Data and Systems, Ed G Schreier. Wichmann, Karlruhe. Pp 373–388.

Earth Observation Sciences Ltd. (1994): Quality and Standards of High Level SAR Data. – Proceedings of the Fourth International Workshop on Image Rectification of Spaceborne Synthetic Aperture, Loipersdorf, Austria, 26–28th May 1993. 135 pages.

Ecker, R.; Gsandtner, M.; Jansa, J.; (1991): Geocoding using hybrid bundle adjustment and a sophisticated DTM. – Proceedings of 11th EARSeL Symposium, Graz, Austria, July 1991. Pp 445–455.

Killiany, R.; (1991): Locating ground control features with sub-pixel accuracy. – Proceedings of 11th EARSeL Symposium, Graz, Austria, July 1991. Pp 418–426.

Meier, E.; Frei, U.: Nüesch, D. (1993): Precise Terrain Corrected Geocoded Images. – SAR Geocoding: Data and Systems, Ed G Schreier. Wichmann, Karlruhe. Pp 173–185.

Pikeroen, B. and *Tannous, I.* (1994): Geometric processings for Spaceborne SAR Images. Quality and Standards of High Level SAR Data. – Proceedings of 4th international Workshop on Image Rectification of Spaceborne SAR, Loipersdorf, Austria, May 1993. EOS Ltd, Farnham. Pp 27–32.

Roth, A.; Craubner, A.; Hügel, T. (1993): Standard Corrected Ellipsoid Corrected Images. – SAR Geocoding: Data and Systems, Ed G Schreier. Wichmann, Karlruhe. Pp 159–172.

Sharroo, R.; Wakker, K.; Mets, G. (1993): The orbit determination accuracy of the ERS-1 mission. – Proceedings of Second ERS-1 Symposium – Space at the Service of Our Environment, Hamburg, October 1993. ESA SP-361. Pp 735–740.

Schreier, G. (1993): – SAR Geocoding: Data and Systems. Wichmann, Karlsruhe. 435pp.

Tarantino, C. and *Pasquali, F.* (1993): I-PAF approach to geocoding. – SAR Geocoding: Data and Systems, Ed G Schreier. Wichmann, Karlruhe. Pp 389–396.

University College London, 1994. Integrating data for a Digital Landscape Model. Proceedings of a Seminar, Frankfurt am Main, Germany, 21 – 22nd March 1994.

Appendix 1

Participants

List of organisations who originally expressed an interest in the project showing their status at the 4th GeoSAR Workshop.

ORGANISATION	Phase 1	Phase 2	1st report	
Alaska SAR facility	√		√	
Univesity of Bonn				Observer only
Institute Carto Catalunya	√	√		New participant 5/93
CORISTA, Naples				Observer only
DLR	√	√	√	
Dibag, Graz	√	√		
Dornier		√	√	
ERDAS	√	√		Data not delivered
Eros Data Centre	√			No info
EOS	√		√	
Hughes STX	√			Withdrawn 5/93
ISTAR	√		√	
JPL	√	√	√	
MacDonald Dettwiler Ass	√	√		No info
Politechnic Milano	√		√	Not active
Agricultural Univ. Norway		√		
Telespazio	√	√	√	
Thomson CSF	√		√	
UCL/GEC-MRC	√	√	√	
TU Vienna	√		√	

Appendix 2

Reports describing the methods and results of participants.

1. Paper describing DLR Geocoding system.
   Matschke M, Marschalk U, Hügel T, 1994. The D-PAF Geocoding System GEOS: Quality of Geocoded SAR Images. Quality and Standards of High Level SAR Data. Proceedings of 4th International Workshop on Image Rectification of Spaceborne SAR, Loipersdorf, Austria, May 1993. EOS Ltd, Farnham. Pp 51–56.

2. Listing of results from DLR presented to Seminar on Integrating Data for a Digital Landcape Model, Frankfurt am Main, 1994.

3. Report from Institut Cartogràfic de Catalunya and Universitat de Barcelona.

4. Paper from Institut Cartogràfic de Catalunya and Universitat de Barcelona.
   Palà V and Corbera J, 1994. ERS-1 SAR Rectification Based on Orbital and Elevation Data. Quality and Standards of High Level SAR Data. Proceedings of 4th International Workshop on Image Rectification of Spaceborne SAR, Loipersdorf, Austria, May 1993. EOS Ltd, Farnham. Pp 19–25.

5. Report from ISTAR

6. Paper from Thomson-CSF
   Pikeroen B and Tannous I, 1994. Geometric Processing for Spaceborne SAR Images. Quality and Standards of High Level SAR Data. Proceedings of 4th International Workshop on Image Rectification of Spaceborne SAR, Loipersdorf, Austria, May 1993. EOS Ltd, Farnham. Pp 27–32.

7. Listing of results from Telespazio presented to Seminar on Integrating Data for a Digital Landcape Model, Frankfurt am Main, 1994.

8. Paper from UCL.
   Upton M, Laycock J and Dowman I, 1994. The OEEPE/GeoSAR ERS-1 SAR geocoding experiment – work at UCL. Quality and Standards of High Level SAR Data. proceedings of 4th international Workshop on Image Rectification of Spaceborne SAR, Loipersdorf, Austria, May 1993. EOS Ltd, Farnham. Pp 47–50.

9. Report of image fusion and interpretation carried out at UCL.

10. Report of interpretation carried out at Agricultural University of Norway.

Appendix 2.1

"The D–PAF Geocoding System GEOS: Quality of Geocoded SAR Images"

M. Matschke, U. Marschalk, T. Hügel

DLR , German Aerospace Research Establishment
D–82234 Oberpfaffenhofen
Germany

ABSTRACT

One and a half year ago the GEOS system at the German Processing and Archiving Facility (D–PAF) started its operational production of geocoded SAR images. There are two different kinds of products: the ellipsoid corrected product (GEC) and the terrain corrected product (GTC). For each GTC also an incidence angle mask (GIM) as a raster file will be generated. The GEOS system allows slant range processed as well as ground range processed images as input.According to the OEEPE ERS–1 SAR geocoding experiment the quality of the testsite (Frankfurt/Main) has been investigated. The test data set with a digital elevation model (DEM) in Gauß–Krüger coordinates has been geocoded and compared with the official ESA GTC product based on the UTM projection. In each scene quality control points will be measured manually and the results and residual statistics will be presented.In this context the development of the geometric accuracy of terrain and ellipsoid corrected images over the last year will be discussed. For GEC and GTC products several test scenes have been selected with regard to different topographic structures. A monthly quality control of GEC products, on the basis of the scene Flevopolder, shows that the accuracy of these products has been permanently stable during the long period of operating.Further it will be demonstrated that the varying resolution of the digital elevation models and the accuracy of tiepoint measurement have a certain influence on the quality of the terrain corrected products.In border areas, which are covered by several map series might occur problems with the adjustment concerning the quality of the tiepoints, because of the different map projections. The investigation of the region around Basel, where the three countries France, Swizerland and Germany adjoin, will be presented.

SHORT DESCRIPTION OF SAR–PRODUCTS (GEC AND GTC)

For the geocoding of GECs only the flat surface of the reference ellipsoid of the desired map projection will be considered. Sensor, orbit and processing parameters as well as the mean height, which is taken from the global elevation data set ETOPO5, to get a minimum of mislocations will be needed for the geocoding. The mislocation is about 2.3 times the height

The detailed topographic height can be considered by the use of digital elevation models (DEM). This allows a precise terrain correction. For the generation of a terrain corrected product tiepoints are measured in the slant– or groundrange image and an adjustment is performed.

In the operational DEM data base of GEOS DEMs in different resolutions are available:

1	x 1	Arc second	former BRD
3	x 3	Arc second	Mideurope and Alps
30	x 30	Arc second	USA
300	x 300	Arc second	(ETOPO5) global

As the quality of the DEM is the main limitation factor for the accuracy of a GTC we only consider DEMs with 1x1 or 3x3 resolution.

For each GTC also an incidence angle, layover and shadow mask (GIM) in form of a 8 bit raster file is generated. This product shows the typical radar effects like layover and shadow areas. Each is traced with a certain grey value and within one bit. The incidence angle is described by the remaining 6 bit.

These informations are important for the evaluation of the terrain corrected product. The accuracy of the GIM is the same as the corresponding GTC so I won't make further inspections on it. The GEOS system allows slant range processed as well as ground range processed images as input

VALIDATION OF GEOCODED ELLIPSOID CORRECTED PRODUCTS (GEC)

For the validation of geocoded ellipsoid corrected products we used Active Radar Calibrators (ARCs). ARCs are active transponders which send an active signal when it receives a radar signal. Corner reflectors instead directly reflect the radarsignal. The intensity of the reflected signal depends on the incident angle of the radarsignal. The signals of the ARCs and their positions are well known so that the geometric control of the geocoded images could be executed. You only have to attention the time delay which calls out of the retardation to send the answer signal.

The geocoded ellipsoid corrected products was validated based on scenes in Flevopolder in the Netherlands (5.5°w. Lo, 52.5°n. La). This scene was chosen from ESA as calibration testsite. It has almost no relief and its height is about the sea level. The surface of the geoid in this area comes very close to the used reference ellipsoid. The mislocations are minimal and allow to determine a sensor specific geometry. Therefore three ARCs were positioned in this area.

ARC NO.	Site	WGS-84 Coordinates	UTM Coordinates	(ns)	Delay (m)	(pixels)
1	Pampushout	52 21 29 N 05 09 07 E 72 m Height	5 803 043 N 646 542 E	1.536	460.5	92
2	Lelystad	52 27 29 N 05 31 39 E 63 m Height	5 814 991 N 671 723 E	1.552	465.3	93
3	Minderhoudhoeve	52 33 18 N 05 40 08 E 63 m Height	5 826 116 N 680 929 E	1.545	463.2	93

Figure 1: Positions of the ARCs in the scene Flevopolder [1]

The ARCs were used for the geometric validation of the products and the radiometric calibration of the sensor.

To determine the accuracy of the GECs the position of the ARCs in the slantrange image were calculated and a digital symbol has been inserted. Afterwards the product has been geocoded. With the visual quality control module the position of the ARCs have been measured and also some other map devided quality control points. The azimuth component of the one ARC in the map 25 OOST Pampushout was to big. This ARC had a foult. For sureness the scene was geocoded once with this ARC and once without it. The northing component is already very accurate the easting which compares with the range geometry was worse. The mislocations were over 130 meters. This results out of the transmit time of the signals. The processing group of the DLR performed an update at the MSAR

processor. The 'sampling start–time bias' was reduced from 6578 ns to 6265 ns to get a minimum of range offsets. After this update the results (see figure 2) were very exact.

Scene (GEC)	Aqui. date mean height	Easting (m)	Northing(m)	Quality
Flevopolder	04/09/91 8 m	40	48	1
Flevopolder	10/09/91 3 m	24	18	1
Frankfurt	20/08/91 288 m	243	140	4
Frankfurt	23/08/91 273 m	326	107	4
Frankfurt	14/08091 247 m	282	121	4

Figure 2: Residuals and qualities of GECs [1]

Scene (GTC)	Aqui. date mean height	Easting (m)	Northing(m)	Quality
Frankfurt	14/08/91	34	24	1
Freiburg	14/08/91	31	15	1

Figure 3: Residuals and qualities of GTCs [1]

VALIDATION OF GEOCODED TERRAIN CORRECTED PRODUCTS (GTC)

In Frankfurt / Germany (8.5°w. Lo, 50°n. La) the validation for the terrain corrected products has been performed because of the availability of a very exact digital elevation model from 1x1 arc second. For the software verification of terrain corrected products manual measured tiepoints and simulated tiepoints has been used.

For the validation of the geocoded terrain corrected products an other GTC has been geocoded (Freiburg / Germany (8°w. Lo, 48°n. La)). This scene is very interesting because there are two different DEMs with different resolutions (1x1 and 3x3 arc seconds) and three countries with its own map systems are meeting there. An other effect is that here a high topographic difference.

Also here the accuracy of the GTC is very high and lays within the frame of errors in the measurements. The mislocations are less then 30 meters. Geocoded terrain corrected products are even in topographic varying areas very exact.

OEEPE ERS–1 SAR GEOCODING EXPERIMENT

According to the OEEPE ERS–1 SAR geocoding experiment the quality of the testsite (Frankfurt/ Main) has been investigated.

The test data set with a digital elevation model (DEM) in Gauß–Krüger coordinates has been geocoded and compared with the official ESA GTC product based on the UTM projection. The digital elevation model in Gauß Krüger coordinates has a resolution from 40 meters the one in UTM 1x1 arc second (25 meter).

The ESA standard product has a size of 100x100 kilometers the OEEPE test scene is only as big as one map sheet 1:50 000 (L 5916). The quality control of both scenes gave these results:

Residuals in Easting / Northing

ESA (WGS84):

Point	east(px)	north(px)	east(m)	north(m)
1	–0.79	0.09	–10.11	1.22
2	0.48	–0.49	6.11	–6.18

OEEPE (Gauss Krüger):

Point	east(px)	north(px)	east(m)	north(m)
1	1.27	–0.01	16.24	–0.14
2	–0.09	0.09	–1.24	1.24
3	0.20	0.00	2.56	0.04
4	0.88	0.19	11.21	2.42

The accuracy in the ESA standard product is a little better because the resolution of the DEM is more exact than the one in Gauß Krüger coordinates. Another fact is that the manually tiepoint measurement is in each scene a little different because of the tiepoint identification accuracy. The error is about one pixel. Both GTC products show the desired accuracy.

CRITICAL ITEMS OF GTC PRODUCTION

Possible errors with the measuring of the point in the map and in the image are within the bounds of the accuracy of the pixel spacing from 12.5 meters. These errors are adjusted by considering more points over the whole image.

In border areas, which are covered by several map series problems might occur with the adjustment concerning the quality of the tiepoints, because of the different map projections. In the central areas of a country the adapting of the reference ellipsoid to the geoid is very exact but at the borders there are large differences. This leads to relatively big shifts. The mislocations in the geocoded image are large. This is documented in the next figure for the scene in Furtwangen with German, French and Swiss maps.

Map from land	Residuals (m)	Root Mean Square	Mean value	Standard deviation	mean height
France	Easting	60	55	25	40 m
	Northing	105	104	15	
Germany	Easting	28	26	12	60 m
	Northing	22	10	22	
Swiss	Easting	19	–15	14	55 m
	Northing	20	20	2	

Figure 4: Dependence of the residuals on the map basement [1]

These residuals do not result from mislocations but from the difference of the reference systems. The residuals in the German and Swiss maps are about the same size, the residuals in the french maps are much bigger. That's because french maps base on the Clarke–Ellipsoid, German and Swiss on the Bessel–Ellipsoid. This leads to pretended larger residuals.

The reference of the DEMs outside from Germany

isn't known. Consequently informations about the height shift are missing. The absolute height is right but for the transformation in an other system details about the difference between the reference ellipsoids are missing. According to the area a shift from about 50 meter is taken because this leads to good results.

The DEM from Germany bases on the ED50 (European Datum form 1950). To get a uniform elevation model the DEMs from all countries were transformed to ED50. The errors by the transformation have a certain influence on the quality of the geocoded terrain corrected products.

QUALITY DURING THE PROCESSING PERIOD

The quality of the terrain corrected products is controlled for each GTC. During the long period of operation the accuracy of these products has been stabile. The mislocations are between 0 and 45 meters in northing, 0 and 70 meters in easting, and also the RMS lays between 0 and 70 meters.

The bigger shifts result probably most from different map systems used for one scene which cause pretended big mislocations. Another reason can be a worse digital elevation model like for scenes in the alps. The mean value of the terrain corrected products is 21 meters in easting, 15 meters in northing and 27 meter RMS. This is about the results of the GTC validation.

To check the accuracy of the GECs a monthly quality control is performed. Each month a scene in Flevopolder is geocoded for quality inspection. Also here you can see that the accuracy has been stabile during the last year. The mislocations are about these from the validation. Only one scene was bad but this resulted out of wrong image annotations.

Residual Statistics of GECs (meters)

residuals	mean RMS	stdev
easting	41	27
northing	28	10
length	52	23

The quality of a product depends also from the used processor. There are considerable radiometric differences between MSAR processed products and fast delivery products. Another effect is that the near range is always brighter then the fare range area. This comes because the FDP, which was planed for "near real time" scenes, makes almost no radiometric compensation. This leads to a radiometric worse product. Because of these aspects GECs are now made from PRIs (groundrange input).

SUMMARY

Geocoded ellipsoid corrected products can be made from each ground or slantrange input. They have a high accuracy in flat areas. In scenes with different topographic areas you have to take inti account that the mislocation in the ellipsoid corrected products is about 2.3 times the height.

System or software modifications wouldn't give better results. Only GTCs deliver a better accuracy but they only can be made in areas where we have a DEM and maps.

The error in azimuth depends on sensor specific parameters the error in range belongs how exact the used digital elevation model is. The DEM in Germany has a resolution of 25 meters. It lays within in the frame of the pixel spacing and causes a maximal error from one pixel.

The accuracy of geocoded terrain corrected products are also in high topographic areas very good. For the evaluation of these products it is useful to know, where the layover and shadow areas are in the scene. That's why we produces for each GTC also an incidence angle, layover and shadow mask.

REFERENCES

[1] Th. Hügel, "Qualitative und Quantitative Analyse der geocodierten ERS1–Bilddaten im Hinblick auf ihre geometrische Genauigkeit und ihrer Anwendungsmöglichkeiten in der Geographie", Ludwig–Maximilian–Universität München, 1992, pp. 37–57

[2] A. Roth, A. Craubner, T. Hügel, "Standard Geocoded Ellipsoid Corrected Images", SAR Geocoding: Data and Systems, Karlsruhe, Herbert Wichmann Verlag GmbH, 1993, ch. 6, pp. 159–172

[3] E. Meier, U. Frei, D. Nüesch, "Precise Terrain Corrected Images", SAR Geocoding: Data and Systems, Karlsruhe, Herbert Wichmann Verlag GmbH, 1993, ch. 7, pp. 172–186

Deutsche Forschungsanstalt für Luft– und Raumfahrt e.V.

OEEPE ERS–1 SAR geocoding experiment

Frankfurt / Main

- OEEPE

  DEM in Gauß–Krüger coordinates

  resolution: 40 meters

  testsite as big as one map sheet 1:50 000 (L 5916)

  residuals between 0 and 16 meters

- ESA

  DEM in UTM projection

  resolution: 25 meters

  size of the scene: 100 x 100 kilometer

  residuals between 1 and 6 meters

DLR

ESA (WGS84)

* Residuals in Easting/ Northing *
****
(System: MAP)

Point ID	east[pxl]	north[pxl]	east[m]	north[m]
POINT 1	3.144198	-0.990315	39.965300	-12.390000
POINT 3	5.716769	0.137485	72.664760	1.720100
POINT 4	1.599598	0.266977	20.332190	3.340200
POINT 5	2.254897	-0.857770	28.661560	-10.731700
POINT 6	1.938759	-0.551275	24.643200	-6.897100
POINT 7	1.752319	1.528035	22.273390	19.117500
POINT 8	1.085632	0.897526	13.799260	11.229100
POINT 9	1.270189	-0.611238	16.145130	-7.647300
POINT 10	3.725435	0.563401	47.353290	7.048800
POINT 11	0.501243	-1.197082	6.371200	-14.976900
POINT 12	1.474815	-0.207399	18.746090	-2.594800
POINT 13	1.776534	1.483227	22.581180	18.556900
POINT 14	1.868304	-0.827101	23.747660	-10.348000
POINT 15	1.295765	0.394432	16.470220	4.934800
POINT 16	1.648873	1.237734	20.958510	15.485500
POINT 17	0.128878	3.811754	1.638140	47.689500
POINT 18	1.578472	0.800996	20.063660	10.021400
POINT 19	-0.795946	0.097625	-10.117120	1.221400
POINT 20	0.481177	-0.494430	6.116150	-6.185900
POINT 21	-1.486610	-0.883658	-18.896020	-11.055600

OEEPE (Gauss Krüger)

Point ID	east[pxl]	north[pxl]	east[m]	north[m]
POINT 1	1.277508	-0.011300	16.240200	-0.141300
POINT 2	-0.097716	0.099393	-1.242200	1.242900
POINT 3	0.201944	0.003647	2.567200	0.045600
POINT 4	0.882358	0.194197	11.216900	2.428400
POINT 5	0.781661	0.196684	9.936800	2.459500
POINT 6	0.197996	-0.106958	2.517000	-1.337500
POINT 7	0.793547	0.489106	10.087900	6.116200
POINT 8	0.107580	1.297512	1.367600	16.225200
POINT 9	0.687368	1.101252	8.738100	13.771000

DLR

Deutsche Forschungsanstalt für Luft– und Raumfahrt e.V.

ESA (WGS84)

* Residuals in Azimuth/ Range *
****
(System: MAP)

Point ID	azimuth[pxl]	range[pxl]	azimuth[m]	range[m]
POINT 1	-0.678519	0.671535	-8.489060	8.535759
POINT 3	0.171271	-0.169509	2.142806	-2.154593
POINT 4	0.093060	-0.092102	1.164292	-1.170697
POINT 5	-0.421479	0.417141	-5.273192	5.302200
POINT 6	-0.232901	0.230504	-2.913861	2.929890
POINT 7	0.583478	-0.577473	7.299997	-7.340154
POINT 8	0.212328	-0.210143	2.656477	-2.671090
POINT 9	-0.169183	0.167442	-2.116679	2.128322
POINT 10	0.457375	-0.452668	5.722299	-5.753778
POINT 11	-0.130753	0.129407	-1.635869	1.644867
POINT 12	-0.066653	0.065967	-0.833911	0.838499
POINT 13	0.574195	-0.568286	7.183851	-7.223369
POINT 14	-0.336732	0.333267	-4.212913	4.236088
POINT 15	0.111372	-0.110226	1.393395	-1.401060
POINT 16	0.444726	-0.440149	5.564048	-5.594656
POINT 17	0.107049	-0.105947	1.339304	-1.346671
POINT 18	0.275515	-0.272680	3.447020	-3.465982
POINT 19	-0.016933	0.016758	-0.211846	0.213011
POINT 20	-0.051843	0.051309	-0.648614	0.652182
POINT 21	0.286260	-0.283313	3.581442	-3.601143

OEEPE (Gauss Krüger)

Point ID	azimuth[pxl]	range[pxl]	azimuth[m]	range[m]
POINT 1	-0.003147	0.003112	-0.039358	0.039558
POINT 2	-0.002118	0.002094	-0.026481	0.026615
POINT 3	0.000161	-0.000159	0.002008	-0.002018
POINT 4	0.037361	-0.036937	0.467191	-0.469559
POINT 5	0.033521	-0.033141	0.419175	-0.421299
POINT 6	-0.004617	0.004565	-0.057740	0.058033
POINT 7	0.084626	-0.083667	1.058240	-1.063603
POINT 8	0.030435	-0.030090	0.380584	-0.382513
POINT 9	0.165046	-0.163174	2.063879	-2.074339

ESA (WGS84)

* Residuals in Length/ Direction *
****
(System: MAP)
(Direction related to easting)

Point ID	length[pxl]	direction[deg.]	length[m]	direction[deg.]
POINT 1	3.296469	342.517350	41.841813	342.775574
POINT 3	5.718422	1.377666	72.685116	1.356037
POINT 4	1.621725	9.475486	20.604730	9.329297
POINT 5	2.412535	339.173032	30.604810	339.472676
POINT 6	2.015612	344.127193	25.590180	344.364213
POINT 7	2.324976	41.088664	29.352729	40.639862
POINT 8	1.408598	39.581610	17.790792	39.136853
POINT 9	1.409607	334.302301	17.864670	334.654964
POINT 10	3.767796	8.599723	47.875042	8.466626
POINT 11	1.297787	292.720049	16.275740	293.044988
POINT 12	1.489326	351.995163	18.924822	352.119297
POINT 13	2.314311	39.858483	29.227867	39.412890
POINT 14	2.043198	336.120960	25.904294	336.454922
POINT 15	1.354468	16.930279	17.193615	16.679244
POINT 16	2.061739	36.893893	26.058777	36.459381
POINT 17	3.813932	88.063533	47.717627	88.032657
POINT 18	1.770076	26.905531	22.427191	26.541218
POINT 19	0.801911	173.007455	10.190581	173.116221
POINT 20	0.689922	314.221713	8.699003	314.675149
POINT 21	1.729411	210.727742	21.892598	210.330861

OEEPE (Gauss Krüger)

Point ID	length[pxl]	direction[deg.]	length[m]	direction[deg.]
POINT 1	1.277558	359.493230	16.240815	359.501503
POINT 2	0.139382	134.512304	1.757231	134.983861
POINT 3	0.201977	1.034498	2.567605	1.017612
POINT 4	0.903476	12.412229	11.476758	12.215714
POINT 5	0.806027	14.123699	10.236656	13.902122
POINT 6	0.225039	331.621805	2.850297	332.014423
POINT 7	0.932171	31.647755	11.797187	31.228044
POINT 8	1.301964	85.260305	16.282735	85.182005
POINT 9	1.298164	58.028850	16.309348	57.603685

DLR

Critical items of GTC production

- manually tiepoint measurement
- different map projections
- basement of DEMs out of Germany isn't known
- transformation of the DEM into ED50 includes arithmetic errors

DLR

Appendix 2.3

OEEPE-GeoSAR EXPERIMENT

Vicenç Palà *
Fernando Pérez *
Jordi Corbera **

* Institut Cartogràfic de Catalunya.
** Universitat de Barcelona. Departament de Geologia Dinàmica.

Report on OEEPE-Experiment
Geocoding of ERS-1 Data

Available Data

35597.tsl: Slant range image.
34497.opd: Orbit points data file. This file was not in the exabyte.
orbit_37231: Preliminary orbit data.
noaa_globe.srf: We did not use this data.
Frankfurt_16bit.srf: 802 columns by 702 rows, 40-meter-spaced elevation model. Gauss-Krüger projection and Bessel ellipsoid.
Frankfurt_8bit.srf: We did not use this data.
35597.gcp: Tie points in WGS-84 geocentric coordinates.
35597.vqc: Quality control points (not used as seen below).
35597_dmp: Parameters used by DLR for image geocoding.
GEC
GTC
Maps

Data Process

1.- Images and DEMs conversion to Institut Cartogràfic de Catalunya (ICC) format.

2.- Useful orbital points extraction. Given that time distance between points is 120 seconds, only a few points are necessary for subsequent orbital adjustment.

3.- DEM conversion. The original Gauss-Krüger DEM was resampled into a UTM-32 DEM. Ellipsoid and datum transformations were applied. Cubic convolution was used for interpolation. The resultant DEM is printed on image **4** (see annex).

Imaging Model

Orbit adjustment

The model describing the orbit is an Eulerian one, meaning that only six unknowns are involved. Since file *34497.opd* was not present in the exabyte we could only use the preliminary orbit data, where we could find a point and its velocity every 120 seconds.Two points from this data, covering the orbit segment in which the image was captured, were used. This choice gives the necessary redundancy for the adjustment and guarantees a good fitting for this points.

The Eulerian model was compared to the polynomial model with the coefficients used by DLR, giving a significant improvement (as could have been expected, since we are dealing with a relatively large orbital segment) when tested on the orbital points around the image (figure 1).

		RMSpos (m)	RMSvel (m/s)
2 orbital points	Polynomial:	8.282	0.433
	Eulerian:	0.001	0.577
4 orbital points:	Polynomial:	301.909	6.517
	Eulerian:	97.539	1.638
6 orbital points:	Polynomial:	1834.214	24.546
	Eulerian:	250.315	2.054

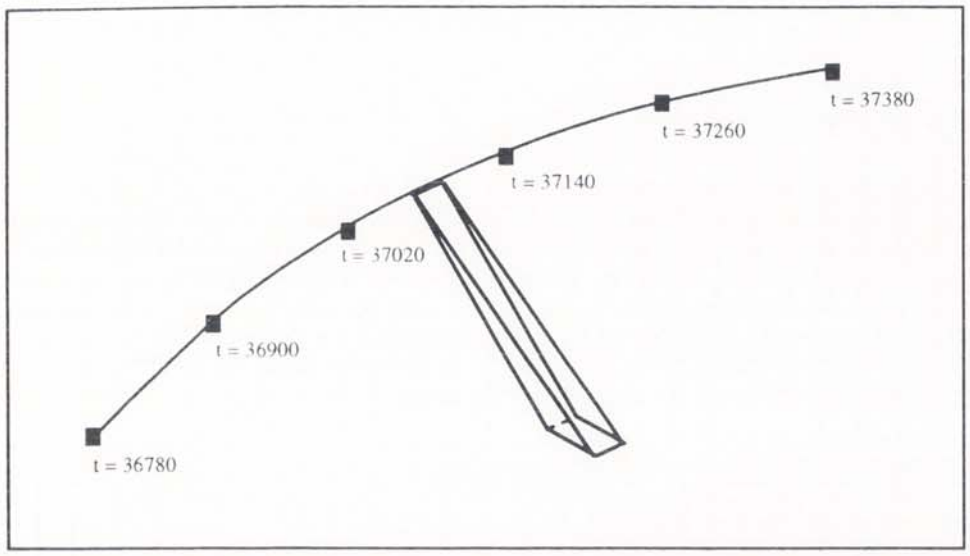

Figure 1. Orbital points around the image. Time (UTC) for each point is shown.

Anyway, the image was captured in the orbital segment between the two central points so similar errors are expected in either model. The advantages of the Eulerian model would be significant when geocoding large image segments.

Imaging parameters adjustment

Two parameters were adjusted based on 25 control points:

1.- Time related to the first row in the image.
2.- Elapsed time between image rows.

The RMS errors measured in pixels on the adjusted points were:

$RMS_{azimuth}$ = 13.42 m
RMS_{range} = 18.44 m

It is worth of note that an adjustment with only two control points gave similar results when compared to those obtained using 25 points. In that case, however, one must start from very reliable points, since its errors would affect the whole image.

GTC Rectification

The geocoding process is performed in three steps. First, a destination row-column coordinate is obtained and stored for each point in the DEM (a, b, c and d points in figure 2). Then, for every destination pixel (p in figure 2), the four nearest DEM neighbours are used to calculate, by means of an interpolation, the corresponding row-column on the original image. Finally, the radiometric value is obtained by interpolating the values of the neighbours in the original image. Images **1** and **1'** (see annex) are the GTCs subscenes on the test area processed by DLR and ICC, respectively, while in image **2** differences between the two former images are shown.

GEC rectification

Following the same procedure, we have performed the GEC rectification introducing a height equal to the mean height in the involved zone. Although we do not know which parameters were used at DLR to produce the GEC, i.e., whether they used the global DEM data or a mean height over the zone, we obtained a good overlapping except for a global shift. Image number three in the annex shows the resultant GEC. As we expected, the errors increased in points with height far from the mean we used, and these errors only affect the column estimate. GECs would be good enough only for mosaicking flat areas.

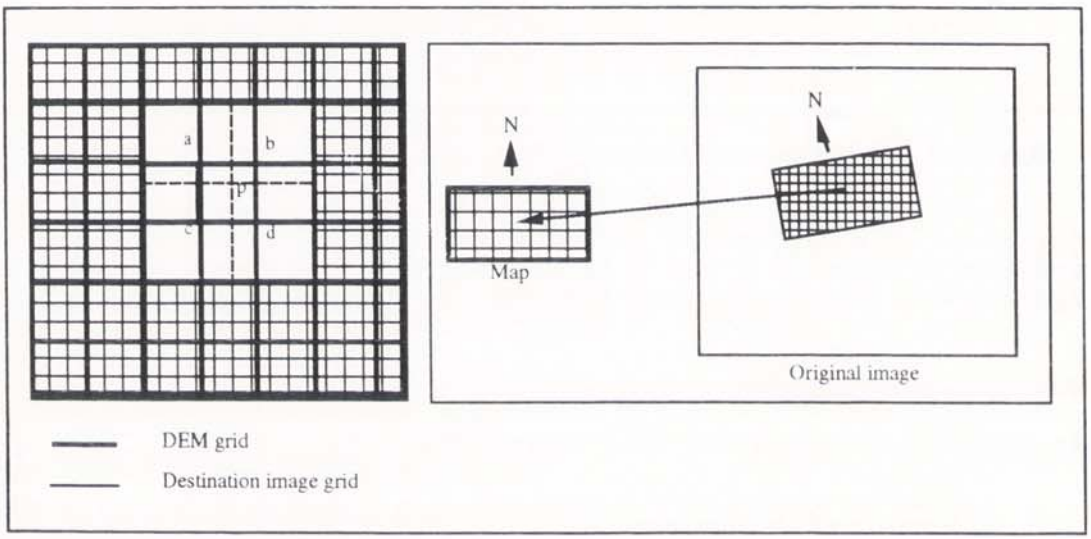

Figure 2. Geocoding process

Quality Control

In order to evaluate the quality of our adjustment, we read the quality-control points file *35597.vqc* and realized that the data in this file relates UTM coordinates on the corrected image to row-column position *on the same* image, not allowing a statistical treatment of the information. (We verified this point by adjusting a linear polynomial and obtained an error near zero). So the only possibility was to perform a visual inspection, trying to recognize the test points on both images and compare their coordinates. However, although we were able to read

the GTC provided by DLR, we could not reference the image from the UTM data in the parameter-pool file, since the UTM limits for the image did not match with the pixel-size and number-of-lines information. That is why we decided to divide the tie points into two groups. One of them was used for adjustment and the other one as test points for quality control.

The RMS errors in pixels on 23 test points were:

$$RMS_{azimuth} = 18.89 \text{ m}$$
$$RMS_{range} = 17.41 \text{ m}$$

Additionally, we extracted a set of 16 points from the map (transformed to UTM coordinates) and obtained their corresponding position in the ICC-geocoded image. We compared these two sets of points and obtained the following results:

$$RMS_{azimuth} = 20.97 \text{ m}$$
$$RMS_{range} = 18.62 \text{ m}$$

ANNEX

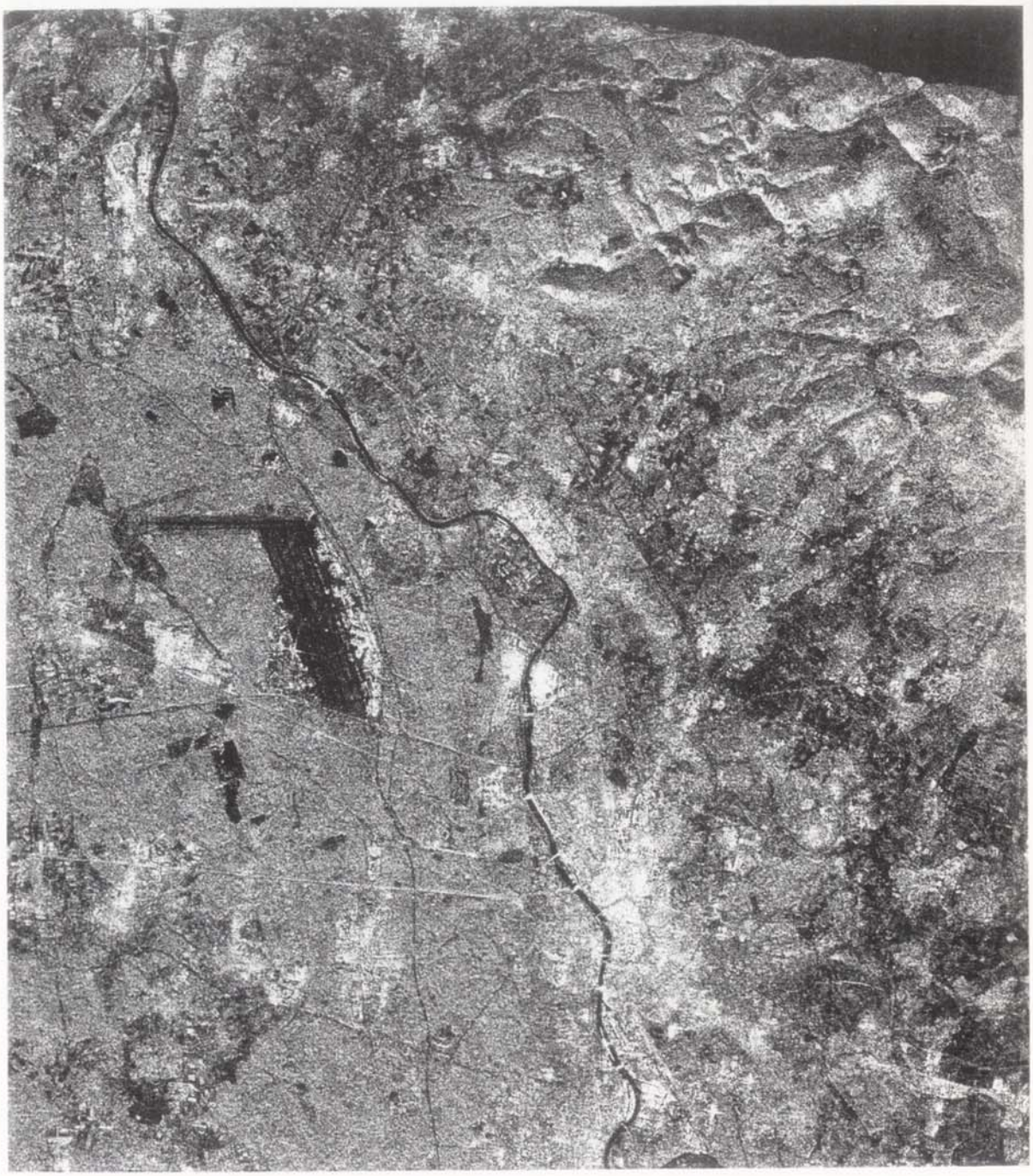

Image 1. GTC provided by DLR

Image 1'. GTC processed by ICC

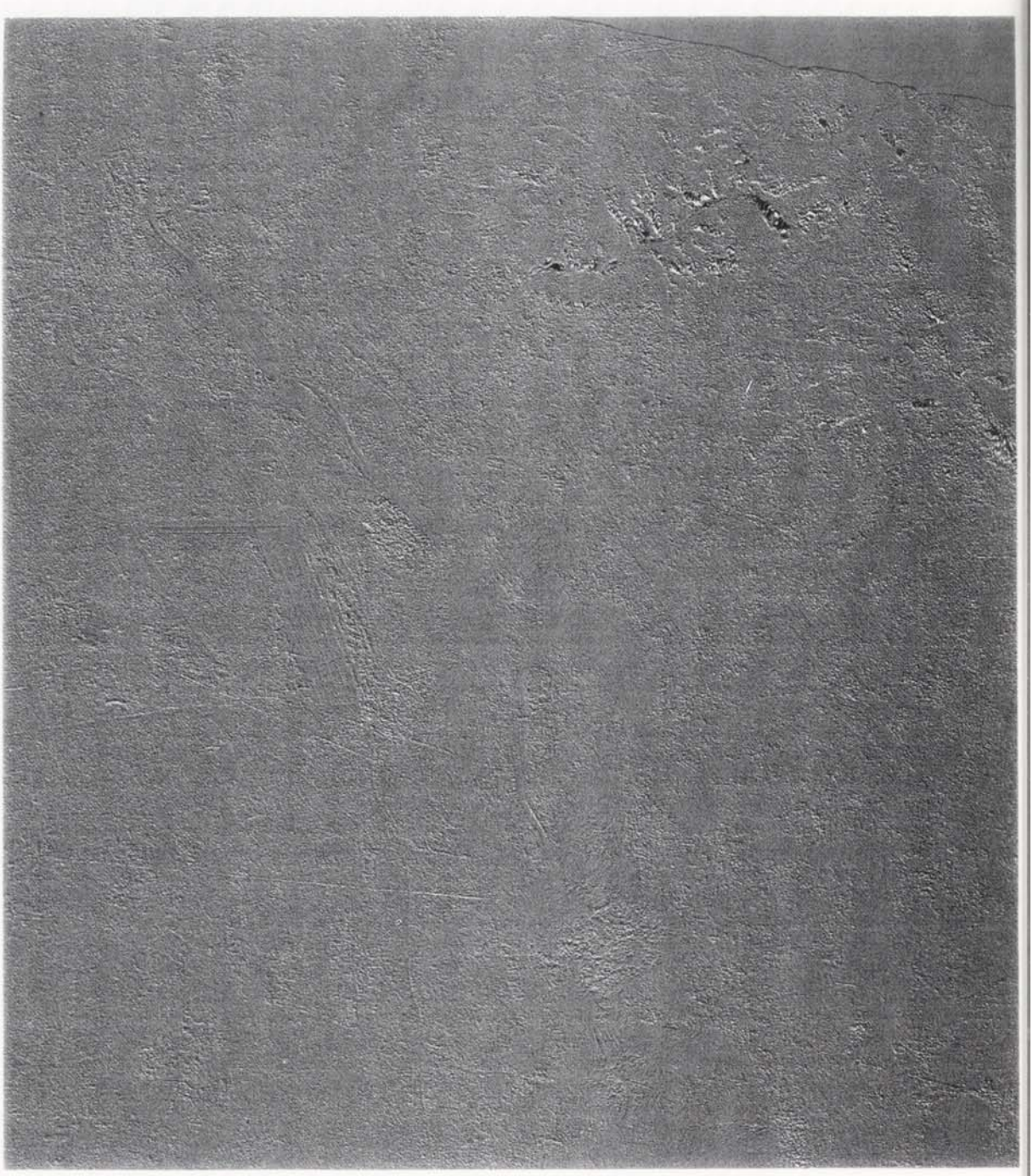

Image 2. Image showing differences (**1 - 1'**)

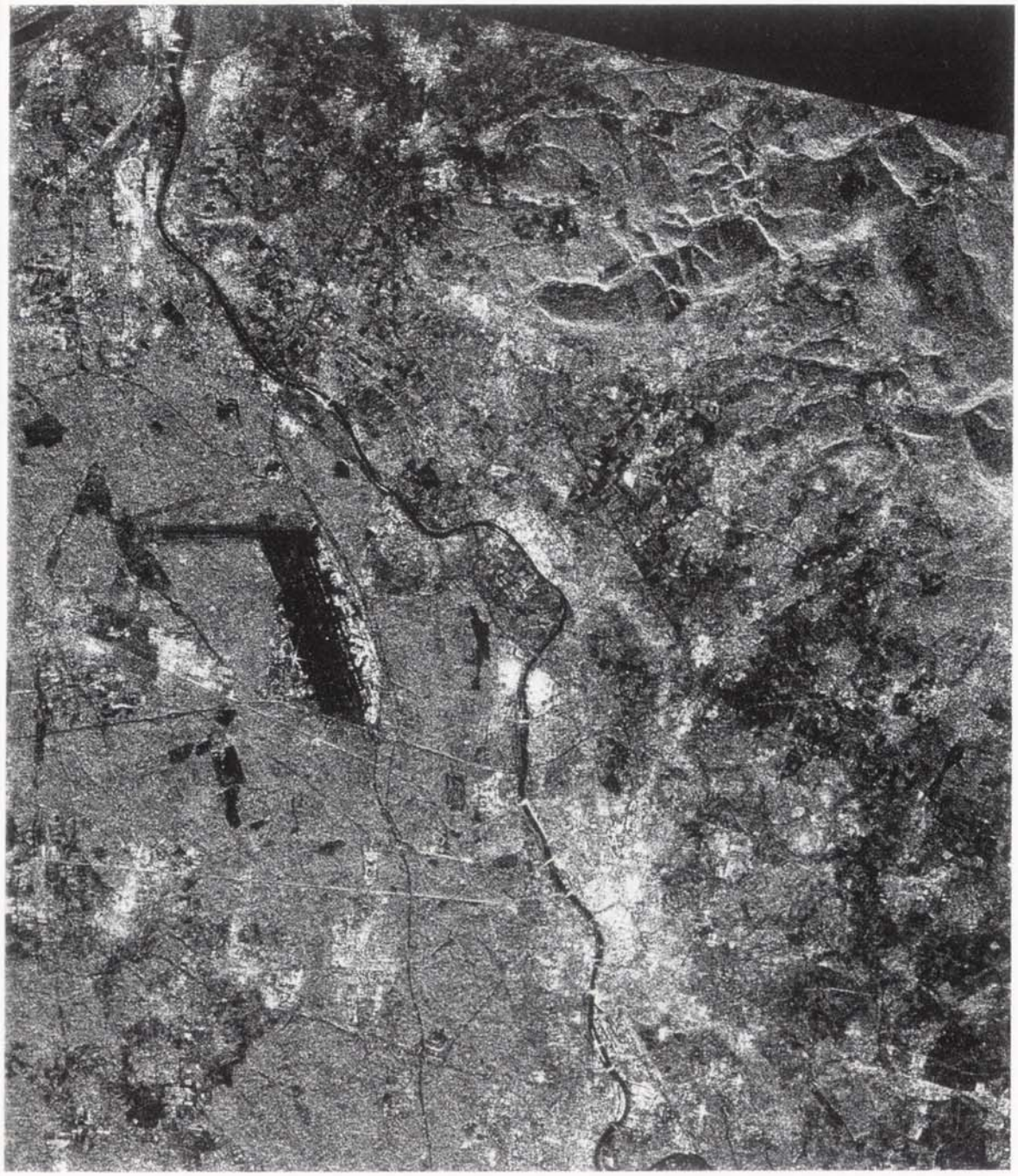

Image 3. GEC processed by ICC

Image 4. DEM provided by DLR

RESULTS FROM OEEPE/GEOSAR TEST OF ERS-1 DATA

Summary sheet

Name Vicenç Palà, Fernando Pérez and Jordi Corbera

Organisation Institut Cartogràfic de Catalunya

Date 07 / 26 / 93

SAR image used for geocoding 35597.tsl

Method of geocoding The geocoding process is performed in three steps. Firstly, a destination row-column coordinate is obtained and stored for each point in the DEM . Then, for every destination pixel, the four nearest DEM neighbours are used to calculate, by means of an interpolation, the corresponding row-column on the original image. Finally, the radiometric value is obtained by interpolating the values of the neighbours in the original image.

Method of resampling Bilinear interpolation

Area geocoded (km x km) 31.9 x 27.9 km

DEM used frankfurt_16bit.srf (converted to UTM coordinates)

No of tie points used in geocoding (whole image, DLR) 25

No of tie points used in checking (whole image, DLR) 23

No of check points extracted from map (test area, ICC) 16

rmse against tie points E N

RMS (range, azimuth)	18.44 m, 13.42 m
Max (range, azimuth)	41.25 m, 35.75 m
Min (range, azimuth)	0.17m, 1.10 m

rmse against check points E N

RMS (range, azimuth)	17.41 m, 18.89 m
Max (range, azimuth)	35.12 m, 43.75 m
Min (range, azimuth)	0.15 m, 0.71 m

rmse against detail from map E N

RMS	18.62 m, 20.97 m
Max	28.03 m, 34.89 m
Min	1.37 m, 2.16 m

Comments

- DEM does not cover the whole image.

- Available information is not sufficient for coordinates assignment to GEC and GTC images (full description of tape header format would be necessary).

- Available data presented in different projections/ellipsoids.

- Only two test points (file 35597.vqc) are in the test area. Moreover, their position (row-column) refers to the geocoded image and do not provide additional information with respect to the cartographic coordinates.

ERS-1 SAR RECTIFICATION BASED ON ORBITAL AND ELEVATION DATA

Vicenç Palà * and Jordi Corbera **

* Institut Cartogràfic de Catalunya,
Barcelona, Spain.

** Departament de Geologia Dinàmica i Paleontologia
Universitat de Barcelona
Barcelona, Spain.

Abstract

Since the European Space Agency's ERS-1 satellite was launched on July 1991, the *Institut Cartogràfic de Catalunya* and the *Departament de Geologia* of the *Universitat de Barcelona* have been working together on the SAR geocoding problem.

The developed method involves a keplerian modelization for the satellite orbit based on the ephemerides orbital points and its velocities. The start time -for the first image row- and increment time between rows may be extracted from the tape information or adjusted on the basis of Ground Control Points (GCPs). In the case of Ground-Range data, polynomial coefficients allowing transformation from Ground-Range to Slant-Range are needed and derived from GCPs, if not provided in the tape header.

The rectification process needs an accurate Digital Elevation Model (DEM) and takes profit of locality when calculating the Synthetic Aperture Radar (SAR) position from the geocentric position. An orbital data table is used in order to improve the rectification speed. The known foreshortening and layover topographic effects on the original images are eliminated.

An ERS-1 image over a rugged area in South Catalonia was rectified and compared with 1:50,000 SPOT PAN orthoimages over the same area, giving a successful overlapping. In the future, we aim to integrate the ERS-1 SAR rectification model with the available models for other imagery (SPOT, TM, Aerial photography,...) and allow a multiple SAR triangulation combined with other observable data when desired.

Introduction

The *Institut Cartogràfic de Catalunya* (ICC) has accumulated a considerable amount of experience on image geocodification -primarily based on optic sensors- in order to obtain cartographic products, i.e. distortion-free orthoimages. Work has been made over LANDSAT (MSS & TM), SPOT (Panchro. & multispectral), NOAA, ATM (Airborne TM) and CASI (Compact Airborne Spectrographic Imager) images.

After the announcement of the ERS-1 launching, the ICC started to explore the capabilities of radar imagery for cartographic use. For this purpose, the ICC came into contact with the *Departament de Geologia* in Barcelona University, at that time interested in the use of ERS-1 images for ice-dynamics studies at Livingston island in Antarctica.

Throughout this collaboration, we have developed a model that takes in account the Earth-satellite system geometry (Corbera, 1992), allowing the suppression of geometric distortions provided that the DEM is known for the imaged zone. This would permit us combine images from different sensors and carry out multitemporal studies.

Even though this implementation takes profit of the particular characteristics of ERS-1 satellite, modifications in order to process SAR images from other satellites can be easily made.

In this paper, we will summarize first the useful data provided in the tape header (auxiliary data). In second place, we will detail the generation of the parametric function in time describing the satellite orbit in geocentric coordinates. Then, we will posit the general radargrammetric model with constraints for ERS-1. After that, we will describe the geocoding algorithm and data adjustment based on GCPs. Finally, we will point out some suggestions for future developing. The general scheme for geocoding is summarized in figure 1.

Auxiliary data

In our particular case, the determination of GCPs is specially difficult due to the great noise level of SAR images, the amount of distortion in rugged terrain and the remoteness of the area, with the lack of cartographic information this fact implies.

The Earthnet ERS-1 Central Facility (EECF) at ESRIN (Frascati, Italy) is distributing images in different application-oriented formats. There are two formats suitable for cartographic purposes. First one is SAR.SLC product, i.e. one-look, complex Slant-Range

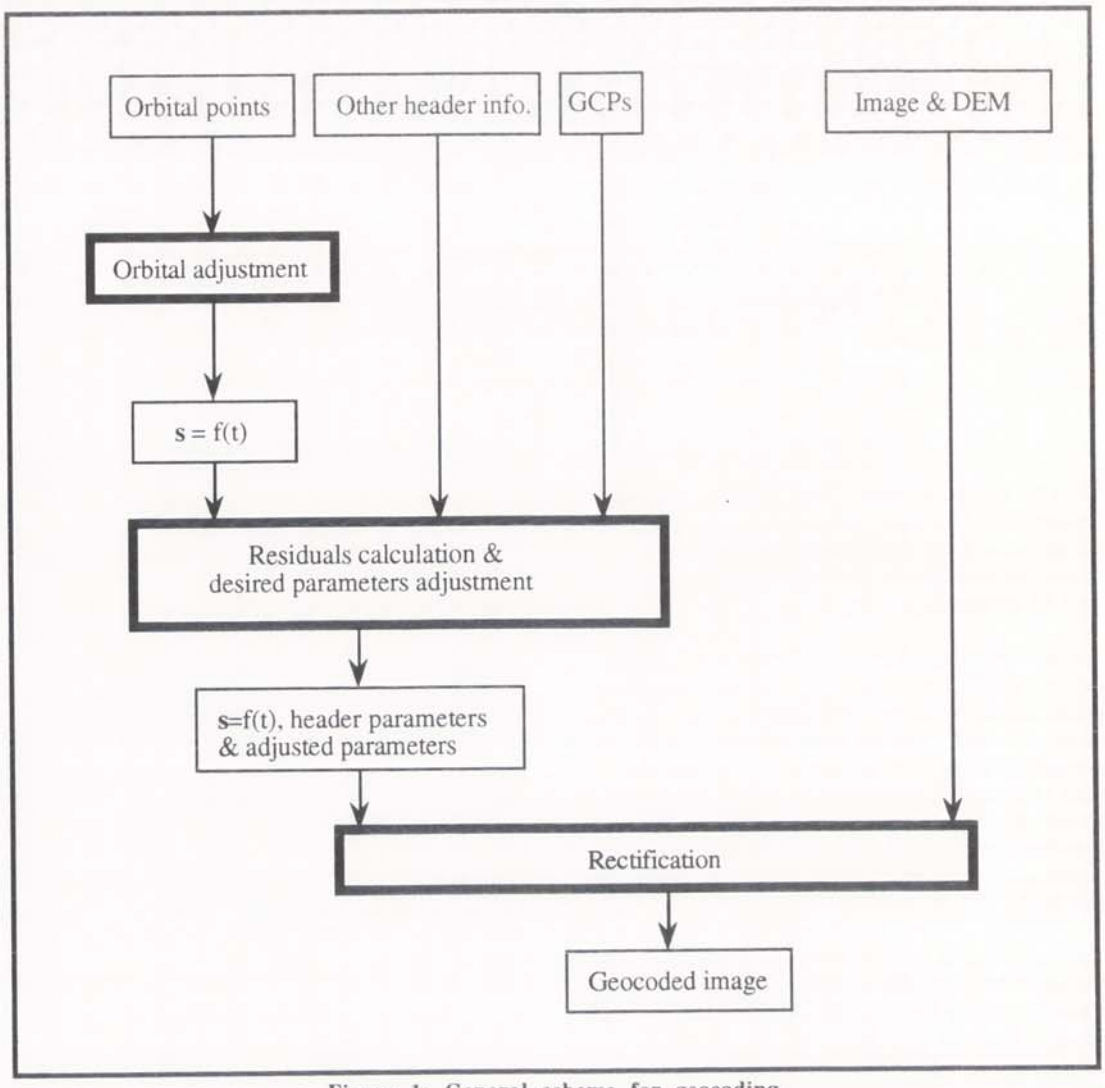

Figure 1: General scheme for geocoding.

images. Second one is the product called SAR.PRI giving multiple-look, real Ground-Range images. The optimum format would be a *hybrid* consisting of multiple-look, real Slant-Range data, unless coefficients for Slant to Ground transformation (performed in ESRIN) were given as auxiliary data.

Some useful information can be retrieved from header:

• Information about a number of points (presently five) on a sector of the satellite orbit over the imaged zone. Coordinates and velocities in a geocentric reference system are supplied for each point. Time increment between these points is also given.

• Zero-doppler azimuth time of first and last azimuth pixel (t_f , t_l). These two values indicate time associated to first and last image rows, that can be easily related to the satellite orbital points.

• Number of rows in the image. Allows computation of time increment between rows.

• Normalization reference range (r_0). Pemiting transformation of Slant-Range values into pixel position inside a row (column).

Orbital adjustment

A function describing the evolution in time of satellite position can be built from the orbital points

$$s(t) = (x(t), y(t), z(t)) \qquad (1)$$

where s is a vector (x,y,z) defining the satellite position at time t .

The simplest approach -and valid in most situations- consists in using polynomials (Raggam, 1990; Roth, 1990):

$$s = s_0 + s_1 \cdot t + s_2 \cdot t^2 + s_3 \cdot t^3 + \ldots , \quad (2)$$

$$v = \partial s / \partial t = s_1 + 2 \cdot s_2 \cdot t + 3 \cdot s_3 \cdot t^2 + \ldots , \quad (3)$$

$$t = t_f + row \cdot \Delta t , \quad (4)$$

where t_f is the time of the first row in the image and Δt is the time increment between rows.

The main disadvantage of polynomial approach is the great amount of coefficients that must be adjusted on the base of orbital points. Although five points would be enough for a single image, they can be insufficient to model large orbital segments (for instance a complete orbital revolution). So, we have chosen a model based on a more physical and realistic conception of orbital evolution, allowing a reduction in the involved unknown parameters and permitting the calculation of large orbital segments.

The function describing the orbital trajectory is completely defined by the six Eulerian elements: **a** (semi-major axis), **e** (orbital eccentricity), **i** (orbital inclination), Ω (the angle, in the equatorial plane, from some fixed direction to the line of nodes), **w** (the angle from the line of nodes to perigee) and $\mathbf{T_0}$ (the time of passage of the satellite through perigee). It is also common to consider as orbital elements the position and velocity in rectangular Cartesian coordinates at a specified time t_0 in the orbit

$$(s_0 , s_0') = (x_0 , y_0 , z_0 , x_0' , y_0' , z_0') .$$

The transformation from position and velocity coordinates to Eulerian elements is detailed by Light (1980). The use of this algorithm is restricted to computation of elliptical orbits and contains several singularities and associated numerical difficulties at zero eccentricity and zero inclination. In the same reference is reported a non-singular solution for the elliptic two-body problem, where, given the initial position and velocity, the procedure calculates the position and velocity at any subsequent time. Here we summarize this called Herrick's "f and g solution":

$$s_0 = (x_0^2 + y_0^2 + z_0^2)^{1/2} , \quad (5)$$

$$s_0' = (x_0'^2 + y_0'^2 + z_0'^2)^{1/2} , \quad (6)$$

$$d_0 = x_0 \cdot x_0' + y_0 \cdot y_0' + z_0 \cdot z_0' , \quad (7)$$

$$a = 1 / (2/s_0 - s_0'^2 / \mu) , \quad (8)$$

where μ is Earth's-mass times gravitational constant ($G \cdot M_\oplus$).

Kepler's modified equation

$$\frac{\mu^{1/2} \cdot (t - t_0)}{a^{3/2}} = \Phi - (1 - s_0/a) \cdot \sin\Phi + \frac{d_0}{(\mu \cdot a)^{1/2}} (1 - \cos\Phi) \quad (9)$$

must be solved for Φ using Newton's root-solving method.

$$f = 1 - a \cdot (1 - \cos\Phi) / s_0 , \quad (10)$$

$$g = (t - t_0) - a^{3/2} \cdot (\Phi - \sin\Phi) / \mu^{1/2} , \quad (11)$$

$$s = f \cdot s_0 + g \cdot s_0' = (x, y, z) , \quad (12)$$

$$s = (x^2 + y^2 + z^2)^{1/2} , \quad (13)$$

$$f' = (- (\mu \cdot a)^{1/2} / (s \cdot s_0)) \cdot \sin\Phi , \quad (14)$$

$$g' = 1 - (a/s) \cdot (1 - \cos\Phi) , \quad (15)$$

$$s' = f' \cdot s_0 + g' \cdot s_0' = (x', y', z') , \quad (16)$$

The orbital function (1) is solved by using equations (5) to (12), whereas equations (13) to (16) allow velocity calculation. It is important to remark that this solution does not take into account orbital perturbations and that it is not sufficient to consider the position and velocity of the first orbital point (given in the tape auxiliary information) as s_0 and s_0', since minimization of error is desired. This error is actually the difference between the given position and velocity for each point and its estimation calculated from equations (5) to (16). A least-squares adjustment will provide s_0 and s_0'.

As given in the tape, orbital points are not located on a plane, since they belong to a fixed-Earth geocentrical coordinate system. In order to fit them into a plane, a simple rotation of the following type must be applied:

$$\psi = - \pi \cdot t / (12 \cdot 3600) , \quad (17)$$

$$x_r = x \cos\psi + y \sin\psi , \quad (18)$$

$$y_r = -x \sin\psi + y \cos\psi , \quad (19)$$

$$z_r = z , \quad (20)$$

where t is elapsed time related to the first orbital point, ψ is the angle the Earth has rotated in this time and x_r, y_r, z_r are rotated coordinates.

Radargrammetric model

The SAR image geocoding problem may be reduced to find some expressions that, from a given point on Earth, provide us with row and pixel position within

this row (column) in the image. The basic SAR equations are perfectly known and have been extensively discussed (Curlander, 1987; Raggam, 1990; Roth, 1990; Schreir, 1990). These are the Doppler and range equations (see figure 2) :

$$\lambda f_{DC} / 2 = (\mathbf{p}' - \mathbf{s}') \cdot (\mathbf{p} - \mathbf{s}) / |\mathbf{p} - \mathbf{s}| \quad , \qquad (21)$$

$$r_s = |\mathbf{p} - \mathbf{s}| \quad , \qquad (22)$$

where $\mathbf{p}$ and $\mathbf{p}'$ denote the location and velocity of a target point, $\mathbf{s}$ and $\mathbf{s}'$ are the satellite position and velocity, λ is the wavelength of the SAR sensor, f_{DC} is the Doppler centroid frequency and r_s is the slant distance between sensor and target.

In the ERS-1 case, these equations may be simplified since f_{DC} is zero

$$(\mathbf{p}' - \mathbf{s}') \cdot (\mathbf{p} - \mathbf{s}) = 0 \quad , \qquad (23)$$

$$r_s = | \mathbf{p} - \mathbf{s} | \quad . \qquad (24)$$

In the case of a Slant-Range ERS-1 image we have

$$r_s = r_0 + col \cdot pix \quad , \qquad (25)$$

or

$$col = (r_s - r_0) / pix \quad , \qquad (26)$$

where r_0 is the normalization reference range available in the tape header, r_s is the Slant-Range distance, pix is the Slant-Range pixel size and col is the column or pixel position within the row.

In the case of a Ground-Range image, a transformation relating Slant-Range to Ground-Range distance has been applied at ESRIN. This transformation consist actually in a third degree polynomial (Oriol, 1992) as follows:

$$r_g = c_0 + c_1 \cdot r_s + c_2 \cdot r_s^2 + c_3 \cdot r_s^3 \quad , \qquad (27)$$

where c_0, c_1, c_2, c_3 are the polynomial coefficients and r_g is Ground-Range distance.

By means of the associated first and last row image times (t_f , t_l), any row may be easily related to time parameter:

$$t = t_f + (t_l - t_f) \cdot row / total\_rows \quad , \qquad (28)$$

where total_rows gives the number of rows in the image.

Geocoding of ERS-1 images

Two different approaches have been considered in order to rectify SAR images: the first one computes, for every image pixel, the related position of this point on Earth; the second one calculates, for every terrain position, the corresponding point in the original (tape provided) image. An interpolation involving the pixels surrounding this point will provide the pixel value to be placed in the geocoded image.

Each method offers some advantages and disadvantages but, in the general case, the second method is simpler and more effective than the first one. In short, for every pixel in the geocoded image to be formed, we know its coordinates in a certain cartographic projection (x_c , y_c) and the procedure operates as follows:

a) Gets the point height z_c from the DEM.
b) Calculates the geocentrical coordinates $\mathbf{p}$.
c) Computes point velocity $\mathbf{p}'$ due to Earth rotation..
d) Calculates time t that yields satellite position $\mathbf{s}$ and velocity $\mathbf{s}'$ accomplishing Doppler equation (23). For each essayed t, rotates the point coordinates $\mathbf{p}$ by means of (18) and (19).
e) By means of equation (24) obtains the slant distance r_s.
f) If we have a Ground-Range image, applies (27) to obtain r_g = col.
f') If we have a Slant-Range image apply (26) to get col.
g) By using equation (28) obtains the row.

The step (d) requires the application of an iterative algorithm since, among all possible satellite positions (or times), only that one accomplishing the Doppler equation should be selected. Given that the rectification procedure operates in a sequential manner, the iterative algorithm calculates consecutive satellite positions and only a few iterations are needed to reach convergence if we take the previous result as an initial value next time the algorithm is used.

It is recommended the use of a table containing satellite positions and velocities for each image row (or time). This table may be computed using equations (28) and (5) to (16), and avoids hard and repetitive computation for every point.

Unknown parameters adjustment

No GCPs will be required in the geocoding process, if the image is in Slant-Range format and the necessary auxiliary data -orbital points, t_f and t_l- are accurate enough.

When only a Ground-Range image is available, we will need GCPs to calculate the polynomial coefficients (27) that allow the transformation from Slant-Range to Ground-Range. Moreover, it may be necessary to recompute, with more precision, the first and last row times (t_f and t_l). In that case, we will perform a least-

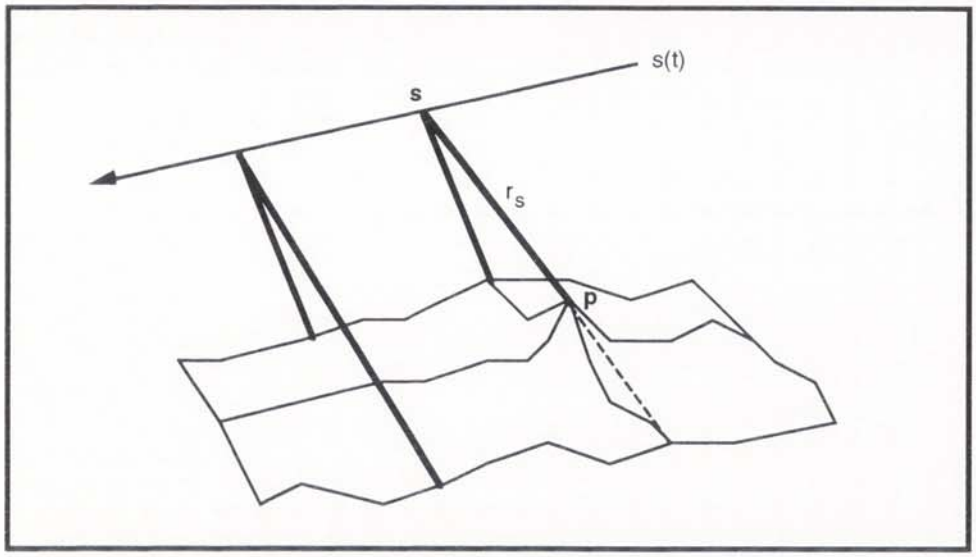

Figure 2: SAR geometry scheme.

squares adjustment of the desired parameters on the basis of GCPs.

Results

To date, we only have had the opportunity to test the developed methodology on one image, covering an area having both flat and very rugged terrain, located around the *Delta de l'Ebre* in South Catalonia.

The image was acquired on August 10, 1991 and it is in Ground-Range format. Its nominal pixel size is 12.5 meters. We decided to adjust the four polynomial coefficients (27) and the first and last row times (t_f, t_l) simultaneously. A 15-meter spaced DEM (RMS=2.5 meters), available for the whole Catalan territory, was used.

The root mean square error (RMS) on 24 test points was

$$RMS_x = 24.75 \text{ meters},$$
$$RMS_y = 26.12 \text{ meters}.$$

An ERS-1 10-meter geocoded image (figure 3) was generated evidencing good overlapping over a geocoded SPOT image.

Future work

In the future we aim to use this methodology to rectify ERS-1 images from the Livingston island in Antarctica. The weather conditions of this area make ERS-1 images an essential tool. In this area, the difficulty of finding GCPs must be specially taken into account when choosing an appropriate format. As we previously mentioned, the desirable format will be that corresponding to SAR.PRI, but in Slant-Range. In case this format were not available, the knowledge of the Slant-Range to Ground-Range transformation coefficients would be desirable.

Furthermore, the ICC has developed the software GeoTeX (Colomina, 1992), oriented to simultaneous adjustment of different kinds of observations. It is planned to integrate the radargrammetric ERS-1 model into this package. This will allow solution of photogrammetric, GPS, LANDSAT, SPOT and ERS-1 observations simultaneously.

References

• **Colomina, I., J.A. Navarro and A. Termens 1992**, GeoTeX: A general point determination system. XVII International Congress of the International Society for Photogrammetry and Remote Sensing, Washington, DC..

• **Corbera, J., 1992**, *El-laboració d'un model orbital de correcció d'imatges SAR - ERS-1.* Master thesis presented at the *Universitat de Barcelona.*

• **Curlander, J.C., R. Kwok and S.S. Pang 1987**, A post-processing system for automated rectification and registration of spaceborne SAR imagery. International Journal of Remote Sensing, 8(4):621-638.

• **Light, D.L. 1980**, Chapter XVII: Satellite Photogrammetry in Manual of Photogrammetry. American Society of Photogrammetry, Falls Church, Virginia.

• **Oriol, E., 1992**. Personal communication. ESRIN, Frascaty, Italy.

• **Raggam, J. 1990**, SAR parameter adjustment and related modules for simulated ERS-1 data. Third International Workshop on Image Rectification of Spaceborne Synthetic Aperture Radar, Farnham Castle, U.K, pp.: 9-14.

• **Roth, A., T. Bayer, G. Shreier and D. Kosmann 1990**, Tuning the D-PAF operational SAR geocoding system for throughput enhancement. Third International Workshop on Image Rectification of Spaceborne Synthetic Aperture Radar, Farnham Castle, U.K, pp.: 87-93.

• **Schreier, G. 1990**, Approach to quality control and long loop quality assessment for SAR geocoded products. Third International Workshop on Image Rectification of Spaceborne Synthetic Aperture Radar, Farnham Castle, U.K, pp.: 115-121.

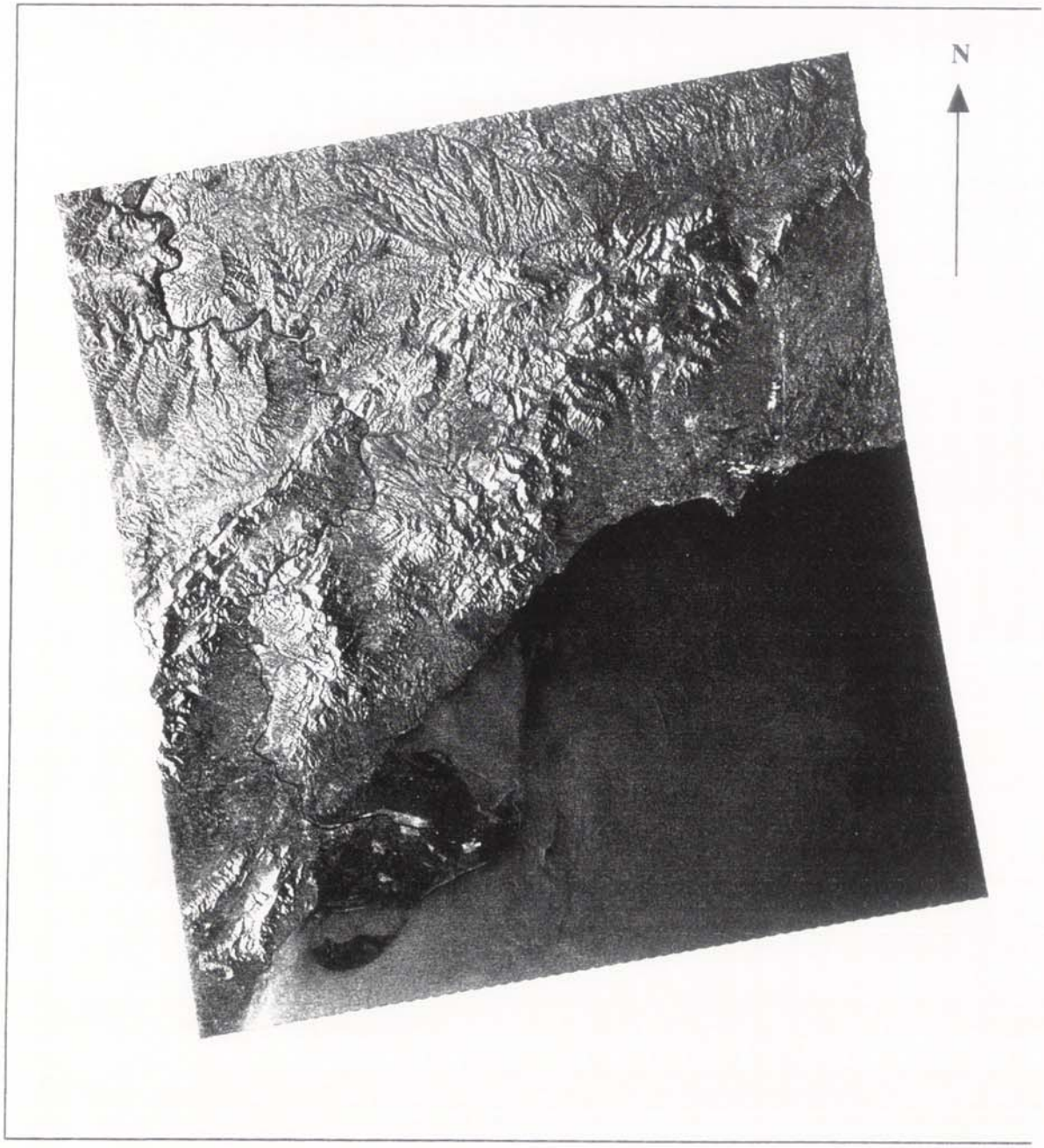

Figure 3: Geocoded image over South Catalonia.

OEEPE-GEOSAR WORKING GROUP
TEST OF ERS-1 DATA

Name: Frédéric PERLANT

Organisation: ISTAR

Date: 17th Septembre 1993

We participate to **Phase 1** on Terrain Geocoding, and we generated also some simple geocoded products to show the influence of the relief on the final geocoded products.

General remarks:

We faced some problems dealing with the data provided for this OEEPE-Geosar test:

- data handling (Single look Slant Range 5 meters resolution in range is not a Standard product).
- we set up a geocoding system compatible with the SPOT products we are generating (10 and 20 meters resolutions). Therefore the products we generated are 10 or 20 meters pixel size.
- we had some difficulties to find out relevant informations in the parameter pool.
- we had some difficulties dealing with the DTM provided as well as control points.

. setting up simply the geometry with the provided GCPs was incompatible with the DTM we were given.

. using Bessel and Gauss-Krueger parameters similar to the one provided, we had to adjust again the parameters and the location of the DTM in order to generate appropriate geocoded product.

- we could not use the Verification points provided with the data pool.
- we had difficulties dealing with the results distributed at the end of June for evaluation, due to the various format used for each results.

SAR image used for geocoding:

The **tsl** image (5m in range and 12.5 meters in azimuth) provided.

Methodology:

The approach is based on a methodology called "Data Geometric Fusion" developped and used at IS-TAR since 1988 for SPOT and aerial imagery and adapted for SAR imagery. It basically consists of a geometric modelling of the sensor acquisition, and of a set of parameters defining each image.

A calibration or adjustement process is used to adjust the particular parameter set according to observations (control or amer points...). This calibration takes into account the uncertainty on the initial parameters defining the image as well as the accuracy of the measured observations (control points).

Geocoding:

We decided to adjust a minimum number of parameters to limit the number of control points required to generate Terrain geocoded product. Actually we are interested in knowing which parameters can be considered as correct and which one have to be adjusted using control points.

In this test we decided to fix the orbit and we adjusted only the Range and the Timing assuming we had a Zero Doppler image.

We first used all the control points provided in file 35597.gcp to adjust the two parameters.

Table 1, 2 and 3 present the different residuals for the 35 control points provided in file 35597.gcp and using the 31 best control points among the 35. Since our adjustement methodology takes into account the accuracy of the control points, we give results for two different sets of parameters qualifying the accuracy on the X,Y precision of the control points on the map (σXY), the precision on the Z (σZ) and the accuracy of the pointing in the image (σxy). For the last results we changed σXY to 5 meters instead of 10. As it is shown the accuracy of the control points influence the final residuals.

Adjusting these two parameters for this set of control points seems to be good enough, given the actual image resolution.

In order to evaluate the robustness of this adjustement (that theoritically needs only one precise control point), we just used 3 control points (for redundancy) to stay within 1.5 pixel for 27 points selected among the 35 control points provided, as can be seen on Table 4 and 5. These table present the residuals in Easting/Northing and Range/Azimuth for the 35 and 27 control points. The residuals are smaller in Azimuth/Northing than in Range/Easting.

		dX (meters) **Easting**				dY(meters) **Northing**			
		moy	eqm	min	max	moy	eqm	min	max
σXY 10 σZ 2 σxy 0.5	35pts	0.54	9.66	-20.78	20.30	-0.14	7.98	-11.84	21.34
	31pts	0.35	8.65	-15.52	18.51	-0.099	5.88	-10.12	11.28
σXY 5	31pts	0.16	4.11	-7.07	9.16	-0.041	3.15	-5.44	6.15

Table 1

		dZ (meters)			
		moy	eqm	min	max
σXY 10 σZ 2 σxy 0.5	35pts	-0.009	0.95	-2.2	1.54
	31pts	-0.006	0.80	-1.66	1.36
σXY 5	31pts	-0.011	1.51	-3.07	2.64

Table 2

		dx (pixel) **Range**				dy(pixel) **Azimuth**			
		moy	eqm	min	max	moy	eqm	min	max
σXY 10 σZ 2 σxy 0.5	35pts	0.0006	0.32	-0.73	0.53	0.0003	0.23	-0.35	0.64
	31pts	0.0003	0.27	-0.56	0.47	0.0000	0.18	-0.31	0.43
σXY 5	31pts	-0.0000	0.51	-1.04	0.91	-0.0003	0.39	-0.68	0.93

Table 3

		dX (meters) **Easting**				dY(meters) **Northing**			
		moy	eqm	min	max	moy	eqm	min	max
σXY 10 σZ 2 σxy 0.5	35pts	–8.9	16.48	-48.9	22.23	6.36	11.43	-10.22	36.57
	27pts	-4.17	11.45	-20.16	17.78	2.64	8.04	-10.22	19.56

Table 4

		dx (pixel) **Range**				dy(pixel) **Azimuth**			
		moy	eqm	min	max	moy	eqm	min	max
σXY 10 σZ 2 σxy 0.5	35pts	-0.73	1.28	-3.43	1.56	0.34	0.83	-0.92	2.60
	27pts	-0.35	0.95	-1.78	1.56	0.13	0.60	-0.92	1.45

Table 5

Resampling:

Bicubic resampling was performed. No special processing was applied to the overlayed regions.

Area geocoded:

We terrain geocode the area that was actually covered by the provided 40 m DTM.

DEM used:

We used the DEM provided for the test, that is to say the 40 meters grid DEM generated from profiles provided by the survey office of Hessen and transferred via an IDL-programm to the 16 bits SUN-raster file.

Extra products:

We also used the ETOPO5 global DTM to define an average height over almost the whole coverage of the ERS-1 image (56km * 64km) and generate simply geocoded product over the area of interest. We also generate a pseudo terrain geocoded product using the ETOPO5 DTM to reduce the errors due to height in the simply geocoded product.

We used these two Geocoded product along with the "true" terrain geocoded product to present the relief influence on the SAR geocoded product over this area by showing the shift xcomputed by correlation between the different image pairs. The results of this analysis show that using ETOPO5 reduce a lot the errors standard deviation in terms of positioning (North, East).

We believe this is an interesting demonstration of the sensitivity of ERS-1 data to relief in order to produce cartographic SAR imagery.

The following tables gather the residuals over the covered image for the two comparisons:

dtmGec-flatGec corresponding to the residuals using a flat dtm for geocoding (similar to GEC ESA products)

dtmGec-ETGec corresponding to the residuals using the ETOP05 height information.

	dX (pixel) **Easting**				dY(pixel) **Northing**			
	moy	eqm	min	max	moy	eqm	min	max
dtmGec - ETGec	-12.82	60.56	-360.0	480.0	-2.04	14.54	-100.0	120.0
dtmGec -flatGec	-48.06	154.5	-520.0	900.0	-11.68	35.66	-100.0	200.0

Table 6

To appreciate the influence of the relief these numbers have to be evaluated according to the height variations in this part of the image shown in the following table:

	dZ (meters)			
	moy	eqm	min	max
dtm - ETOP05	-5.36	26.0	-152.0	209.0
dtm - flat	-20.57	66.78	-223.0	390.0

Table 7

Comments:

As a conclusion, although we were finally able to generate different geocoded products, we found difficult to deal with the different data (parameter pool, DTM, control points, cartography...) provided for this test, and more precisely we had a hard time dealing with some inconsistencies.

The **tsl** data seems to be be a good product for precise geometric processing of ERS SAR AMI data, since is has a good radiometry along with a Slant Range geometry.

DTM Geocoded product

Flat Geocoded product

ETOP05 Geocoded product

GEOMETRIC PROCESSINGS FOR SPACEBORNE SAR IMAGES

Bernard Pikeroen and Issam Tannous
THOMSON-CSF
7, rue des Mathurins
92223 - Bagneux, France

Abstract - In this paper, an unifying approach for geometric processings of multi-sensor remote sensing images is presented. It is based on two fundamental key points. The first is the need of an accurate parametric modelling of the Sensor-Earth system geometry for each sensor under consideration. The second point is what we call the geometric fusion kernel which delivers the best estimate of all the parameters sets associated with each model using external observations (such as ground control points). The correct ground position of the observations can be estimated as well. Three geometric processings, often used in remote sensing applications (geocoding, registration and digital elevation model computation using stereo technique), performed on ERS-1 SAR images, are presented in order to illustrate this approach.

INTRODUCTION

Geometric processings for remote sensing images are essential for cartographic applications such as image geocoding or Digital Elevation Model (DEM) extraction, but also for thematic applications like multisensor images fusion because of the very accurate image registration requirement. In all events, geometric processings are based on transformations that change the coordinates system of the images. That can be represented in a generic way by the transformation :

$$(x, y, z) \xmapsto{\mathcal{T}} (x', y', z')$$

where (x, y, z) are the pixel coordinates in the source referential, (x', y', z') the pixel coordinates in the desirable referential and $\mathcal{T}$ the required transformation.
The common point between all the applications is the use of the image projection function F, which gives the image coordinates of a point from its ground coordinates. Its inverse F^{-1} (noted G and called image location function) is used as well. Generally, these functions relate the point longitude l and latitude φ to its image column and line cooordinates (p, q), knowing its elevation h :

$$(l, \varphi, h) \xmapsto{F} (p, q, h)$$
$$(p, q, h) \xmapsto{G} (l, \varphi, h)$$

The transformation $\mathcal{T}$ is then worked out by compounding functions F and/or G with elementary transformations depending on the application.
Geometric processings pose therefore two problems :

- computation of functions F and G,
- accuracy of functions F and G.

F or G are delivered by accurate modelling of the imaging system geometry. The accuracy of these functions depends therefore on the imaging system parameters accuracy. This accuracy (called initial accuracy) is often insufficient for most applications. Under some conditions, the accuracy of F and G can be improved by taking into account external measurements such as tie-points (ground control points between an image and a map (p, q, l, φ, h) and/or homologous points between two images (p_1, q_1, p_2, q_2) or (p_1, q_1, p_2, q_2, h)) through optimization techniques.
In this paper, we give a general description (in a multisensor sense) of the geometric modelling which delivers functions F and G. The optimization of functions F and G using external informations are then presented following the multisensor concept we call "geometric fusion kernel" (the "fusion" term is employed because this geometric kernel is able to manage multisensor modelling). Three major geometric processings for remote sensing images based on this unifying approach and applied to ERS-1 SAR images are then presented. They are :

- image geocoding,
- image registration,
- DEM extraction using stereo technique.

GEOMETRIC MODELLING

Geometric modelling intends to deliver the basic functions F and G used to build transformation $\mathcal{T}$ for geometric processings.

PRINCIPLES OF GEOMETRIC MODELLING

F or G are worked out by solving a set of equations describing the Sensor-Earth system geometry. Generally, the physical properties of the imaging geometry are such that the modelling is parametric. Then F and G depend on a set of parameters Θ, which can be seen as the state vector of the imaging system. The shape of F and G defines the imaging model. For one image, Θ is a set of numerical values. The accuracy of the geometric processings depends on the knowledge of F or G, and Θ. Schematically, the knowledge of F or G is connected to the knowledge of the Sensor-Earth system. It is a modelling problem. The knowledge of Θ depends on the accuracy of the imaging ancillary data measurements for a given image. These measurements are an a priori information provided to the geometric modelling. Another informations sources are generally available : they are the tie-points measurements. The geometric modelling of the Sensor-Earth system simply ensures the optimal taking into account of these external informations sources. The best estimate of both the parameters vector Θ and the tie-points ground positions is computed from all the available a priori informations, and from the modelling constraint. We can show that the final error comes from :

- an error on the estimation of the parameters vector (depending respectively on the a priori parameters measurements accuracy and the tie-points accuracy),
- an error on the imaging system model itself (error on F and G).

So, the first condition to ensure is a minimal modelling error.

SENSOR-EARTH SYSTEM MODELLING

The Sensor-Earth system geometric modelling is generally divided into four segments :

- the spacecraft trajectory modelling (i.e. orbit modelling),
- the spacecraft attitude modelling,
- the instrument modelling (including processing in the SAR case) which gives the imaging model equations,
- an Earth model.

This general decomposition is essential for multisensor images analysis systems because it allows the possible use of the same sub-model for two different sensor (for exemple, SPOT and ERS-1 orbit model is identical). In the SAR case, the attitude model has not to be considered because of the synthetic aperture processing (raw data azimuth processing).
Each of these sub-models provides a sub-set of parameters the union of which gives the parameters vector Θ.

INITIAL VALUES OF THE PARAMETERS AND ERRORS

Initial values of the parameters - There are two classes of parameters :

- "system" parameters, highly connected to the sensor definition. Their values are generally constant for one image to another and are known with a high accuracy (for exemple, the wavelength of the emitted signal in the SAR case),
- variable parameters, connected to one image, which are a priori known with poor accuracy (called unknown parameters).

Only these last parameters form the vector Θ, and must be estimated. An initial value of this vector is computed from the ancillary data associated to the image under consideration, either directly from these data (for exemple the near range in the SAR case) or indirectly from a set of measurements using a known function relating them to Θ (for exemple, the orbit parameters are computed from a set of ephemeris data). This initial value allows an a priori location of the image which accuracy is related to the errors on the parameters values.

Errors on the parameters values - The inherent goal of the modelling approach is the optimal decrease of location errors for a given amount of informations. Inversely, that allows to reduce the required amount of external information (tie-points) in order to reach a desirable error (for exemple registration of two images with an accuracy better than the pixel size).
With this aim in view, one of the important points of the modelling is its ability to deal with an initial error model, to propagate it, and to predict the final errors. In other words, any measurement must be associated with an error to have a meaning with this approach. This error is often represented by a variance. The error value is as fundamental as the initial value. Considering an error as unknown is equivalent to attache no confidence to the associated parameter measurement (for exemple a tie-point with no error measurement has a minimum weight in the modelling). A zero variance for a parameter allows to consider it as very well known and ensures that it induces no location error. That allows to reduce the modelling number of parameters (only the unknown parameters form Θ), leading to very robust models with very few parameters (for exemple, the SPOT model and the ERS-1 model have respectively only 8 and 7 parameters).

GEOMETRIC FUSION KERNEL

The aim of the geometric fusion kernel is to deliver the best estimate of the model parameters vector Θ in order to improve accuracy of function F and G, using the following inputs :

- initial value of vector Θ and associated errors,
- tie-points measurements and associated errors.

The best estimate of the tie-points ground positions can be delivered as well (because tie-points are themselves measurements associated with an error). Including tie-points as unknowns in the estimation process allows to compensate for false points so that the parameter estimation is more accurate.
Assume N images of a scene (acquired by different sensors). Assume P tie-points. Let $\overline{M}_i$ be the ground measurement of tie-point i with error ε_{M_i}, and let $\overline{P}_{ik}$ be its measurement on image k with error $\varepsilon_{P_{ik}}$. The problem is to work out the values of Θ and M_i (the actual ground position of tie-points i) that minimize the difference between $\overline{P}_{ik}$ and $F_{\Theta_k}(M_i)$ (called projection residual) for all i and k, with F_{Θ_k} being the parametric projection function of image k. The initial solution for Θ_k is its initial value, noted $\overline{\Theta}_k$, and characterized by the error ε_{Θ_k}.
Assuming all errors being gaussian with zero mean and standart deviation σ, this problem can be solved using a bayesian approach [1]. This formulation leads to minimize the sum of two terms :

$$J = J_1 + J_2 \qquad (1)$$

where J_1 and J_2 are respectively called the total projection residual and the total rigidity residual. J_1 is given by :

$$J_1 = \sum_{i=1}^{P}\sum_{k=1}^{N}(\overline{P}_{ik} - F_{\Theta_k}(M_i))^t \Gamma_{ik}^{-1}(\overline{P}_{ik} - F_{\Theta_k}(M_i)) \qquad (2)$$

where ^{t} symbol denotes transposition operation. Γ_{ik} is the covariance matrix of tie-point i measurement error on image k. Assuming components of P_{ik} are independant, this matrix is diagonal and is given by

$$\Gamma_{ik} = \left[(\sigma_{P_{ik}})^2\right]. \qquad (3)$$

J_2 is given by :

$$J_2 = \sum_{k=1}^{N}(\Theta_k - \overline{\Theta}_k)^t \Lambda_{\Theta_k}^{-1}(\Theta_k - \overline{\Theta}_k) + \qquad (4)$$

$$\sum_{i=1}^{P}(M_i - \overline{M}_i)^t \Lambda_{M_i}^{-1}(M_i - \overline{M}_i) \qquad (5)$$

where Λ_{Θ_k} is the covariance matrix of errors vector on Θ_k, and Λ_{M_i} the covariance matrix of the errors on $\overline{M}_i$ components. Assuming the parameters are independant Λ_{Θ_k} is a diagonal matrix given by :

$$\Lambda_{\Theta_k} = \left[(\sigma_{\Theta_k})^2\right]. \qquad (6)$$

Assuming the components of M_i are independant, Λ_{M_i} is a diagonal matrix given by :

$$\Lambda_{M_i} = \left[(\sigma_{M_i})^2\right] \quad (7)$$

This minimization problem is an optimization problem and is equivalent to a non-linear least square problem solved by any suitable technique (Gradient, Newton, Kalman filtering).

The outputs of the optimization is the optimal estimated parameters vector $\widehat{\Theta}_k$ for all k, the optimal estimated ground position $\widehat{M}_i$ of tie-points i, and the final covariance matrices of errors on respectively the parameters and the tie-points.

These final covariance matrices give the estimation accuracy and allow to assess the accuracy of functions F and G, so consequently the accuracy of further geometric processings. For exemple, the location error of image k is characterized by the covariance matrix given by :

$$\left[\frac{\partial G_{\Theta_k}}{\partial \Theta_k}\right] \Lambda_{\Theta_k} \left[\frac{\partial G_{\Theta_k}}{\partial \Theta_k}\right]^t \quad (8)$$

APPLICATIONS TO ERS-1 SAR IMAGES

In this section, we give three exemples of geometric processings using ERS-1 SAR images. But first of all, the modelling that delivers functions F and G for spaceborne SAR sensors is presented.

ERS-1 SAR GEOMETRIC MODELLING

Let $\mathcal{R}_B = (O, e_x, e_y, e_z)$ be the referential centered at the center of the Earth and rotating with the Earth, where (O, e_x, e_y) is the equatorial plane and (O, e_z) axe is pointed toward the North pole.

Instrument modelling and imaging equations - The equations of the SAR imaging model are the so called range and Doppler equations given in $\mathcal{R}_B$ by [2] :

$$r^2 = (X - X_S(t))^2 + (Y - Y_S(t))^2 + (Z - Z_S(t))^2 \quad (9)$$

$$\frac{\lambda r f_D}{2} = (X - X_S(t))V_{X_S}(t) + (Y - Y_S(t))V_{Y_S}(t) + (Z - Z_S(t))V_{Z_S}(t) \quad (10)$$

where (X, Y, Z) are the imaging point coordinates, $(X_S(t), Y_S(t), Z_S(t))$ the SAR position, $(V_{X_S}(t), V_{Y_S}(t), V_{Z_S}(t))$ the SAR velocity, t the time, r the SAR-point range, f_D the Doppler centroid used in raw data azimuth processing, and λ the radar wavelength.

The SAR data collection process allows to compute t and r from the pixel position in the image. t is computed from the azimuth pixel position p using $t = kp + t_0$ where t_0 is a reference time given in the ancillary data (for exemple, center image time) and k the azimuth time pixel size. k is got from the pulse repetition frequency F_r and the number of azimuth looks N using $k = N/F_r$. r is computed from the range pixel position q using $r = \mu q + r_0$ where r_0 is a reference range given in the ancillary data (for exemple near range) and μ the range pixel size. μ is got from the sampling frequency F_s using $\mu = c/2F_s$ where c is the light speed.

The Doppler centroid f_D could be a function of range and/or azimuth pixel position. It is equivalent to the so called skew angle (function of the spacecraft attitude angles) [3]. However, using the same Doppler centroid as used for azimuth processing does not necessarily correspond to the actual skew angle (case of non-zero f_D estimation error during azimuth processing) but allows to deal with the correct point which has been processed [4][5].

Trajectory modelling - The spacecraft trajectory modelling allows to compute the spacecraft position and velocity for all time t.

This modelling is sensor dependent. In ERS-1 case [6], which is of interest in this paper, the trajectory is a perturbed keplerian orbit characterized by 6 time varying osculatory parameters (same type than SPOT's orbit). We can show that in this case the spacecraft motion on a small orbit arc (about 2000 km) can be modelled with a very high accuracy (of the order of centimeter) by a Taylor series expansion of the osculatory parameters at a low order [7]. In fact, only the following 4 osculatory parameters are enough to compute the position and the velocity of the spacecraft [7] :

- ρ, range from center of Earth to spacecraft. Its expansion order is 3 : $\rho(t) = \rho_0 + \rho_1 t + \rho_2 t^2 + \rho_3 t^3$
- W, spacecraft argument. Its expansion order is 3 : $W(t) = W_0 + W_1 t + W_2 t^2 + W_3 t^3$,
- Ω, longitude of ascending node. Its expansion order is 1 : $\Omega(t) = \Omega_0 + \Omega_1 t$
- I, orbit inclination. Its expansion order is 1 : $I(t) = I_0 + I_1 t$

The coefficients of the previous series expansions are the orbit parameters. Their initial values are computed from a set of ephemeris data ($X_S(t_i)$, $Y_S(t_i)$, $Z_S(t_i)$, $V_{X_S}(t_i)$, $V_{Y_S}(t_i)$, $V_{Z_S}(t_i)$), $i = 1, .., n$, given in the ancillary data, as follow. The set of values $(\rho(t_i), W(t_i), \Omega(t_i), I(t_i))$, $i = 1, ..., n$, is computed from the ephemeris data using a known transformation T [4][5]. The orbit parameters are then worked out by a least square fit using the 4 previous series expansion. Once that has been done, position and velocity of the spacecraft can be computed for any time t (any azimuth pixel position p) using the series expansions and the transformation T^{-1}.

ERS-1 SAR location and projection functions - The ERS-1 SAR location function G is immediatly got by solving equations (9) and (10) for X,Y and Z with the constraint that the point belongs to the Earth surface modelled by an ellipsoid as given by :

$$\frac{X^2 + Y^2}{(A + h)^2} + \frac{Z^2}{(B + h)^2} = 1 \quad (11)$$

where A and B are respectively the semi-major and the semi-minor axe of the reference ellipsoid, and h the elevation of the point above the reference ellipsoid (the actual elevation is then computed given the geoid model with respect to the ellipsoid). The geographic coordinates (l, φ) are then got from (X, Y, Z) by known transformations [4]. The projection function F is got by inverting G using a numerical technique.

The parameters of the ERS-1 SAR model are then $\{r_0, t_0, \mu, k, f_D, \lambda\}$ (common to any SAR system) plus the orbit model parameters $\{\rho_i, W_i, \Omega_i, I_i\}$ (specific to ERS-1). The location error caused by the error on each parameter (error budget) is computed in order to build the parameters vector to be estimated in the geometric fusion kernel (the unknown parameters). This vector depends on the sensor under consideration. In the ERS-1 case, the system specifications [6] allow to consider only the following parameters vector (all other parameters are set as constant) [4] :

$$\{\rho_0, \rho_1, W_0, W_1, \Omega_0, r_0, f_D\}.$$

f_D is considered as unknown, not for estimation error during azimuth processing, but for inherent error in the received azimuth signal phase and for azimuth timing errors [4][5].

TEST OF GEOSAR ERS-1 SAR DATA

The OEEPE-GeoSAR test data had been used along with the previous ERS-1 SAR geometric model in the geometric fusion kernel. The ancillary data allow to compute the initial value of the model parameters (The initial value of the orbit parameters had been computed from the trajectory coefficients delivered in File 35597_dmp — and no, as required, from File orbit_37231 which contains the ephemeris data of the preliminary orbit because of the lack of its format description —. It seems that the trajectory coefficients used had been already adjusted). The parameters optimization had been performed using the 35 available tie-points. The statistics of the residues on the 35 tie-points are presented in Table 1 and 2. They are given in ground coordinates (East-Noth) and in image coordinates (Range-Azimuth), before and after optimization. Table 1 presents the results without optimizing the position of the 35 tie-points while Table 2 gives the results when the tie-points positions are estimated along with the model parameters (in order to compensate for the tie-points measurement errors). These results show that it is essential to adjust the tie-points position when the measurement errors are significant. Final assessment of the result must be performed using accurate control points (such as GPS points).

Residue in Ground Coordinates (meters)				
	Mean East	Mean North	Stand. Dev. East	Stand. Dev. North
Before Opt.	-81.62	14.10	14.28	26.35
After Opt.	-0.38	1.64	12.04	10.84

Residue in Image Coordinates (pixels)				
	Mean Range	Mean Azimuth	Stand. Dev. Range	Stand. Dev. Azimuth
Before Opt.	-6.29	-1.17	1.07	2.20
After Opt.	0.01	0.13	0.99	0.82

Table 1: Statistics on residues without optimizing tie-points positions

Residue in Ground Coordinates (meters)				
	Mean East	Mean North	Stand. Dev. East	Stand. Dev. North
Before Opt.	-81.62	14.10	14.28	26.35
After Opt.	-0.02	0.09	1.58	0.50

Residue in Image Coordinates (pixels)				
	Mean Range	Mean Azimuth	Stand. Dev. Range	Stand. Dev. Azimuth
Before Opt.	-6.29	-1.17	1.07	2.20
After Opt.	0.00	0.00	0.12	0.02

Table 2: Statistics on residues with optimization of tie-points positions

GEOMETRIC PROCESSINGS

Once the geometric model parameters are optimally estimated (like in the previous exemple), function F and G can be used to perform geometric processings (or rectifications) of the associated images.

Image geocoding - Image geocoding consists of transforming a source image in a cartographic representation (UTM projection, stereographic projection, ...). In this case, transformation T is given by $T_c \circ G$ where T_c is the required cartographic projection and $\circ$ the compound operation :

$$(p, q, h) \xmapsto{G} (l, \varphi, h) \xmapsto{T_c} (x, y, h)$$

A DEM is required as input to get the point elevation. In practice, the inverse transform is used. We compute for every point (x, y, h) on the DEM the image position (p, q). The DEM point grey level is then computed by interpolation in a neighbourhood of (p, q). That had been applied on the OEEPE-GeoSAR ERS-1 SAR test image (©ESA). The accuracy of the geocoded image is given in Table 2 (further assessment must be performed using accurate control points). Figure 1 shows a perspective view of a portion of the computed geocoded image over the DEM of the area (Frankfurt airport area).

Image registration - In the case of two images, the registration of image 2 and image 1 involves the following transformation :

$$(p_2, q_2, h) \xmapsto{G_2} (l, \varphi, h) \xmapsto{P_1} (p_1, q_1, h)$$

A DEM is required as input to get the point elevation. That has been applied to register an ERS-1 SAR SLC detected image (©ESA) and a SPOT image (©SPOT-IMAGE) using 16 tie-points. The registration accuracy is better than both images pixel size. On Figure 2, two registered areas extract from both images are superimposed on a map (Strasbourg-Eintzheim airport area).

Stereo DEM computation - If two images of a non-constant elevation scene are registered without knowledge of the elevation (using the optimized geometric models), the residual registration errors come from the error on the elevation used as input and is usually called parallax. The scene elevation can then be computed provided the parallax can be measured. This elevation restoration technique is called stereo.
Generally, the parallax is computed for all pixel by correlating both images. This correlation process becomes very heavy for large images. In order to reduce the correlation cost, the epipolarity concept is introduced [7]. The epipolar direction for a couple of images is equal to the direction of the relative relief effect of the images (provided the epipolar curves exist). It is given in the cartographic referential $\mathcal{R}_c$ by :

$$\mathcal{E}(h) = \frac{\partial (T_c \circ (G_1 - G_2))}{\partial h} = \frac{\partial R(h)}{\partial h} \qquad (12)$$

where G_i is the location function of image i, T_c is the cartographic projection and R the parallax vector. In order to compute the parallax, the correlation process can be constraint to search for homologous points along the epipolar curves. In addition, if the epipolar curves are locally straight lines (on a significant length), both images can be resampled such that the epipolar curves become the lines of the new images. The search for homologous points are then naturally performed line by line (1-D correlation) im-

proving the correlation cost by a large amount. The transformation applied for each image is :

$$(p_i, q_i, h_0) \xmapsto{G_i} (l, \varphi, h_0) \xmapsto{T_c} (x_i, y_i, h_0) \xmapsto{T_e} (x_{ei}, y_{ei}, h_0)$$

where h_0 is a reference altitude and T_e is simply a rotation transformation in order to represent the source image in the epipolar referential $\mathcal{R}_e$. $\mathcal{R}_e$ is got by rotating $\mathcal{R}_c$ around the z axe by the angle $\chi = \arctan(\mathcal{E}_y(h_0)/\mathcal{E}_x(h_0))$. The new images are then correlated line by line in order to get the parallax value in $\mathcal{R}_e$ for each pixel (in $\mathcal{R}_e$, only the first component of R, say R_u, is non-zero). Given the actual elevation h for a point, we must have $R_u(h) = 0$. Expanding $R_u(h)$ in Taylor series about h_0 and neglecting terms of order higher than 1 [4] allow to compute the point elevation h :

$$h = h_0 - \frac{R_u(h_0)}{||\mathcal{E}(h_0)||} \qquad (13)$$

where $R_u(h_0)$ is the paraliax got by correlation.
This technique had been applied on a couple of ERS-1 SAR SLC detected images (©ESA) over the Aix-En-Provence area (in [4], existence of epipolar curves for a couple of ERS-1 SAR images had been proved and interval on which they can be considered as straight lines had been computed). 9 tie-points have been used in order to estimate the parameters vector of each image. The resulting accuracy of line correspondance of the epipolar images is about 0.5 pixel. Figure 3(a) shows the two source images resampled in $\mathcal{R}_e$, and Figure 3(b) shows the computed DEM in $\mathcal{R}_c$ (without any further smoothing processing). Considering the baseline between the two orbit paths (about 50 km), the altimetric accuracy of the DEM is not better than 40 meters.

CONCLUSION

In this paper an unifying approach for geometric processings of remote sensing images had been introduced. Production of geocoded images, registered images, and DEM by stereo technique, using ERS-1 SAR images, had been then presented as application of this concept. Of course, production of DEM using interferometry technique can be easily embedded in this approach.
The geometric fusion kernel presented in this paper coupled to a geographic information system can be the heart of an operational multisensor fusion and geographic system. With the multiplicity of remote sensing data available in the near future, such a system should become highly recommended.

REFERENCES

[1] J.M. Mendel, *Discrete Techniques of Parameter Estimation*, New York : Marcel Dekker Inc., 1973.

[2] J.C. Curlander, "Location of Spaceborne SAR Imagery", *IEEE Trans. Geosc. Rem. Sens.* Vol. 20(3), pp. 359-364, July 1982.

[3] F.W. Leberl, *Radargrammetric Image Processing*, Norwood : Artech House Inc., 1990.

[4] I. Tannous, *Modélisation paramétrique de la géométrie de prise de vue du radar à ouverture synthétique embarqué sur satellite. Application à la superposition radar/optique*, Thèse de Doctorat, Univ. Paris 7, 1991.

[5] I. Tannous and B. Pikeroen, "Parametric Modeling of Spaceborne SAR image Geometry", *Phot. Eng. and Rem. Sens.*, in press.

[6] ERS-1 System & Mission, *ERS-1 Programme. ERS-1 Satellite to Ground Segment Interface Specification*, Technical Report ER-IS-ESA-GS-0001, February 1191.

[7] H. Guichard, *Géométrie des images de satellite à défilement et application à la photogrammétrie spatiale*, Technical Report, SPOT IMAGE, 1986.

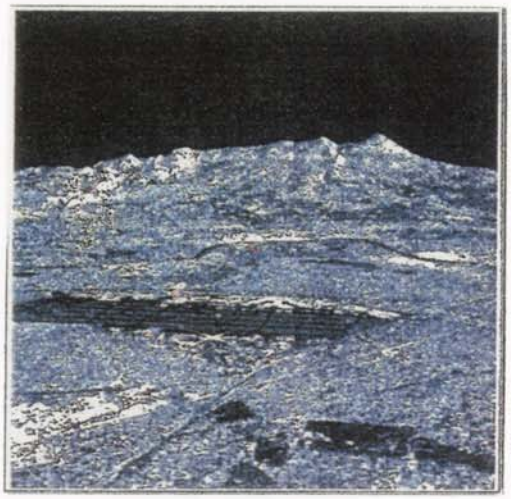

Figure 1 : Perspective view of the geocoded ERS-1 SAR image using the DEM.

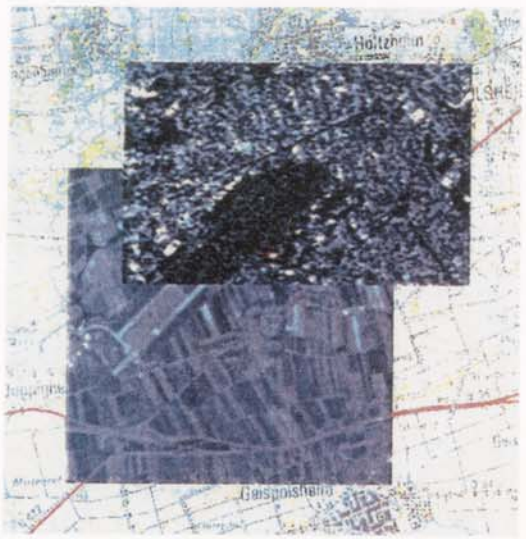

Figure 2 : Registration of an ERS-1 SAR image, a SPOT image and a map.

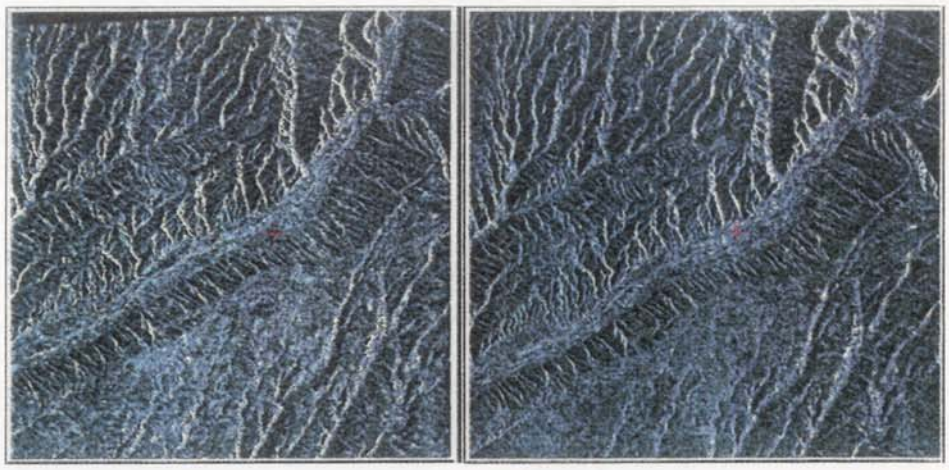

Figure 3(a) : Couple of ERS-1 SAR images resampled in the epipolar referential (line-to-line correspondence).

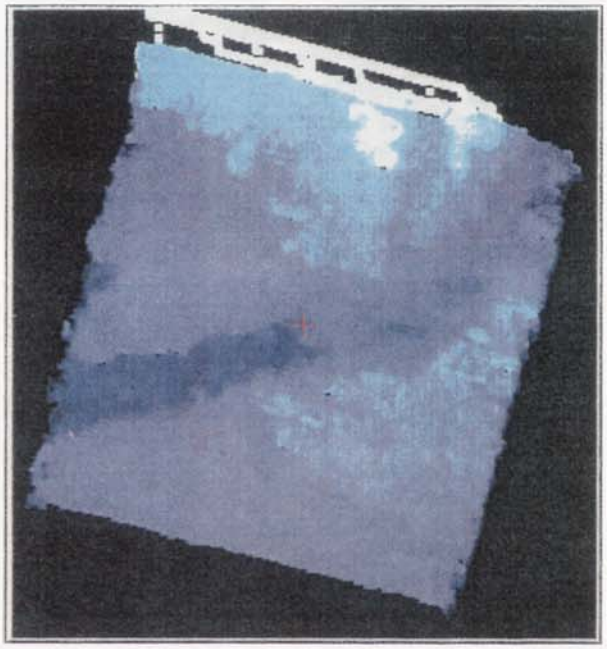

Figure 3(b) : Extracted DEM in a cartographic projection (without any smoothing processing).

GTC OF FRANKFURT AREA

(Geometrical residuals values):

GCP	E_{image} (UTM)	E_{image} (GK)	E_{map} (GK)	E_m-E_i (GK	N_{image} (UTM)	N_{image} (GK)	N_{map} (GK)	N_m-N_i (GK)
1	461908.0	3461967.2	3462000.0	32.8	5541893.5	5543676.8	5543675.0	-1.88
2	456195.5	3456252.4	3456250.0	-2.4	5544956.0	5546740.5	5546750.0	9.5
3	465858.0	3465918.7	3465930.0	11.3	5547106.0	5548891.5	5548900.0	8.5
4	467570.5	3467631.9	3467620.0	-11.	5541918.5	5543702.0	5543700.0	-2.0
5	472170.5	3472233.7	3472230.0	-3.7	5546043.5	5547828.7	5547850.0	21.3
6	471033.0	3471095.8	3471100.0	4.2	5539481.0	5541263.5	5541300.0	36.5
7	469508.0	3469570.1	3469600.0	29.9	5548931.0	5550717.3	5550700.0	-17.3
8	472645.5	3472708.8	3472700.0	-8.8	5548531.0	5550317.2	5550320.0	2.8
9	458620.5	3458678.4	3458670.0	-8.4	5539293.5	5541075.8	5541100.0	24.2
10	466720.5	3466781.5	3466780.0	-1.5	5548681.0	5550467.1	5550475.0	7.9
11	464295.5	3464355.6	3464380.0	24.4	5543568.5	5545352.6	5545350.0	-2.6
12	472595.5	3472658.9	3472650.0	-8.9	5542018.5	5543802.1	5543800.0	-2.1
13	453095.5	3453151.2	3453110.0	-41.	5538793.5	5540575.5	5540600.0	24.5
14	470620.5	3470683.0	3470700.0	17.0	5548518.5	5550304.6	5550310.0	5.4
15	463070.5	3463130.1	3463100.0	-30.	5543556.0	5545340.0	5545350.0	10.0
16	462395.5	3462454.9	3462450.0	-4.9	5543193.5	5544977.4	5545000.0	22.6
17	462120.5	3462179.8	3462200.0	20.2	5542481.0	5544264.6	5544250.0	-14.6
18	461708.0	3461767.2	3461800.0	32.8	5541393.5	5543176.7	5543180.0	3.3
19	470833.0	3470895.7	3470900.0	4.3	5540731.0	5542514.0	5542550.0	36.0
20	470320.5	3470383.0	3470420.0	37.0	5543393.5	5545177.6	5545190.0	12.4
21	460558.0	3460616.6	3460600.0	-16.	5542381.0	5544164.5	5544200.0	35.5
22	465208.0	3465268.3	3465270.0	1.7	5553568.5	5555356.5	5555350.0	-6.5
23	471533.0	3471596.0	3471600.0	-4.0	5542243.5	5544027.2	5544050.0	22.8
24	466520.5	3466581.5	3466575.0	-6.5	5541943.5	5543727.0	5543750.0	23.0
25	475720.5	3475785.2	3475775.0	-10.	5540993.5	5542776.7	5542790.0	13.3
26	476045.5	3476110.3	3476100.0	-10.	5544156.0	5545940.5	5545965.0	24.5
27	475583.0	3475647.6	3475640.0	-7.6	5541906.0	5543689.6	5543670.0	-19.6
28	464370.5	3464430.6	3464425.0	-5.6	5547468.5	5549254.1	5549250.0	-4.1
29	462495.5	3462554.9	3462550.0	-4.9	5541693.5	5543476.8	5543500.0	23.2
30	465883.0	3465943.6	3465940.0	-3.6	5551118.5	5552905.6	5552925.0	19.4

STATISTICAL GEOMETRICAL RESULTS OF THE FRANKFURT GTC PRODUCT

	EAST	NORTH
MIN	**-2.5 m.**	**-2.0 m.**
MAX	**37.0 m.**	**36.5 m.**
AVG	**1.083 m.**	**10.567 m.**
RMS	**17.857 m.**	**18.521 m.**
ST. DEV.	**11.810 m.**	**10.665 m.**

Appendix 2.8

THE OEEPE/GEOSAR ERS-1 SAR GEOCODING EXPERIMENT — WORK AT UCL

M. Upton[1], J. E. Laycock[2] and I. J. Dowman[1]

[1] University College London, Gower Street, London, WC1E 6BT, United Kingdom.
Tel. 44 71 380 7050 x.2747. Fax. 44 71 380 0453.
[2] Space and Defence Research Laboratory, GEC-Marconi Research Centre,
West Hanningfield Road, Great Baddow, Chelmsford, Essex, CM2 8HN, United Kingdom.
Tel. 44 245 473331 x.3665. Fax. 44 245 475244.

ABSTRACT

University College London have participated in the OEEPE/GEOSAR ERS-1 SAR geocoding experiment using a geocoding demonstrator system developed for the Defence Research Agency by a consortium led by GEC-Marconi Research Centre. The objective of the experiment is to geocode an ERS-1 SAR image included as part of a standard data set. The resulting products are to form part of a comparitive test alongside other geocoding systems.

The standard data set supplied to participants has been processed and the results validated. The products include the geocoded image, and shadow, layover and energy conservation maps. Problems were encountered along the way, mainly to do with the documentation for the data set, and the large amount of preprocessing the data required before presentation to the geocoder. Tiepointing had to be performed in a context outside of the geocoding system, and the validation tiepoints could not be used.

The RMS tiepoint residuals converted to map space were approximately 120 metres uncorrected, and 10 metres corrected. The shadow map was blank, which is shown to be correct. By comparison with the images, the content of the layover maps appeared reasonable, and the spatial accuracy of the geocoding was shown to be good. The content of the energy conservation maps appeared reasonable, but could not be checked properly.

It is argued that the image space layover map is more useful for validation than the one in map space. The addition of an incidence angle map to the set of products is stated to be desirable.

Keywords: ERS-1, SAR, Geocode, OEEPE/GEOSAR.

1. INTRODUCTION

The OEEPE/GEOSAR ERS-1 SAR geocoding experiment is a comparitive test of the various SAR geocoding systems that have been developed for use with ERS-1 data, organized by OEEPE and the GEOSAR working group. As input to this experiment, DLR have produced a standard data set that includes an ERS-1 SAR image, and the auxiliary data necessary to terrain geocode it. Each geocoding system participating in the experiment uses this same data set as input, thus permitting meaningful comparison of their various products.

The first stage in the experiment is for each geocoding system to generate the geocoded image corresponding to the input data in the standard data set. The geocoded image should then be validated by whatever means are provided by the geocoding system. The next stage is for mapping centres to evaluate the accuracy and content of the geocoded images, and to use them to produce and revise topographic maps.

MRC (GEC-Marconi Research Centre) led a consortium which built a geocoding demonstrator system for producing terrain corrected geocoded ERS-1 SAR images. The system was developed as an experimental geocoding facility for the Defence Research Agency, Farnborough. The consortium included Earth Observation Sciences and UCL (University College London).

At UCL, this geocoding demonstrator has been applied to the standard data set, producing a geocoded image, and ancillary products. Some validation of the results has been performed. This paper reports upon this work in more detail, and presents the results.

2. THE GEOCODING SYSTEM

The primary function of the system is to produce terrain corrected geocoded images. In order to aid image interpretation, bitmaps indicating areas affected by layover and shadow can be generated, as well as an energy conservation map that records the change in image energy due to geocoding. Prior to geocoding, the system can generate an error budget predicting the accuracy of the geocoded image based upon the accuracy of the input data, such as the available orbit data. If appropriate, the user can then select the manual tiepointing option. This causes the geometric transformation function from map to image space to be modified so that the tiepointing residuals are minimized. In parallel to the geocoding system, MRC developed a validation and visualization system comprising a set of tools, implemented in AVS (Application Visualization System), for analysing and visualizing geocoded images and related data sets.

The project was split into three development phases. Phase 2, which ended in July 1992 resulted in an interim geocoding system, excluding the complete tiepointing implementation, with a very basic user interface, and with only nearest neighbour or linear resampling kernels usable. Phase 3 of the project, with the above functionality fully implemented, was completed in July 1993. The OEEPE/GEOSAR experiment was therefore conducted using the interim Phase 2 system, which made input data preparation and tiepoint correction more difficult.

3. INPUT DATA

The standard data set supplied by DLR covers the Frankfurt am Main area. Two topographic maps of the test area are provided: one at 1:200,000 for approximately the whole area, another at 1:50,000 for a smaller area that includes West Frankfurt. The 1:50,000 map has Gauß-Krüger coordinates marked. A DEM approximately coinciding with this map is provided. This DEM is on a grid in the Gauß-Krüger projection and is 32km × 28km in size, with a grid spacing of 40m. Heights are in the range 78m to 781m, in units of 1m, and the maximum height difference between adjacent samples is 35m. Near the centre of this DEM, there is a strange linear height discontinuity. Also provided is the ETOPO5 global elevation model.

The orbit provided is the preliminary orbit, giving position and velocity in CIS (Conventional Inertial reference System) every 2 minutes for 7 days. Time is given in TDT (Terrestrial Dynamic Time).

Tiepoints for adjustment are given in DLR's GCP file. For each tiepoint, the scene and image coordinates are given. Scene coordinates are given in ECR (Earth Centre Rotated). There are 35 points for adjustment, 7 of which lie in the area covered by the 40m DEM. Tiepoints for validation are given in DLR's VQC file.

The image provided is DLR's TSD product. This is a slant range precision image. It is 8207 × 8000 pixels in size, with each value represented in 15 bits.

The remaining parameters are given in a dump of DLR's parameter pool for the processing at DLR of this data set, along with the supplied documentation.

4. PREPROCESSING OF INPUT DATA

DLR processed the input data to produce a geocoded image in the projection UTM zone 32 using the datum WGS84. The input data supplied by DLR fits naturally into this process. Our geocoding demonstrator, unlike the fully developed system, has no support for datum shifts, and only supports a limited number of ellipsoids and projections. In particular, although UTM is supported, it is not possible to specify the WGS84 ellipsoid. The most reasonable alternative to WGS84 for UTM in Europe is to use the datum ED50, whose ellipsoid (International) is supported by the demonstrator. The lack of support for datum shifts means that all input data must be shifted to this datum [6,7] before presentation to the geocoder.

The DEM used was the 40m one; ETOPO5 was not used. The projection that this DEM is presented in is not supported by the geocoding demonstrator. This, together with the need to shift to ED50, led to the decision to preprocess the DEM to the same datum and projection as that of the geocoded image. This was accomplished by projecting each individual point in the DEM through the relevant map projection, geographic/cartesian, and datum shift transformations, followed by kriging to obtain values on a grid. The demonstrator also requires each DEM value to be represented in one byte. The height values in the input DEM span a greater range than can be represented in one byte without compression, therefore a scale factor of 3.2 was applied.

The geocoding demonstrator requires the orbit to consist of three state vectors spanning the image, giving position and velocity in either an inertial reference system or the terrestrial one. The two reference systems are related by a straightforward rotation about the z axis. It was not clear how to convert the CIS values given in the input orbit to the inertial system used by the demonstrator, and so the orbit was preprocessed to the terrestrial reference system ED50 cartesian. This involved transformations from CIS to CTS (Conventional Terrestrial reference System), from WGS84 cartesian to ED50 cartesian, taking WGS84 cartesian to be a good approximation to CTS, from TDT to UTC (Universal Time Coordinated), and from UTC to MJD (Modified Julian Date). Velocity values were transformed as pairs of points separated by 1 second.

Source	Time	Position (x, y, z)		
VMP	19:00.000	4819211.50	1012196.50	5194282.00
Unmodified	19:58.184	4823463.93	991733.07	5194282.58
Modified	19:00.000	4819212.71	1012189.42	5194282.60

Table 1. An orbit state vector transformed to CTS.

The resulting state vectors in ED50 cartesian were clearly incorrect; they were too far from the scene. In the dump of DLR's parameter pool there is a section for input to the VMP (Verification Mode Processor), in which there are the parameters v_statv_* giving one state vector near the scene. Table 1 "VMP" shows some of this vector; it has more plausible values. Table 1 "Unmodified" shows one of the input state vectors transformed by us to CTS; it has essentially the same value for z, but a different time. Table 1 "Modified" shows the same thing, but with the input state vector modified before transformation to have the same time as that of the VMP state vector; it has essentially the same value as the VMP state vector. This observation led to the inclusion in the preprocessing of the input orbit of the subtraction of 58.184 seconds from the time for each state vector. Proper justification for this, or an alternative, has yet to be found.

The geocoding demonstrator applies a polynomial correction to the range projection as it is computed; there is no other adjustment. Unlike the fully developed system, the geocoding demonstrator requires that the parameters of this polynomial be supplied by the user. Preprocessing of the input tiepoints into these polynomial parameters was therefore necessary, and required access to the range projection. This was generated into a file by an initial execution of the demonstrator with no polynomial correction. ECR, which the tiepoint scene coordinates are given in, was taken to be WGS84 cartesian. The range projection could only be generated for the area covered by the DEM, so only the 7 tiepoints in that area could be used. The validation tiepoints could not be used, as no sense could be made of the input file format.

The geocoding demonstrator requires each image value to be represented in one byte. The values in the input image span a greater range than can be represented in one byte without compression, therefore a scale factor of 0.4 was applied. The parameters for the transformation from image coordinates (i, j) to time and range are given in the dump of DLR's parameter pool. They are intended to be used in the following equations; the first pixel is (1, 1).

$$time = \text{g\_time\_ref} + \text{g\_time\_az0} + i \times \text{g\_time\_az1}$$
$$range = \text{g\_range\_rg0} + j \times \text{g\_range\_rg1}$$

The full UTC time of the first pixel is given by v_start_utc. These parameters had to be preprocessed into those required by the demonstrator. The demonstrator also requires the approximate geographic coordinates of each of the corners of the image. These are given in the parameter dump by the parameters r_sla_* and r_ele_*, which are in WGS84 geographic. Before presentation to the demonstrator, they were transformed to ED50 geographic and resequenced according to the sensor track direction. This latter is given by the parameter g_sens_edir.

The remaining input parameters required by the geocoding

demonstrator were extracted either directly from the supplied documentation, or from the dump of DLR's parameter pool. In addition to the preprocessing already mentioned, all the input data had to be reformatted to that required by the demonstrator.

5. EXECUTION OF THE GEOCODER

The geocoded image was chosen to cover the same area as the DEM, but with a pixel spacing of 12.5m. DEM resampling was chosen to be nearest neighbour, and image resampling was chosen to be bilinear. The geocoding demonstrator was executed two times. The initial execution, as described above, was for tiepointing purposes, and was without polynomial correction, and with the generation of ancillary products disabled. The main execution had the generation of ancillary products enabled. The machine used was a Sun 4/50EGX (SPARCstation IPX) with 64Mbyte RAM. A rough guide to the execution times is given by table 2, which gives approximate elapsed times for the generation of each product in minutes. Little else of significance was running on the machine at the same time. The large time for the shadow map is due to adverse memory page access behaviour.

The polynomial correction has 4 parameters, and the 7 tiepoints represent 14 constraints upon it. The range projection residuals at the tiepoints are therefore a reasonable measure of the geocoding accuracy obtained. Table 3 gives these residuals for each execution of the demonstrator. These values can be approximately converted to metres in ground range by taking 1 pixel in azimuth to be 12.5m, and 1 pixel in range to be 12.8m (scene centre value).

The geocoding demonstrator has the facility to view any of the images or ancillary products in a window, with zooming. The shadow and layover maps can be overlain upon the images or energy conservation maps, in either map or image space. This provides a means to visually check the content of the shadow and layover maps, the accuracy of the range projection, and the spatial accuracy of the geocoded image. There is no means to check the radiometry.

The generated shadow map was blank, representing the total absence of shadow in the scene. This can be shown to be the correct result through a comparison of the incidence angle against the slopes in the DEM. The DEM has a grid spacing of 40m, and the maximum height difference between adjacent samples is 35m. This means the maximum slope is 48.8° from vertical. The incidence angle does not exceed 26.4° from vertical [1], and so shadow cannot occur from the DEM.

Product	Time (minutes)
Resampled DEM	30
Range projection and geocoded image	30
Shadow map	309
Layover maps	6
Energy conservation maps	9

Table 2. Execution times (elapsed).

Point	Uncorrected		Corrected		Units
	Azimuth	Range	Azimuth	Range	
2	-2.950	-7.944	-0.144	0.202	pixels
5	-2.629	-8.457	0.178	0.050	
6	-1.982	-8.840	0.825	0.017	
7	-2.655	-8.763	0.152	-0.595	
8	-4.191	-8.442	-1.384	0.073	
10	-3.117	-10.053	-0.311	-0.170	
24	-2.123	-8.245	0.684	0.490	
RMS	2.888	8.700	0.680	0.310	pixels
RMS	36.100	111.360	8.500	3.968	metres

Table 3. Tiepoint residuals.

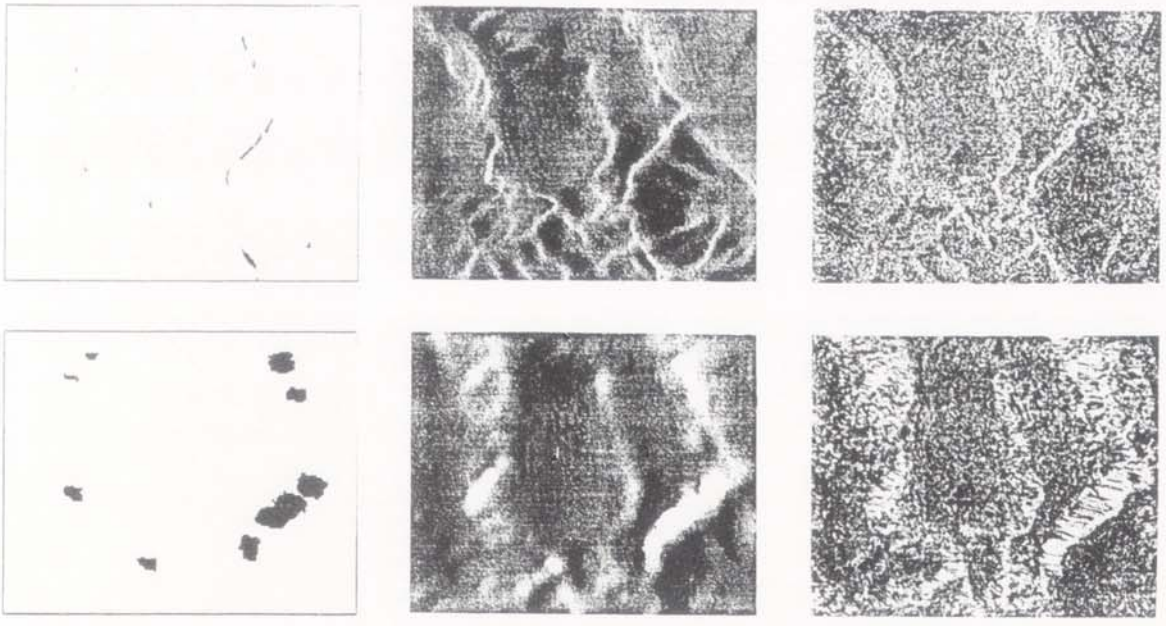

Figure 1. Geocoder products. Region shown is in the NW of the DEM area.
Image space (a) layover, (b) energy conservation, (c) image.
Map space (d) layover, (e) energy conservation, (f) image.

The content of the layover maps appeared reasonable, in that areas of layover coincided with bright areas in the images and energy conservation maps. Spatial accuracy was also good, in that it was not possible to discern any disparity between any of the items. The content of the energy conservation maps appeared reasonable, but no proper checks were possible. Figure 1 shows the images, and layover and energy conservation maps for a small region in the NW of the DEM area; a region of rugged terrain.

6. CONCLUSIONS

The test was dominated by the work necessary to preprocess the input data into a form suitable for input to the geocoding demonstrator. This was partly due to the nature of the input data, and partly due to the nature of the geocoding demonstrator. Many additional tools were required in order to perform this preprocessing.

The main problems with the input data were to do with the documentation. The formats of some of the data files were either incompletely documented or not documented at all. The orientation of data in the DEM and image files was undocumented. Some coordinate systems referred to were unfamiliar; for example TDT and ECR. The descriptions for each parameter in DLR's parameter pool were terse. Many of the parameters needed from the dump of the parameter pool were in unknown coordinate systems. Most of this uncertainty was resolved by intelligent guesswork and experimentation; however, uncertainty about the validation tiepoints and the orbit remained, to the extent that the validation tiepoints could not be used at all. The parameters were based around a geocoded image in the projection UTM using the datum WGS84, this is an unusual combination.

The main problems with the geocoding demonstrator were to do with the fact that it is a prototype for a fully developed system. Many functions were therefore incompletely implemented. These included the lack of support for datum shifts, and minimal support for tiepointing. The fully developed system supports both of these functions fully. The range of ellipsoids and projections supported is not large.

Tiepointing had to be performed, but although this mostly had to be done using tools external to the demonstrator, the method used was the same as that implemented in the fully developed system.

The execution time for the generation of the shadow map is large. This is due to the way memory is accessed.

The range projection residuals at the tiepoints exist naturally in image space. In map space, residuals would be for the inverse projection. Unlike the forward projection, errors in the inverse projection are affected by the slopes in the DEM. Spatial errors in map space are therefore uneven, particularly so in areas of rugged terrain, making generalization of residuals into overall accuracy difficult. Spatial errors in image space should be more even, so it is probably more useful to present residuals in image space.

DEMs are limited in the steepness of slope that can be represented, thus making shadow and layover from DEMs less likely to occur than from the terrain. It is not at all uncommon to find that a DEM generates no shadow. Layover is more common, as the slopes do not have to be so steep as for shadow.

In regions that are near layover, a small change in image position can correspond to a large change in map position. This leads to a spreading out of such regions in the geocoded image. For this reason, the comparison in image space of the layover map against the image is a better check on spatial accuracy than the same comparison in map space. The image space layover map is therefore a useful product.

The energy conservation map exists to record the change in image energy due solely to the geocoding projection; it thus records the change of area between map and image space. Some users also want to make corrections for terrain slope effects, for which an incidence angle map is necessary; the incidence angle map records the angle between the incident radar signal and the surface normal. The geocoding demonstrator does not produce an incidence angle map, but it may be added in the future.

REFERENCES

[1] Pam Vass & Malcolm Handoll, 1991, *UK ERS-1 reference manual*, Earth Observation Data Centre, Farnborough, UK, DC-MA-EOS-ED-0001.

[2] Laycock J E, Meadows P J, Dowman I J & Upton M, 1991, *Precision geocoding project — Algorithm definition*, GEC-Marconi Research Centre, GEO-MRC-XX-2001/5.

[3] Meadows P J, Laycock J, *Geocoding demonstrator error budget analysis*, GEC-Marconi Research Centre, GEO-XR-00003-MRC-3300.

[4] Dowman I, Laycock J & Whalley J, 1993, Geocoding in the UK, *SAR geocoding — Data and systems*, Wichmann-Verlag, Karlsruhe.

[5] Dowman I, Upton M, de Knecht J & Davison C, 1993, Preliminary studies on the application of ERS-1 data to topographic mapping, *Proc First ERS-1 Symposium 1992*, Cannes, France, ESA, SP-359, 543-549.

[6] Graf C, Nüesch D, Meier E & Frei U, 1988, *Map projections for SAR geocoding*, University of Zürich, ERS-D-TN-22910-A/9/88.

[7] Evenden G I, 1991, *Cartographic projection procedures for the UNIX environment — A user's manual*, US Geological Survey, Open-file report 90-284.

Appendix 2.9

An evaluation of geocoded ERS-1 SAR data for mapping when combined with Landsat Thematic mapper and KFA 1000 photography

Sofia Theodoridou and Ian Dowman

University College London

1 Introduction

A study was carried out at UCL to determine the utility of SAR data for mapping by itself or with other satellite data. Two geocoded images from phase 1 of the geocoding test were available as well as other data from the OEEPE Digital Landscape Model project. These included Landsat Thematic mapper data and KFA 1000 photographs. The images were registered together and an assessment made of the image content. The results of different image combinations are compared. Figures are also available on the accuracy of the geocoded SAR data in comparison with the other satellite data.

2 Data

In this study, a digitised vector-map of the test area, provided by TU Vienna, served as the geometric reference data. This digital data was derived from the 1 : 50.000 map sheet "Frankfurt am Main West". Coordinates are given in the German Gauss-Krüger system. The accuracy of this product is considered to be about ±25 m due to cartographic displacements related to the limited pointing accuracy when digitising a map of 1 : 50.000 scale.

The digitised map was provided in the following formats:

- AutoCAD 10.0-drawing file (frankmap.dwg).
- DXF-file (frankmap.dxf).
- ERDAS DIG-file (frankmap.dig), a vector format ASCII-file, that can be used in ERDAS package.
- HPGL-plotfile (frankmap.plt), a wide-spread plotter-format file which can be plotted on many devices, and also can be imported into other programmes.

The area covered by the map contains:

- roads and railway,
- water features,
- woodland borders,
- large buildings (airport, industrial, railway-stations)
- basic contour lines

For checking purpose points derived by Saundercock (Dowman et al, 1993), were used. 51 GCPs were identified and co-ordinated in the German Gauss-Krüger system. Those points were carefully measured five times from the 1 : 50.000 paper map so as to avoid blunders, and the average taken so as to ensure a measurement accuracy to less than 0.2 mm (10 m at ground scale). Hence the derivation of the GCP locations was to sub-pixel precision.

The data used for this project, listed in table 1 came from three different satellite platforms. Thus, different parameters should be considered in the image quality and information content.

Sensor	**Description**	**Pixel Size**
ERS-1 SAR	geocoded scene by DLR	12.5 x 12.5 m
ERS-1 SAR	geocoded scene by TU Vienna	12.5 x 12.5 m
Landsat-TM	7 bands of the Thematic Mapper	25 x 25 m
KFA-1000	spaceborne camera orthophoto	25 x 25 m

Table 1. Data used to evaluate content.

The following ERS-1 data was provided:

- An ERDAS-7.4 file with ERS-1 data of Frankfurt site, geocoded by TU Vienna. The original SAR scene has been optimised from the 16-bit to an 8-bit range by using histogram equalisation. This change transfers the real grey scale value of about 32.000, to an 8-bit 255 grey scale values distribution which helps the visual interpretation.

  As it is described on the documentation provided by DLR, this product has been generated without using any external orbit-

information. The orbit and the relevant projection-parameters were calculated via a photogrammetric-bundle-adjustment program (ORIENT) using as an input 35 control-point-measurements covering the whole scene, provided by DLR. This calculation were performed in a Cartesian 3D-space (based on a plane tangential to ellipsoid at the given site). Contradictions between the given control point measurements and the derived model were within ±5 m with a maximum error of 62 m.

Then, the given ERS-1 scene was geocoded, using a DEM (32 x 28 km) of 40 m original grid (16-bit), resampled to a 12.5 m pixel size. Every 3D-terrain point was transformed into the Cartesian space (where the orbit model is defined) and the slant-range distance to the orbit could be calculated within a plane orthogonal to the orbit vector. The intersection of this plane with the orbit gave the relevant scan, where the location of the terrain-point is determined using the orbit model for offset and scale in slant-range. The grey values at the calculated position was determined by bilinear interpolation among the four closest neighbour pixels. This value finally was assigned to the position in the geocoded-image, according to the x/y-coordinates of the terrain point. The imaging defects like layover and shadow were ignored, and also no corrections to grey levels in foreshortening areas were applied.

- An ERDAS-7.4 file with ERS-1 data of Frankfurt site, geocoded by the German Aerospace Research Establishment (DLR). It is a subset from the original ESA GTC scene, using a different DEM from that provided for the OEEPE test.

3 Methodology

In order to evaluate the content of SAR data in terms of accuracy and interpretability for mapping purposes, it is necessary to carry out a number of pre-processing procedures. The aim is to compare the two different geocoded SAR scenes with the single image data of that area, derived from the other sources. In order to compare SAR with other satellite data, Landsat Thematic Mapper data and KFA 1000 data used in the OEEPE Digital Landscape Model test, also of the Frankfurt area, were used and combinations of these products were formed to test their content. To carry out a comparison and create the merged images, all the data must be registered to each other and referred to a common ground co-ordinate system.

The following paragraphs describe the methodology, which was based to the availability of Image Processing tools of ERDAS Imagine.

The work was done in the UNIX-based ERDAS IMAGINE software, Version 8.1. The ERDAS system is a fully featured raster GIS image processing system, which incorporates functions for raster data starting from the very first stage of collecting, and ending with the production of a cartographic-quality map composition.

ERDAS allows the user to deal with data coming from different sources such as satellite data, airborne sensor data, digital topographic data and scanned or digitised maps or photographs. It can also interchange known raster file formats coming from other systems, as well vector file formats such as ARCInfo and DXF files. Vector files that are imported to the system can be further processed in the vector format or either can be transformed into raster format.

The environment uses a friendly Graphical User Interface with icons. The raster images can be displayed on multiple windows, having the option of a geographical linkage in order to provide different views of the same area.

For the purpose of this project, the ERDAS IMAGINE tools that were mostly used are:

- Import/ Export dialogue box, in order to import in ERDAS environment the ARCInfo format vector map as well as the satellite scenes which were in a LAN format. The import creates raster files, which are called image files (.img), for the raster imported data, and vector files in the case that the input is in vector format. Alternatively, the vector file can be transformed in a raster form and therefore in an image file.

- SAR scenes as well as LANDSAT-TM scene were extended outside the reference map "limits". In order to reduce the size of the large imagery, all scenes were subset to the co-ordinate limits of the map 1 : 50.000. Subset command (Utilities option of the Image Interpreter dialogue box) can be used to copy a selected portion of an image file to an output file.

- A very useful tool is the Contrast and Brightness Adjustment dialogue box, which performs image enhancement allowing to

view, edit the contrast and brightness and save the new look up tables of a continuous raster data.

- Radar dialogue box, contains the Speckle Suppression tool which was used in order to reduce the presence of speckle noise on radar imagery.

- For the superimposition of different image files a technique which stacks layers from different files in any order was used. This special tool is called Layer Stack and it is in the Utilities option of the Image Interpreter dialogue box.

- Image fusion based on the IHS transformation was performed using the tools of the Spectral Enhancement dialogue box, RGB to IHS. and IHS to RGB.

- Rectification can be done using the GCP Editor which allows to record and view GCP data with the top raster layer in the viewer as well as to create a kind of data base to store coordinates. Finally, resampling in ERDAS can be done by one of the three known techniques (nearest neighbour, bilinear interpolation, cubic convolution) using the dialogue box Resample. This tool allows to choose the transformation type and the kind of projection.

Before any process involving the registration, the radar data had to be filtered to remove the speckle effect. The speckle suppression filter which was chosen from an available list of ERDAS Imagine, was the Sigma. A 3 x 3 window with an estimated value for sigma of 0.26, was applied to both images. The resultant images were assessed visually as better than the original images affected from the speckle effect for visual interpretation.

The seven separate files, one for every the seven Landsat-TM band, were combined into one using the image processing package HIPS (Human Image Processing Software). The resultant file which is containing the seven spectral bands in seven different layers, can be displayed either as a colour image when 3 layers are combined, or a as a grey scale image when one layer is chosen.

Vector-format files can be imported and used in ERDAS Imagine. Among the formats that the ERDAS supports are the DXF and the ARCInfo files. Here, the digitised reference map was imported from a DXF file. Afterwards, this file was also converted from vector into raster format for the purpose of registration.

Theoretically, geometric registration must be done using well located ground control points, distributed all over the image area.

In this study, the images that were registered are:

- ERS -1 SAR scene, geocoded by DLR
- ERS -1 SAR scene, geocoded by TU Vienna
- Landsat-TM file containing the 7 bands
- KFA-1000 orthophoto

and additionally

- the raster format of the digitised map

All those files were registered to the same ground co-ordinate system, which is the German Gauss-Krüger, using as a destination a file containing the ground control coordinates in that system. The procedure involves the identification and accurate positioning of the GCPs on every image, using the pointing device on the screen display. At this point, the source coordinates are measured to be used for the polynomial transformation to the destination coordinates.

Ground control points were mostly road or railway intersections, river bridges, and top of hills. The flatter parts of the test site were occupied by more cultural features, so that road and railway intersections, corners of differing land use types, and the Frankfurt airport hard standings are used as GCPs. On the hilly part of the test site, hill-tops, valley intersections, and sharp changes of direction in valley bottoms are used as a GCPs.

The registration of the image data and raster-map to a list of GCPs in the German Gauss-Krüger co-ordinate system, was done using least-squares based, second and third orders polynomial rectification algorithms. The degrees of polynomials used for transformation, produced the best residuals for the number of GCPs used in each case. A high order polynomial is the more rigorous solution, especially in mountainous areas, but takes more computational time. The linear transformations produce acceptable results in flat areas, and are usually preferred because of their fast computing. Appendix B shows the list of GCPs used for each of the image registrations and the results derived from the transformations. The results of the registration are discussed in the next chapter.

After the registration was finished, all images were resampled to fit a 12.5 x 12.5 pixel size grid by the bilinear interpolation method.

After the registration procedure was finished, all images were subset to the area of the reference map origins.

Two methods for merging were used in this study. In the first case, single images were assigned separately to each of the RGB colour guns, in order to produce a colour composite. Those combinations involved the registered SAR images, firstly with the rasterised digital map, and secondly with the KFA-1000 orthophoto. The merged products using this method are:

- GTC1 with digitised map
- GTC1 with KFA-1000 image
- TUV1 with digitised map
- TUV1 with KFA-1000 image

In the second case, the method for merging multisensor image data using the IHS transformation was applied. This technique involves three basic steps:

1. Forward transformation of Landsat-TM file from RGB space to IHS space.
2. Substitution of Intensity component by the SAR image which has similar resolution.
3. Reverse transformation of that composite into original RGB space for better visual interpretation.

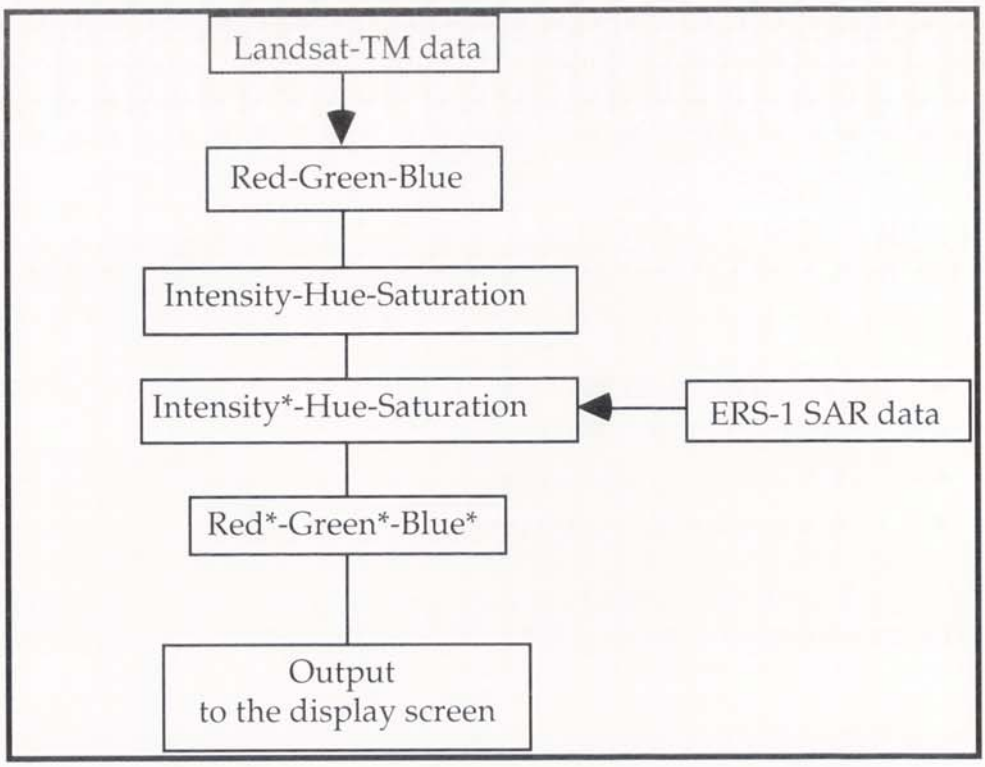

Figure 1. The IHS transform for merging Landsat-TM bands with SAR data.

In that form, the RGB file can be displayed on the screen. The merged products are:

- GTC1 with Landsat-TM scene
- TUV1 with Landsat-TM scene

For this method three spectral bands from the seven of the Landsat-TM scene, were chosen as input to the IHS transform. TM2/TM5/TM7 bands provided the best combination for map production. After the Landsat-TM2/TM5/TM7 bands were transformed to IHS coordinates, the intensity channel was replaced by the radar image and these modified triplets were used as input to the reverse IHS to RGB transform for the display on the screen.

The last step of the project concerned the evaluation of the ERS-1 SAR data for mapping purposes. The aim was to examine the influence of image resolution to the image content, by collecting as much reliable information for mapping purposes as possible, for each of the tested sets of

data. The quality of the extracted features from the imagery was verified against a reference map. The quality assessment of the content of ERS-1 radar imagery, was examined using the method of visual interpretation.

First, the sets of data were displayed on the screen viewer and then adjusted in contrast and brightness to optimise the visual interpretation. The recognition of topographic objects was based on a categorisation for areal and linear features. The zoom-in zoom-out tools were used in order to help the discrimination between vaguely recognised objects. In many cases, superimposition of image data with the rasterised vector map helped the interpretation. The identification and localisation of topographic objects was investigated following a three-class scale.

4. Data analysis

4.1 Data sets

For the accuracy assessment of the two SAR images, for mapping purposes, the following data sets were also chosen to be examined:

- KFA-1000 orthophoto,
- Landsat-TM5, because it gives the best interpretability as a single band display,
- Landsat-TM4/TM5/TM1, assigned to the Red-Green-Blue components respectively, as a 3-band combination that contains the most information because it consists of one visible bands (TM1), one near-infrared bands (TM4), and one mid-infrared bands (TM5),

and the integrated data sets:

- ERS-1 SAR scene by DLR, combined with the KFA-1000 orthophoto,
- ERS-1 SAR scene by TU Vienna, combined with the KFA-1000 orthophoto,
- ERS-1 SAR scene by DLR, combined with the Landsat-TM2/TM5/TM7,
- ERS-1 SAR scene by TU Vienna, combined with the Landsat-TM2/TM5/TM7.

4.2 Geometric assessment

As expected, the different kind of data resulted in differences in terms of registration accuracies, and this was related to the problems of identi-

fication of GCPs in the whole area. The quality of each data set is what determines the accuracy to which control points in the images can be defined. The root mean square errors that were determined for the different registrations are given in table 2.

Data	rmse (m)	Order of polynomial	No of GCPs
GTC1	16.6	2	14
TUV1:	25.6	3	19
Landsat-TM:	36.5	2	14
KFA orthophoto:	35.5	2	18
Digitised map:	12.3	2	16

Table 2. Results of fitting geocoded products to ground check points.

The TUV1-product is showing contradictions of up to 50 m compared to the digitised reference map, while GTC1-product is even better. But the latter is caused by the local adoption applied to the GTC, due to lack of absolute co-ordinate-reference (lack of reliable GCPs). Most of the offsets - up to 200 m - are in the Northwest corner of the image, where terrain is hilly, which may be due to a probably smoother DEM used by DLR for the geocoding.

The relative accuracy derived from the registration, has to be considered with respect to the pixel resolution of the images. Having in mind that the SAR scenes were geocoded to a pixel resolution of 12.5 m, SAR rms error refers to 1.5 - 2 pixels accuracy. Likewise, the digitised map refers to a half-pixel accuracy and, Landsat-TM as well as KFA orthophoto refers to 1.5 accuracy. If one considers that the map coordinates from the scale 1 : 50.000, could only be determined to within 10 m ground accuracy, measurement to the nearest pixel was certainly a satisfactory optimum. However, the superimposition of the registered data sets, showed significantly large contradiction in the North-Western part of the test site, which is a mountainous and hilly area. This cast doubt on the overall effectiveness of the geocoding process although the checks carried out in phase 1 indicate good overall accuracy. The discrepancies may be due to problems in identification of control points in hilly, forested areas.

Most of the problems that were met involved the GCPs identification in the SAR images, especially in the North-Western part of the scene. In

those rural areas the polynomial fit showed large discrepancies, influenced by the relief, which limited the number of the identifiable GCPs. Despite the techniques for the speckle reduction and also contrast stretching that were applied to enhance the SAR scenes, the identification of road crossings in areas with rough terrain relief were almost impossible. Due to the orientation of the radar sensor with respect to the target, terrain relief distortions such as foreshortening, layover and shadow affect the mountainous and hilly areas. The steep incidence angle of ERS-1 of 23° causes active shadow for regions with slopes greater 67°. In those areas linear features such as roads, although their good width for recognition, were not identifiable, and missing information presents as "black holes". Moreover, a large zoom-in factor proved to be not useful for the visibility improvement of the ground control points, due to the SAR low resolution. Within build-up areas it was quite easy to locate control points, with fewer exceptions of vague identification. Eventually, the ground control points that were used for the registration of the SAR scenes were located mainly on the flat part of the imagery, and for that reason the results in the urban area show a better fit. In rural areas the fit doesn't match and the superimposition of the registered scenes with the map showed great contradictions especially on the hilly areas. Little or no difference has found between the two sets of images.

Problems with the registration of the other types of imagery of the area did not arise, because of their better resolution and good ground control point localisation and distribution all over the test site.

Finally, the relative accuracy of the registration was verified by superimposing the reference map on the resampled images, and was considered quite good in flat areas, where were most of the GCPs were located. The image fitting is very good along the river where the location of GCPs at the bridges was easy. In the hilly area of the SAR images showed great contradictions due to the lack of GCPs selection.

Emphasis is on how much the geometric resolution influences a large area (e.g.. total ERS-1 scene) and the limitations due to radiometric resolution, since discrimination between low-backscattering fields is not possible with ERS-1.

4.3 Interpretation of the fused images

The image products were examined visually in order to gain a general sense of their recognition ability in areal, linear and point features. A classification of the objects that are contained in the test site was decided, considering the requirements for topographic mapping. Those features were

categorised in two broad classes in order to show the ability to detect features to be mapped that fall in those classes:

Areal objects	**Linear objects**
Forests	Motorways
Waterbodies	Second-order streets
Densely-built up areas	Railway
Sparsely built-up areas	Major river
Airport	Minor rivers
Major buildings	Bridges
(airport, railway, industrial)	Field boundaries

The interpretation of radar data has to be approached in a differnt way from that of aerial photography or satellite data because of the different image formation. In this study a very basic approach was adopted in which the map was used in combination with the SAR image to decide what features are. Clearly only a simple classification was used.

The ability to interpret visually the boundaries, the areal and linear objects, and their distinct separation, was categorised according to a three-level scale. The reuslts are shown in Tables 3 to 6. Features that were identified without any doubt are classified as easily discernable, those over which some doubt exists were classified as discernable and those misidentified are classified not discernable.

Natural features

The shoreline of the Main River of Frankfurt area is the most easy plotted feature of the test site. It is the dominant characteristic of the scene which clearly visible on all types of imagery including the SAR scenes.

Apart from that river, minor rivers proved to be difficult to identify. In many cases were misidentified with other linear features such as second-order roads, because of their spatial pattern similarity. An exception was made with the KFA-1000 orthophoto and the examined Landsat-TM3-band colour composite (Table 4). In those images, the relief roughness of the north-western edge of the site helped river recognition, and some minor rivers were identified. The use of a map to obtain auxiliary information could help a lot the identification of such features.

Table 3.

	ERS-1 DLR	ERS-1 TU Vienna
Areal objects		
Forests/ Parks	0	0
Waterbodies	0	0
Densely built-up areas	+	+
Sparsely built-up areas	0	0
Airport	+	+
Major buildings	0	0
(airport, railway, industrial)		
Linear objects		
Motorways	0	0
Second-order streets	0	0
Railway	0	0
Major river	++	++
Minor rivers	0	0
Bridge	++	++
Field boundaries	0	0

0 = not discernible; + = discernible; ++ = easily discernible.

Table 4.

	KFA-1000	LandsatTM5	LandsatTM4/TM5/TM1
Areal objects			
Forests/ Parks	+	0	+
Waterbodies	++	+	++
Densely built-up areas	+	+	+
Sparsely built-up areas	+	+	+
Airport	++	++	++
Major buildings	++	0	+
(airport, railway, industrial)			
Linear objects			
Motorways	++	++	++
Second-order streets	+	+	+
Railway	+	+	+
Major river	++	+	++
Minor rivers	+	0	+
Bridges	++	+	++
Field boundaries	+	0	++

0 = not discernible; + = discernible; ++ = easily discernible.

Other areal waterbodies such as lakes, were easily plotted only from the fused Landsat-TM scenes with the SAR data, and vaguely seen on the merged SAR/ KFA-1000 scene (Tables 5 and 6).

The woodland plotting was easy from the colour composites with Landsat imagery, where the true and false colour display improved a lot the recognition of forestry, and just discernible from the KFA orthophoto and again the Landsat-TM 3-band colour composite. The recognition of woodland helped a lot in cases where it was surrounded by open space.

Table 5.

	ERS-1 DLR/KFA-1000	ERS-1 DLR/LandsatTM5/TM7
Areal objects		
Forests/ Parks	+	++
Waterbodies	+	++
Densely built-up areas	+	+
Sparsely built-up areas	+	+
Airport	++	++
Major buildings	+	+
(airport, railway, industrial)		
Linear objects		
Motorways	++	++
Second-order streets	+	0
Railway	+	0
Major river	++	++
Minor rivers	0	0
Bridges	++	++
Field boundaries	+	+

0 = not discernible; + = discernible; ++ = easily discernible.

Boundaries

Property boundaries in rural areas were indicated only on the Landsat-TM/ SAR colour composites (Tables 5 and 6) where it was also identifiable the land use type.

Other areal features such as the boundaries of the hard standing of airport (Figures 2 and 3) were clearly visible on all types of imagery including radar images as well.

Buildings

Buildings due to their small dimensions, are the most misidentified features on SAR imagery. Only the boundaries of an urban area can be

recognised on a radar image. Large buildings at the industrial and airport zones (Figure 2), were indicated very vague and houses in residential areas were not recognised. Again the colour image-composites helped identification a lot, especially for individual buildings discrimination in open country.

Communications Network

Main roads could be identified easily without the use of a map in every data set except the single SAR scenes. Some difficulties arose with the major roads interpretation within the urban area, as the signal from the buildings tend to dominate the image.

The rail network and channels were only identifiable with the aid of a map on all types of data except the SAR scenes. The bridges of the main river on the other hand, gave a good pattern and could be plotted clearly from all data sets.

Table 6.

	ERS-1 TU Vienna/KFA-1000	ERS-1 TU Vienna/LandsatTM5/TM7
Areal objects		
Forests/ Parks	+	++
Waterbodies	+	++
Densely built-up areas	+	+
Sparsely built-up areas	+	+
Airport	++	++
Major buildings (airport, railway, industrial)	+	+
Linear objects		
Motorways	++	++
Second-order streets	+	0
Railway	+	0
Major river	++	++
Minor rivers	0	0
Bridges	++	++
Field boundaries	+	+

0 = not discernible; + = discernible; ++ = easily discernible.

The use of ERS-1 SAR data for the purpose of topographic mapping can cause difficulties because of its nature. Optical spaceborne data from other sources proved to be much more useful in direct plotting. Results from the visual interpretation showed that SAR data can be better used in conjunction with a map of the area for map revision purposes, or in combination with multispectral data.

5. Conclusions

The usefulness of the ERS-1 SAR imagery for topographic mapping has to be considered with respect to the appropriate cartographic scale selection. The considerations that have to be made about the presentation scale depend on geometric accuracy and a resolution of details. Previous research for the map scale selection for remotely sensed imagery proposes that Landsat-MSS data must be shown at scale 1 : 250.000, Landsat TM data at

1 : 100.000, SPOT data at 1 : 50.000, considering that about 3 pixels should be presented in a millimetre. In 1987, Leberl *et al.*, investigated the appropriate scale selection for the spaceborne radar imagery. Considering classical orthophotography, the argument is made that enlargements between the original negative and the final presentation should not exceed a factor of 11. Assuming an equivalent pixel size in an original aerial photograph of 10 mm, the enlargement would place 9 pixels in a millimetre. The space image consideration about the 3 pixels presentation in a millimetre, would suggest that a radar image with 6 m pixels can be presented at a scale 1 : 25.000. The orthophoto consideration would suggest a scale of 1 : 50.000. This is the reason to select a scale of 1 : 50.000 for the radar image map. Furthermore, if we assume ERS-1 SAR expected accuracies for a terrain corrected scene (GTC using a DEM) of 25 m, and permitting a planimetric error of 0.5 to 1.0 mm that an image map product should have, the corresponding mapping scales are the 1 : 50.000 and 1 : 150.000, respectively. However, the radiometric peculiarities of SAR significantly reduce the usefulness of these data for topographic mapping applications.

References

Dowman I, Chen Pu-Huai, O Clochez and *G Saundercock*, 1993. Heighting From Stereoscopic ERS-1 Data. Proceedings of Second ERS-1 Symposium - Space at the Service of Our Environment, Hamburg, October 1993. ESA SP-361. Pp 735–740.

Leberl F, Domic G, Mercer B, 1987. Methods and accuracy of operational digital image mapping with aircraft SAR. ASPRS/ACSM Technical papers 1987 4:148–158.

Figure 2. Subsets of the same area of 4 data sets.

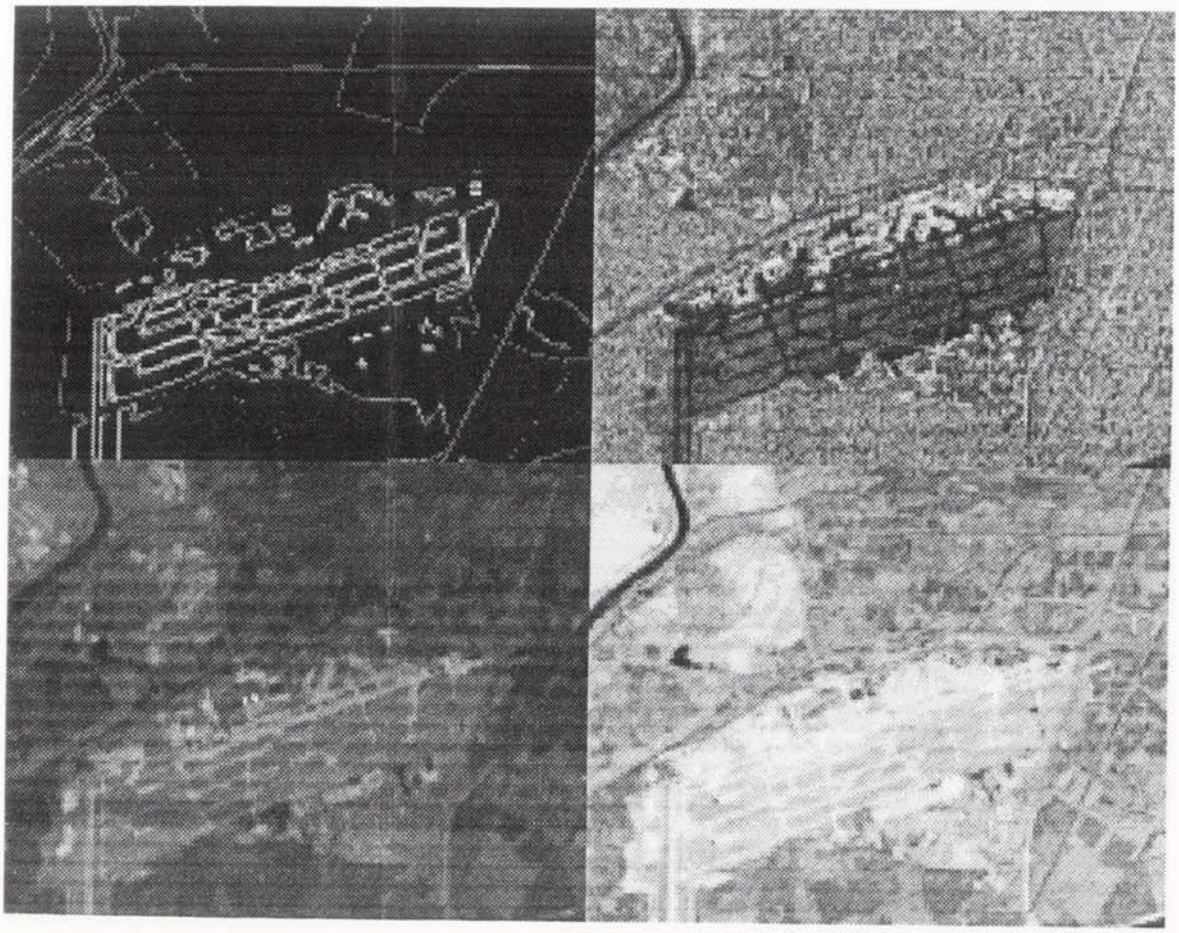

A subset of the Frankfurt airport area. Notice the hardstandings and the route network. The four frames are:

a. the rasterised digital map of the area
b. the ERS-1 SAR geocoded by DLR
c. the Landsat-TM5 scene
d. the KFA-1000 orthophoto

Figure 3. ERS-1 SAR image compositions.

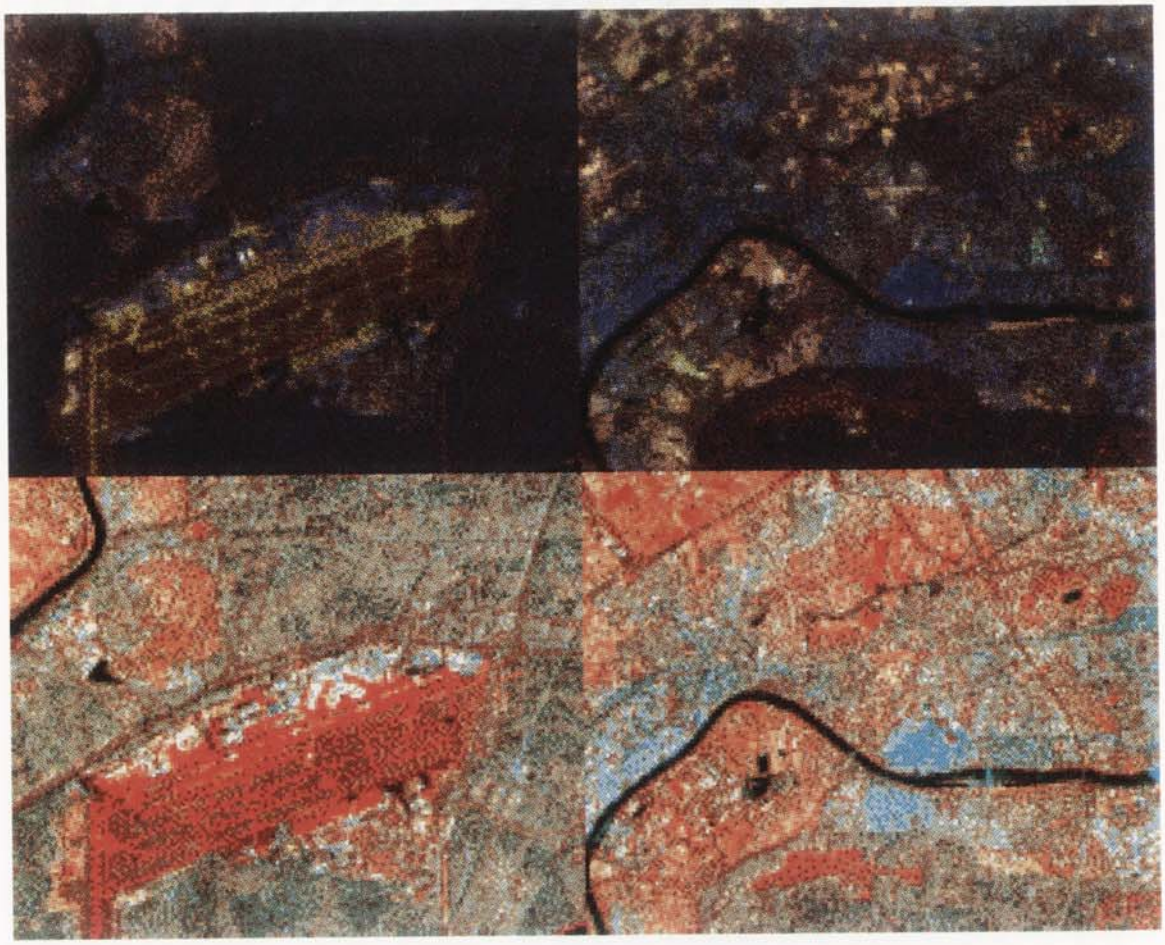

Colour image composite produced by merging the ERS-1 SAR scene geocoded by DLR and the Landsat-TM5/TM7 bands.

a. subset of the airport area,

b. subset of a densely built-up area.

Colour image composite produced by merging the ERS-1 SAR scene geocoded by DLR and the KFA-1000 orthophoto.

c. subset of the airport area,

d. subset of a densely built-up area.

Appendix 2.10

Agricultural University of Norway

Summary report on interpretation of ERS-1 SAR image data for OEEPE test.

Method.
In order to make an assessment of the suitability of ERS-1 SAR image data for mapping purposes, a qualitative approach was chosen. Five subareas, each area comprising 400 lines and 500 pixels, were selected from the file MAP_TUV.LAN supplied by the Technical University of Vienna. For each area, a visual interpretation was carried out directly from the image display screen on the ERDAS image processing system. The interpretation was initially recorded in vector format (as ERDAS.DIG-file), and was later converted to raster representation (as ERDAS.GIS-file). The interpretation was carried out by five people, each person interpreting one area each. In addition to the interpretation proper, each interpreter gave his or her comments on the problems encountered in the interpretation of this type of data compared to interpretation of data from the optical sensors in Landsat and SPOT satellites.

Interpreters' background.
All five interpreters taking part in the test are graduate students with 4.5 years studies in mapping sciences behind them. At the end of the spring term of 1995, they completed their studies at the Agricultural University. During their studies they have been trained in conventional Photogrammetry and air photo interpretation. They have also completed courses in " Satellite Mapping", and have thus also very good experience with digital as well as visual analysis of satellite imagery, particularly images from the Landsat and SPOT satellites. The interpretation carried of in this test, was their first "hands-on" experience with the ERS-1 SAR type of data. In addition to general theoretical knowledge of the SAR principle, a special lecture on interpretation of ERS-1 SAR image data was given during a visit to the Norwegian Defence Research Establishment (NDRE) at the end of October 1994 year. On the basis, it is not unreasonable to say that the persons who have carried out the interpretation in this test, are among those who have the most qualifications for carrying out such a task. the fact that the interpreters could meet the ERS-1 SAR image data with "fresh-eyes", is in this connection considered advantageous.

Presentation of Results.
The results for each interpreter is presented together with the corresponding topographic map and the original ERS-1 SAR image data accompanied by a qualitative and subjective assessment of the interpretation possibilities of this type of data. An attempt has been made to summarise the individual comments and point out what are the main impressions of ERS-1 SAR image data within this group of interpreters. This summary is given below.

Results from interpreter No 1.

Comments:

An attempt was made to interpret 6 classes: 1: Roads, Airport area, 3: Built up areas, 4: "Distinct white", 5 "White spots", 6: " Dark spots". Class 1: Astonishingly few roads could be detected, the type of landscape taken into consideration. Class 2: The airport area was the feature which could be most easily interpreted. Runways and taxi ways could be distinguished from the rest of the airport area. Only the border line of the general airport area was digitised. Class 3: The dark area in the south was interpreted as a built up area. Texture was also used as an indication of area type.

In general: Very difficult to interpret details in a SAR image. The image has a blurred appearance. Certain details with special properties concerning microwave reflectance are clearly shown, but it is difficult to identify these features. The terrain slope has a strong influence on the radar reflection. This represents a problem in connection with the interpretation. Distinction between different land cover categories can be more easily interpreted using optical satellite images which more clearly show cultivated areas, built up areas, forest roads etc. In the SAR image there is too much noise. SAR images are not ideal for mapping purposes. For certain purposes, they can however represent a valuable supplement.

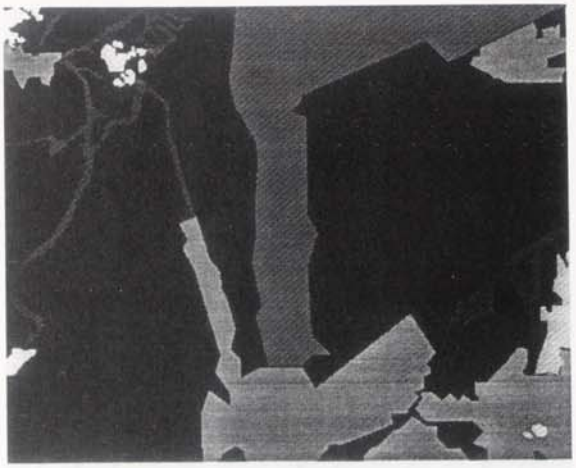

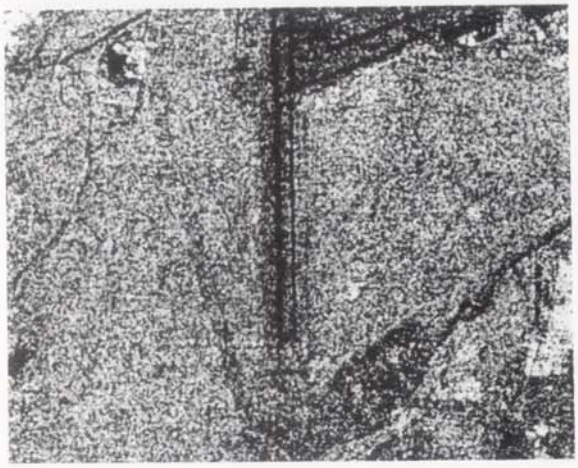

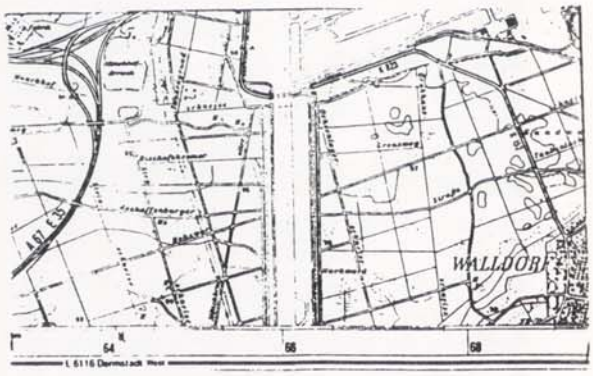

Results from interpreter No 2:

Comments: An attempt was made to interpret the categories Roads, Built up areas and forest.

In general: The interpretation was very difficult, even with support from the topographic 1:50 000 map of the corresponding area. The reflection from roofs in built areas is multidirectional and gives a very noisy-looking result. Certain roads could be detected, particularly those aligned parallel to the direction of the satellite movement. Small straight valleys are also clearly shown, due to a similar effect.

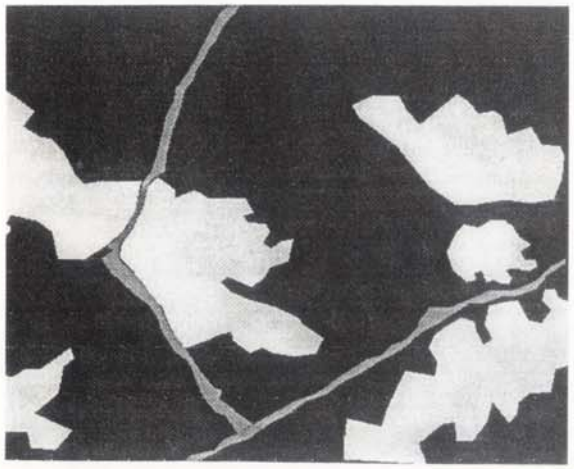

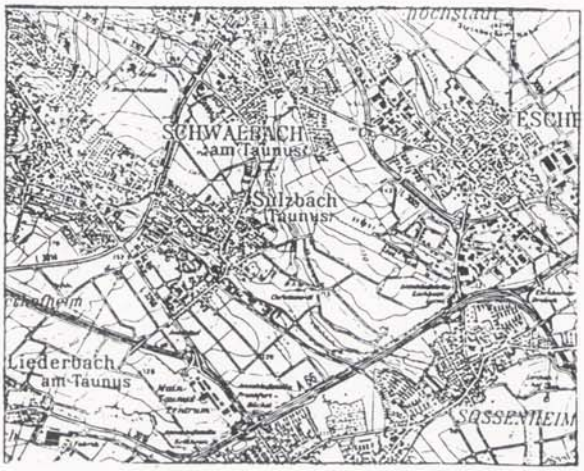

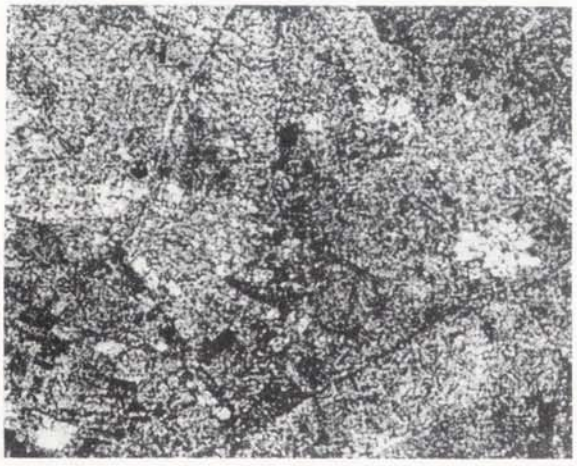

Results from interpreter No 3:

Comments: The classes 1: Roads, 2: Lakes, 3: Built up areas, 4: river, large and 5: River, small/creek were interpreted.

In general: The interpretation of the SAR image was extremely difficult because of the "salt and pepper" appearance. Very few homogenous areas could be distinguished. Only the motorways, the lakes and also the large river could be interpreted directly. Certain built-up areas could be seen, but for some others it was impossible to find the border-line defining the area.

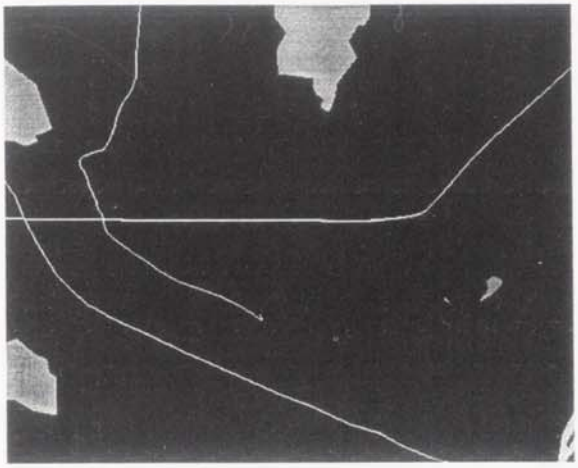

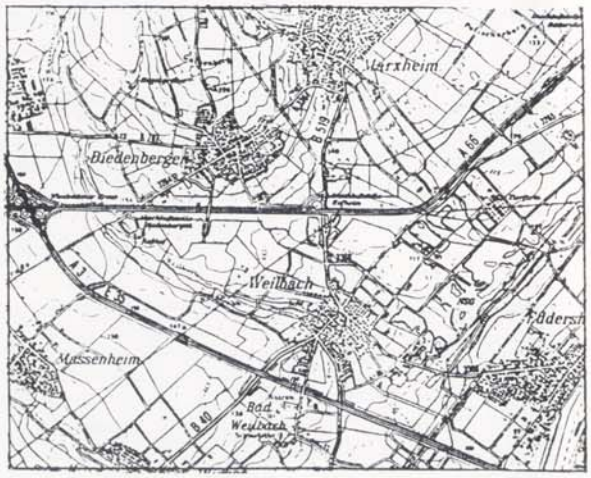

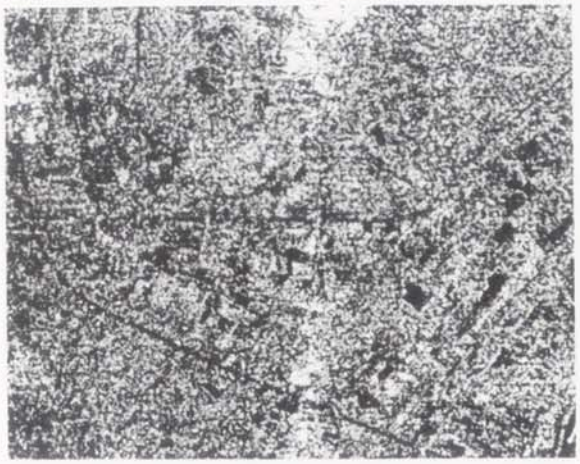

Results from interpreter No 4:

Comments: Following categories were interpreted: 1: Built-up areas, 2: Park-like area(?) and 3: Mixed forest.

In general: The most striking feature in this image subset was the valley-structures. This appears to be only feature which can be interpreted directly without any support from other sources as for example a map. The side of the valley facing the satellite is very bright, and the other side of the valley is rather dark. *This effect is probably more distinct in SAR images than optical satellite sensors. Built -up areas could hardly be distinguished without map support. Certain areas could then be interpreted using texture variation. The influence of the topography on the overall reflection pattern makes it very difficult to interpret smaller details. Images from optical satellite sensors seem to be better suited for interpretation of built-up areas and cultivated areas. Certain roads could be detected, probably due to alignment parallel to satellite movement. Some of these roads were so narrow that they most probably can be detected only by optical sensors with very high spatial resolution.

*Coordinator's comment: The bright valley side is presumably due to the geometric correction based on the digital terrain model. Few pixels are smeared out to cover the area visible in the orthographic projection.

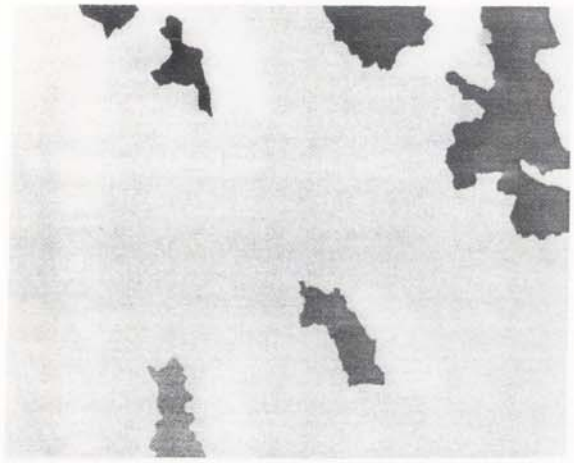

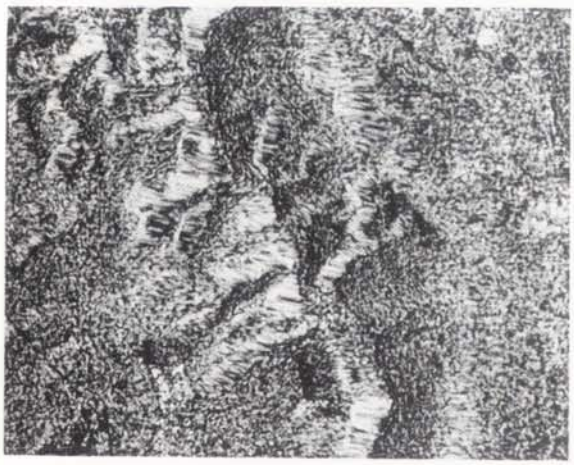

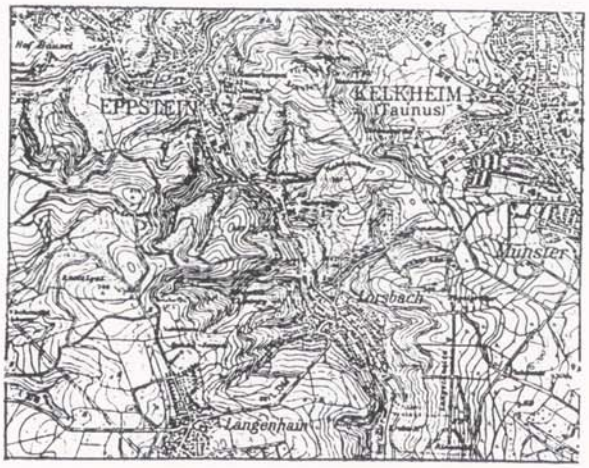

Results from interpreter No 5:

Comments: Following 10 classes were interpreted: 1: Runways, 2: Hangar, 3: River, Lake, 5: Mixed forest, 6: Road, 7: Railway-line, 8: Built-up areas, 9: decidious forest, 10: Park/meadow, 11: "Inter-road area". 5-6 of these classes could be interpreted directly without any support from the map. The remaining classes could be "everything".

In general: It is much more difficult to recognise features in a SAR image than in for instance a SPOT image. Certain border-lines between areas with different texture can be interpreted directly fro the image. To find out what the actual area really represents is much more difficult, and can in most cases not be obtained without support from other sources. The noisy appearance of the SAR images represents a problem. Experiments should be carried out in order to find out to what extent low-pass filtering would improve the interpretation possibilities of such images.

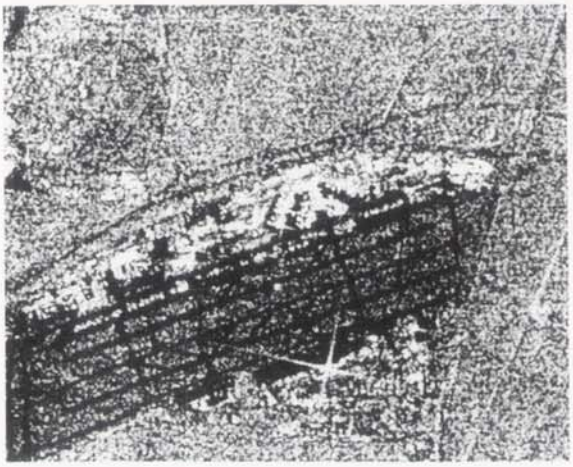

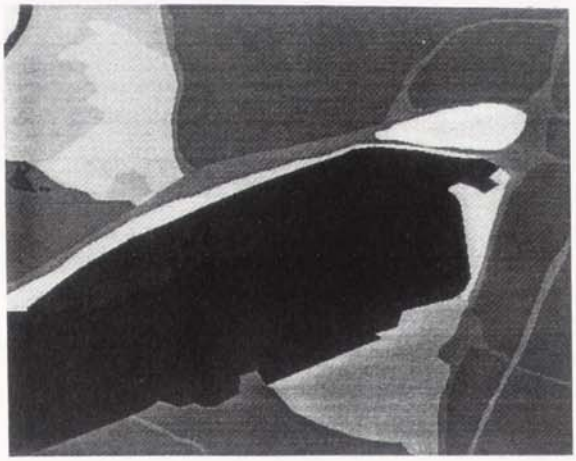

LIST OF THE OEEPE PUBLICATIONS

State – March 1996

A. Official publications

1 *Trombetti, C.:* „Activité de la Commission A de l'OEEPE de 1960 à 1964" – *Cunietti, M.:* „Activité de la Commission B de l'OEEPE pendant la période septembre 1960 –j anvier 1964" – *Förstner, R.:* „Rapport sur les travaux et les résultats de la Commission C de l'OEEPE (1960–1964)" – *Neumaier, K.:* „Rapport de la Commission E pour Lisbonne" – *Weele, A. J. v. d.:* „Report of Commission F." – Frankfurt a. M. 1964, 50 pages with 7 tables and 9 annexes.

2 *Neumaier, K.:* „Essais d'interprétation de »Bedford« et de »Waterbury«. Rapport commun établi par les Centres de la Commission E de l'OEEPE ayant participé aux tests" – „The Interpretation Tests of »Bedford« and »Waterbury«. Common Report Established by all Participating Centres of Commission E of OEEPE" – „Essais de restitution »Bloc Suisse«. Rapport commun établi par les Centres de la Commission E de l'OEEPE ayant participé aux tests" – „Test »Schweizer Block«. Joint Report of all Centres of Commission E of OEEPE." – Frankfurt a. M. 1966, 60 pages with 44 annexes.

3 *Cunietti, M.:* „Emploi des blocs de bandes pour la cartographie à grande échelle – Résultats des recherches expérimentales organisées par la Commission B de l'O.E.E.P.E. au cours de la période 1959–1966" – „Use of Strips Connected to Blocks for Large Scale Mapping – Results of Experimental Research Organized by Commission B of the O.E.E.P.E. from 1959 through 1966." – Frankfurt a. M. 1968, 157 pages with 50 figures and 24 tables.

4 *Förstner, R.:* „Sur la précision de mesures photogrammétriques de coordonnées en terrain montagneux. Rapport sur les résultats de l'essai de Reichenbach de la Commission C de l'OEEPE" – „The Accuracy of Photogrammetric Co-ordinate Measurements in Mountainous Terrain. Report on the Results of the Reichenbach Test Commission C of the OEEPE." – Frankfurt a. M. 1968, Part I: 145 pages with 9 figures; Part II: 23 pages with 65 tables.

5 *Trombetti, C.:* „Les recherches expérimentales exécutées sur de longues bandes par la Commission A de l'OEEPE." – Frankfurt a. M. 1972, 41 pages with 1 figure, 2 tables, 96 annexes and 19 plates.

6 *Neumaier, K.:* „Essai d'interprétation. Rapports des Centres de la Commission E de l'OEEPE." – Frankfurt a. M. 1972, 38 pages with 12 tables and 5 annexes.

7 *Wiser, P.:* „Etude expérimentale de l'aérotiangulation semi-analytique. Rapport sur l'essai »Gramastetten«." – Frankfurt a. M. 1972, 36 pages with 6 figures and 8 tables.

8 „Proceedings of the OEEPE Symposium on Experimental Research on Accuracy of Aerial Triangulation (Results of Oberschwaben Tests)"

Ackermann, F.: „On Statistical Investigation into the Accuracy of Aerial Triangulation. The Test Project Oberschwaben" – „Recherches statistiques sur la précision de l'aérotriangulation. Le champ d'essai Oberschwaben" – *Belzner, H.:* „The Planning. Establishing and Flying of the Test Field Oberschwaben" – *Stark, E.:* Testblock Oberschwaben, Programme I. Results of Strip Adjustments" – *Ackermann, F.:* „Testblock Oberschwaben, Program I. Results of Block-Adjustment by Independent Models" – *Ebner, H.:* Comparison of Different Methods of Block Adjustment" – *Wiser, P.:* „Propositions pour le traitement des erreurs non-accidentelles" – *Camps, F.:* „Résultats obtenus dans le cadre du project Oberschwaben 2A" – *Cunietti, M.; Vanossi, A.:* „Etude statistique expérimentale des erreurs d'enchaînement des photogrammes" – *Kupfer, G.:* „Image Geometry as Obtained from Rheidt Test Area Photography" – *Förstner, R.:* „The Signal-Field of Baustetten. A Short Report" – *Visser, J.; Leberl, F.; Kure, J.:* „OEEPE Oberschwaben Reseau Investigations" – *Bauer, H.:* „Compensation of Systematic Errors by Analytical Block Adjustment with Common Image Deformation Parameters." – Frankfurt a. M. 1973, 350 pages with 119 figures, 68 tables and 1 annex.

9 *Beck, W.:* „The Production of Topographic Maps at 1 : 10,000 by Photogrammetric Methods. – With statistical evaluations, reproductions, style sheet and sample fragments by Landesvermessungsamt Baden-Württemberg Stuttgart." – Frankfurt a. M. 1976, 89 pages with 10 figures, 20 tables and 20 annexes.

10 „Résultats complémentaires de l'essai d'«Oberriet» of the Commission C de l'OEEPE – Further Results of the Photogrammetric Tests of «Oberriet» of the Commission C of the OEEPE"

Hárry, H.: „Mesure de points de terrain non signalisés dans le champ d'essai d'«Oberriet» – Measurements of Non-Signalized Points in the Test Field «Oberriet» (Abstract)" – *Stickler, A.; Waldhäusl, P.:* „Restitution graphique des points et des lignes non signalisés et leur comparaison avec des résultats de mesures sur le terrain dans le champ d'essai d'«Oberriet» – Graphical Plotting of Non-Signalized Points and Lines, and Comparison with Terrestrial Surveys in the Test Field «Oberriet»" – *Förstner, R.:* „Résultats complémentaires des transformations de coordonnées de l'essai d'«Oberriet» de la Commission C de l'OEEPE – Further Results from Co-ordinate Transformations of the Test «Oberriet» of Commission C of the OEEPE" – *Schürer, K.:* „Comparaison des distances d'«Oberriet» – Comparison of Distances of «Oberriet» (Abstract)." – Frankfurt a. M. 1975, 158 pages with 22 figures and 26 tables.

11 „25 années de l'OEEPE"

Verlaine, R.: „25 années d'activité de l'OEEPE" – „25 Years of OEEPE (Summary)" – *Baarda, W.:* „Mathematical Models." – Frankfurt a. M. 1979, 104 pages with 22 figures.

12 *Spiess, E.:* „Revision of 1 : 25,000 Topographic Maps by Photogrammetric Methods." – Frankfurt a. M. 1985, 228 pages with 102 figures and 30 tables.

13 *Timmerman, J.; Roos, P. A.; Schürer, K.; Förstner, R.:* On the Accuracy of Photogrammetric Measurements of Buildings – Report on the Results of the Test "Dordrecht", Carried out by Commission C of the OEEPE. – Frankfurt a. M. 1982, 144 pages with 14 figures and 36 tables.

14 *Thompson C. N.:* Test of Digitising Methods. – Frankfurt a. M. 1984, 120 pages with 38 figures and 18 tables.

15 *Jaakkola, M.; Brindöpke, W.; Kölbl, O.; Noukka, P.:* Optimal Emulsions for Large-Scale Mapping – Test of "Steinwedel" – Commission C of the OEEPE 1981–84. – Frankfurt a. M. 1985, 102 pages with 53 figures.

16 *Waldhäusl, P.:* Results of the Vienna Test of OEEPE Commission C. – *Kölbl, O.:* Photogrammetric Versus Terrestrial Town Survey. – Frankfurt a. M. 1986, 57 pages with 16 figures, 10 tables and 7 annexes.

17 *Commission E of the OEEPE:* Influences of Reproduction Techniques on the Identification of Topographic Details on Orthophotomaps. – Frankfurt a. M. 1986, 138 pages with 51 figures, 25 tables and 6 appendices.

18 *Förstner, W.:* Final Report on the Joint Test on Gross Error Detection of OEEPE and ISP WG III/1. – Frankfurt a. M. 1986, 97 pages with 27 tables and 20 figures.

19 *Dowman, I. J.; Ducher, G.:* Spacelab Metric Camera Experiment – Test of Image Accuracy. – Frankfurt a. M. 1987, 112 pages with 13 figures, 25 tables and 7 appendices.

20 *Eichhorn, G.:* Summary of Replies to Questionnaire on Land Information Systems – Commission V – Land Information Systems. – Frankfurt a. M. 1988, 129 pages with 49 tables and 1 annex.

21 *Kölbl, O.:* Proceedings of the Workshop on Cadastral Renovation – Ecole polytechnique fédérale, Lausanne, 9–11 September, 1987. – Frankfurt a. M. 1988, 337 pages with figures, tables and appendices.

22 *Rollin, J.; Dowman, I. J.:* Map Compilation and Revision in Developing Areas – Test of Large Format Camera Imagery. – Frankfurt a. M. 1988, 35 pages with 3 figures, 9 tables and 3 appendices.

23 *Drummond, J.* (ed.): Automatic Digitizing – A Report Submitted by a Working Group of Commission D (Photogrammetry and Cartography). – Frankfurt a. M. 1990, 224 pages with 85 figures, 6 tables and 6 appendices.

24 *Ahokas, E.; Jaakkola, J.; Sotkas, P.:* Interpretability of SPOT data for General Mapping. – Frankfurt a. M. 1990, 120 pages with 11 figures, 7 tables and 10 appendices.

25 *Ducher, G.:* Test on Orthophoto and Stereo-Orthophoto Accuracy. – Frankfurt a. M. 1991, 227 pages with 16 figures and 44 tables.

26 *Dowman, I. J.* (ed.): Test of Triangulation of SPOT Data – Frankfurt a. M. 1991, 206 pages with 67 figures, 52 tables and 3 appendices.

27 *Newby, P. R. T.; Thompson, C. N.* (ed.): Proceedings of the ISPRS and OEEPE Joint Workshop on Updating Digital Data by Photogrammetric Methods. – Frankfurt a. M. 1992, 278 pages with 79 figures, 10 tables and 2 appendices.

28 *Koen, L. A.; Kölbl, O.* (ed.): Proceedings of the OEEPE-Workshop on Data Quality in Land Information Systems, Apeldoorn, Netherlands, 4–6 September 1991. – Frankfurt a. M. 1992, 243 pages with 62 figures, 14 tables and 2 appendices.

29 *Burman, H.; Torlegård, K.*: Empirical Results of GPS – Supported Block Triangulation. – Frankfurt a. M. 1994, 86 pages with 5 figures, 3 tables and 8 appendices.

30 *Gray, S.* (ed.): Updating of Complex Topographic Databases. – Frankfurt a. M. 1995, 133 pages with 2 figures and 12 appendices.

31 *Jaakola, J.; Sarjakoski, T.*: Experimental Test on Digital Aerial Triangulation. – Frankfurt a. M. 1996, 155 pages with 24 figures, 7 tables and 2 appendices.

B. Special publications

- Special Publications O.E.E.P.E. – Number I

  Solaini, L.; Trombetti, C.: Relation sur les travaux préliminaires de la Commission A (Triangulation aérienne aux petites et aux moyennes échelles) de l'Organisation Européenne d'Etudes Photogrammétriques Expérimentales (O.E.E.P.E.). I^{ére} Partie: Programme et organisation du travail. – *Solaini, L.; Belfiore, P.:* Travaux préliminaires de la Commission B de l'Organisation Européenne d'Etudes Photogrammétriques Expérimentales (O.E.E.P.E.) (Triangulations aériennes aux grandes échelles). – *Solaini, L.; Trombetti, C.; Belfiore, P.:* Rapport sur les travaux expérimentaux de triangulation aérienne exécutés par l'Organisation Européenne d'Etudes Photogrammétriques Expérimentales (Commission A et B). – *Lehmann, G.:* Compte rendu des travaux de la Commission C de l'O.E.E.P.E. effectués jusqu'à présent. – *Gotthardt, E.:* O.E.E.P.E. Commission C. Compte-rendu de la restitution à la Technischen Hochschule, Stuttgart, des vols d'essai du groupe I du terrain d'Oberriet. – *Brucklacher, W.:* Compte-rendu du centre «Zeiss-Aerotopograph» sur les restitutions pour la Commission C de l'O.E.E.P.E. (Restitution de la bande de vol, groupe I, vol. No. 5). – *Förstner, R.:* O.E.E.P.E. Commission C. Rapport sur la restitution effectuée dans l'Institut für Angewandte Geodäsie, Francfort sur le Main. Terrain d'essai d'Oberriet les vols No. 1 et 3 (groupe I). – I.T.C., Delft: Commission C, O.E.E.P.E. Déroulement chronologique des observations. – Photogrammetria XII (1955–1956) 3, Amsterdam 1956, pp. 79–199 with 12 figures and 11 tables.

- Publications spéciales de L'O.E.E.P.E. – Numéro II

  Solaini, L.; Trombetti, C.: Relations sur les travaux préliminaires de la Commission A (Triangulation aérienne aux petites et aux moyennes échelles) de l'Organisation Européenne d'Etudes Photogrammétriques Expérimentales (O.E.E.P.E.). 2^{e} partie. Prises de vues et points de contrôle. – *Gotthardt, E.:* Rapport sur les premiers résultats de l'essai d'«Oberriet» de la Commission C de l'O.E.E.P.E. – Photogrammetria XV (1958–1959) 3, Amsterdam 1959, pp. 77–148 with 15 figures and 12 tables.

- *Trombetti, C.:* Travaux de prises de vues et préparation sur le terrain effectuées dans le 1958 sur le nouveau polygone italien pour la Commission A de l'OEEPE. – Florence 1959, 16 pages with 109 tables.

- *Trombetti, C.; Fondelli, M.:* Aérotriangulation analogique solaire. – Firence 1961, 111 pages, with 14 figures and 43 tables.

- Publications spéciales de l'O.E.E.P.E. – Numéro III

  Solaini, L.; Trombetti, C.: Rapport sur les résultats des travaux d'enchaînement et de compensation exécutés pour la Commission A de l'O.E.E.P.E. jusqu'au mois de Janvier 1960. Tome 1: Tableaux et texte. Tome 2: Atlas. – Photogrammetria XVII (1960–1961) 4, Amsterdam 1961, pp. 119–326 with 69 figures and 18 tables.

- „OEEPE – Sonderveröffentlichung Nr. 1"

  Gigas, E.: „Beitrag zur Geschichte der Europäischen Organisation für photogrammetrische experimentelle Untersuchungen" – *N. N.:* „Vereinbarung über die Gründung einer Europäischen Organisation für photogrammetrische experimentelle Untersuchungen" – „Zusatzprotokoll" – *Gigas, E.:* „Der Sechserausschuß" – *Brucklacher, W.:* „Kurzbericht über die Arbeiten in der Kommission A der OEEPE" – *Cunietti, M.:* „Kurzbericht des Präsidenten der Kommission B über die gegenwärtigen Versuche und Untersuchungen" – *Förstner, R.:* „Kurzbericht über die Arbeiten in der Kommission B der OEEPE" – „Kurzbericht über die Arbeiten in der Kommission C der OEEPE" – *Belzner, H.:* „Kurzbericht über die Arbeiten in der Kommission E der OEEPE" – *Schwidefsky, K.:* „Kurzbericht über die Arbeiten in der Kommission F der OEEPE" – *Meier, H.-K.:* „Kurzbericht über die Tätigkeit der Untergruppe „Numerische Verfahren" in der Kommission F der OEEPE" – *Belzner, H.:* „Versuchsfelder für internationale Versuchs- und Forschungsarbeiten." – Nachr. Kt.- u. Vermesss.-wes., R. V, Nr. 2, Frankfurt a. M. 1962, 41 pages with 3 tables and 7 annexes.

- *Rinner, K.:* Analytisch-photogrammetrische Triangulation eines Teststreifens der OEEPE. – Österr. Z. Vermess.-wes., OEEPE-Sonderveröff. Nr. 1, Wien 1992, 31 pages.

- *Neumaier, K.; Kasper, H.:* Untersuchungen zur Aerotriangulation von Überweitwinkelaufnahmen. – Österr. Z. Vermess.-wes., OEEPE-Sonderveröff. Nr. 2, Wien 1965, 4 pages with 4 annexes.

- „OEEPE – Sonderveröffentlichung Nr. 2"

  Gotthardt, E.: „Erfahrungen mit analytischer Einpassung von Bildstreifen." – Nachr. Kt.- u. Vermess.-wes., R. V, Nr. 12, Frankfurt a. M. 1965, 14 pages with 2 figures and 7 tables.

- „OEEPE – Sonderveröffentlichung Nr. 3"

  Neumaier, K.: „Versuch »Bedford« und »Waterbury«. Gemeinsamer Bericht aller Zentren der Kommission E der OEEPE" – „Versuch »Schweizer Block«. Gemeinsamer Bericht aller Zentren der Kommission E der OEEPE." – Nachr. Kt.- u. Vermess.-wes., R.V, Nr. 13, Frankfurt a. M. 1966, 30 pages with 44 annexes.

- *Stickler, A.; Waldhäusl, P.:* Interpretation der vorläufigen Ergebnisse der Versuche der Kommission C der OEEPE aus der Sicht des Zentrums Wien. – Österr. Z. Vermess.-wes., OEEPE-Sonderveröff. (Publ. Spéc.) Nr. 3, Wien 1967, 4 pages with 2 figures and 9 tables.

- „OEEPE – Sonderveröffentlichung Nr. 4"

  Schürer, K.: „Die Höhenmeßgenauigkeit einfacher photogrammetrischer Kartiergeräte. Bemerkungen zum Versuch »Schweizer Block« der Kommission E der OEEPE." – Nachr. Kt.- u. Vermess.-wes., Sonderhefte, Frankfurt a. M.,1968, 25 pages with 7 figures and 3 tables.

- „OEEPE – Sonderveröffentlichung Nr. 5"

  Förstner, R.: „Über die Genauigkeit der photogrammetrischen Koordinatenmessung in bergigem Gelände. Bericht über die Ergebnisse des Versuchs Reichenbach der Kommission C der OEEPE." – Nachr. Kt.- u. Vermess.-wes., Sonderhefte, Frankfurt a. M. 1969, Part I: 74 pages with 9 figures; Part II: 65 tables.

- „OEEPE – Sonderveröffentlichung Nr. 6"

  Knorr, H.: „Die Europäische Organisation für experimentelle photogrammetrische Untersuchungen – OEEPE – in den Jahren 1962 bis 1970." – Nachr. Kt.- u. Vermess.-wes., Sonderhefte, Frankfurt a. M. 1971, 44 pages with 1 figure and 3 tables.

- „OEEPE – Sonderveröffentlichung Nr. D–7"

  Förstner, R.: „Das Versuchsfeld Reichenbach der OEEPE." – Nachr. Kt.- u. Vermess.-wes., Sonderhefte, Frankfurt a. M. 1972, 191 pages with 49 figures and 38 tables.

- „OEEPE – Sonderveröffentlichung Nr. D–8"

  Neumaier, K.: „Interpretationsversuch. Berichte der Zentren der Kommission E der OEEPE." – Nachr. Kt.- u. Vermess.-wes., Sonderhefte, Frankfurt a. M. 1972, 33 pages with 12 tables and 5 annexes.

- „OEEPE – Sonderveröffentlichung Nr. D–9"

  Beck, W.: „Herstellung topographischer Karten 1 : 10 000 auf photogrammetrischem Weg. Mit statistischen Auswertungen, Reproduktionen, Musterblatt und Kartenmustern des Landesvermessungsamts Baden-Württemberg, Stuttgart." – Nachr. Kt.- u. Vermess.-wes., Sonderhefte, Frankfurt a. M. 1976, 65 pages with 10 figures, 20 tables and 20 annexes.

- „OEEPE – Sonderveröffentlichung Nr. D–10"

  Weitere Ergebnisse des Meßversuchs „Oberriet" der Kommission C der OEEPE. *Hârry, H.:* „Messungen an nicht signalisierten Geländepunkten im Versuchsfeld «Oberriet»" – *Stickler, A.; Waldhäusl, P.:* „Graphische Auswertung nicht signalisierter Punkte und Linien und deren Vergleich mit Feldmessungsergebnissen im Versuchsfeld «Oberriet»" – *Förstner, R.:* „Weitere Ergebnisse aus Koordinatentransformationen des Versuchs «Oberriet» der Kommission C der OEEPE" – *Schürer, K.:* „Streckenvergleich «Oberriet»." – Nachr. Kt.- u. Vermess.-wes., Sonderhefte, Frankfurt a. M. 1975, 116 pages with 22 figures and 26 tables.

- „OEEPE – Sonderveröffentlichung Nr. D–11"

  Schulz, B.-S.: „Vorschlag einer Methode zur analytischen Behandlung von Reseauaufnahmen." – Nachr. Kt.- u. Vermess.-wes., Sonderhefte, Frankfurt a. M. 1976, 34 pages with 16 tables.

- „OEEPE – Sonderveröffentlichung Nr. D–12"

  Verlaine, R.: „25 Jahre OEEPE." – Nachr. Kt.- u. Vermess.-wes., Sonderhefte, Frankfurt a. M. 1980, 53 pages.

- „OEEPE – Sonderveröffentlichung Nr. D–13"

  Haug, G.: „Bestimmung und Korrektur systematischer Bild- und Modelldeformationen in der Aerotriangulation am Beispiel des Testfeldes „Oberschwaben." – Nachr. Kt.- u. Vermess.-wes., Sonderhefte, Frankfurt a. M. 1980, 136 pages with 25 figures and 51 tables.

- „OEEPE – Sonderveröffentlichung Nr. D–14"

  Spiess, E.: „Fortführung der Topographischen Karte 1 : 25 000 mittels Photogrammetrie" (not published, see English version in OEEPE official publication No. 12)

- „OEEPE – Sonderveröffentlichung Nr. D–15"

  Timmerman, J.; Roos, P. A.; Schürer, K.; Förstner, R.: „Über die Genauigkeit der photogrammetrischen Gebäudevermessung. Bericht über die Ergebnisse des Versuchs Dordrecht der Kommission C der OEEPE." – Nachr. Kt.- u. Vermess.-wes., Sonderhefte, Frankfurt a. M. 1983, 131 pages with 14 figures and 36 tables.

- „OEEPE – Sonderveröffentlichung Nr. D–16"

  Kommission E der OEEPE: „Einflüsse der Reproduktionstechnik auf die Erkennbarkeit von Details in Orthophotokarten." – Nachr. Kt.- u. Vermess.-wes., Sonderhefte, Frankfurt a. M. 1986, 130 pages with 51 figures, 25 tables and 6 annexes.

- „OEEPE – Sonderveröffentlichung Nr. D–17"

  Schürer, K.: „Über die Genauigkeit der Koordinaten signalisierter Punkte bei großen Bildmaßstäben. Ergebnisse des Versuchs „Wien" der Kommission C der OEEPE." – Nachr. Kt.- u. Vermess.-wes., Sonderhefte, Frankfurt a. M. 1987, 84 pages with 3 figures, 10 tables and 42 annexes.

C. Congress reports and publications in scientific reviews

- *Stickler, A.:* Interpretation of the Results of the O.E.E.P.E. Commission C. – Photogrammetria XVI (1959–1960) 1, pp. 8–12, 3 figures, 1 annexe (en langue allemande: pp. 12–16).
- *Solaini, L.; Trombetti, C.:* Results of Bridging and Adjustment Works of the Commission A of the O.E.E.P.E. from 1956 to 1959. – Photogrammetria XVI (1959–1960) 4 (Spec. Congr.-No. C), pp. 340–345, 2 tables.
- *N. N.:* Report on the Work Carried out by Commission B of the O.E.E.P.E. During the Period of September 1956–August 1960. – Photogrammetria XVI (1959–1960) 4 (Spec. Congr.-No. C), pp. 346–351, 2 tables.
- *Förstner, R.:* Bericht über die Tätigkeit und Ergebnisse der Kommission C der O.E.E.P.E. (1956–1960). – Photogrammetria XVI (1959–1960) 4 (Spec. Congr.-No. C), pp. 352–357, 1 table.
- *Bachmann, W. K.:* Essais sur la précision de la mesure des parallaxes verticales dans les appareils de restitution du I^{er} ordre. – Photogrammetria XVI (1959–1960) 4 (Spec. Congr.-No. C), pp. 358–360).
- *Wiser, P.:* Sur la reproductibilité des erreurs du cheminement aérien. – Bull. Soc. Belge Photogramm., No. 60, Juin 1960, pp. 3–11, 2 figures, 2 tables.
- *Cunietti, M.:* L'erreur de mesure des parallaxes transversales dans les appareils de restitution. – Bull. Trimestr. Soc. Belge Photogramm., No. 66, Décembre 1961, pp. 3–50, 12 figures, 22 tables.
- „OEEPE – Arbeitsberichte 1960/64 der Kommissionen A, B, C, E, F"

  Trombetti, C.: „Activité de la Commission A de l'OEEPE de 1960 à 1964" – *Cunietti, M.:* „Activité de la Commission B de l'OEEPE pendant la période septembre 1960–janvier 1964" – *Förstner, R.:* „Rapport sur les travaux et les résultats de la Commission C de l'OEEPE (1960–1964)" – *Neumaier, K.:* „Rapport de la Commission E pour Lisbonne" – *Weele, A. J. van der:* „Report of Commission F." – Nachr. Kt.- u. Vermess.-wes., R. V. Nr. 11, Frankfurt a. M. 1964, 50 pages with 7 tables and 9 annexes.
- *Cunietti, M.; Inghilleri, G.; Puliti, M.; Togliatti, G.:* Participation aux recherches sur les blocs de bandes pour la cartographie à grande échelle organisées par la Commission B de l'OEEPE. Milano, Centre CASF du Politecnico. – Boll. Geod. e Sc. affini (XXVI) 1, Firenze 1967, 104 pages.
- *Gotthardt E.:* Die Tätigkeit der Kommission B der OEEPE. – Bildmess. u. Luftbildwes. 36 (1968) 1, pp. 35–37.
- *Cunietti, M.:* Résultats des recherches expérimentales organisées par la Commission B de l'OEEPE au cours de la période 1959–1966. Résumé du Rapport final. – Présenté à l'XI^{e} Congrès International de Photogrammétrie, Lausanne 1968, Comm. III (en langues française et anglaise), 9 pages.

- *Förstner, R.:* Résumé du Rapport sur les résultats de l'essai de Reichenbach de la Commission C de l'OEEPE. – Présenté à l'XI^{e} Congrès International de Photogrammétrie, Lausanne 1968, Comm. IV (en langues française, anglaise et allemande), 28 pages, 2 figures, 2 tables.
- *Timmerman, J.:* Proef „OEEPE-Dordrecht". – ngt 74, 4. Jg., Nr. 6, Juni 1974, S. 143–154 (Kurzfassung: Versuch „OEEPE-Dordrecht". Genauigkeit photogrammetrischer Gebäudevermessung. Vorgelegt auf dem Symposium der Kommission IV der I.G.P., Paris, 24.–26. September 1974).
- *Timmerman, J.:* Report on the Commission C. "OEEPE-Dordrecht" Experiment. – Presented Paper for Comm. IV, XIIIth Congress of ISP, Helsinki 1976.
- *Beck, W.:* Rapport de la Commission D de l'OEEPE sur l'établissement de cartes topographiques au 1/10 000 selon le procédé photogrammétrique. – Presented Paper for Comm. IV, XIIIth Congress of ISP, Helsinki 1976.
- *Verlaine, R.:* La naissance et le développement de l'OEEPE – Festschrift – Dr. h. c. *Hans Härry*, 80 Jahre – Schweizerische Gesellschaft für Photogrammetrie und Wild Heerbrugg AG, Bern 1976.
- *Förstner, R.:* Internationale Versuche (Essais contrôlés) – Festschrift – Dr. h. c. *Hans Härry*, 80 Jahre – Schweizerische Gesellschaft für Photogrammetrie und Wild Heerbrugg AG, Bern 1976.
- *Bay, E.; Cunietti, M.; Vanossi, A.:* Détermination Expérimentale des Erreurs Systématiques des Faisceaux Perspectifs. – Société Belge de Photogrammétrie, Bulletin trimestriel, Brüssel 1977, pp 21–49.
- *Timmerman, J.:* Fotogrammetrische stadskaartering de OEEPE-proef Dordrecht. – Geodesia 19, Amsterdam 1977, pp. 291–298.
- *Waldhäusl, P.:* The Vienna Experiment of the OEEPE/C. Proceedings – Standards and Specifications for Integrated Surveying and Mapping Systems. – Schriftenreihe HSBw, Heft 2, München 1978.
- *Bachmann, W. K.:* Recherches sur la stabilité des appareils de restitution photogrammétriques analogiques. – Vermessung, Photogrammetrie, Kulturtechnik, Zürich 1978, pp. 265–268.
- *Parsic, Z.:* Untersuchungen über den Einfluß signalisierter und künstlicher Verknüpfungspunkte auf die Genauigkeit der Blocktriangulation. – Vermessung, Photogrammetrie, Kulturtechnik, Zürich 1978, pp. 269–278.
- *Waldhäusl, P.:* Der Versuch Wien der OEEPE/C. – Geowissenschaftliche Mitteilungen der Studienrichtung Vermessungswesen der TU Wien; Heft 13, Wien 1978, pp. 101–124.
- *Waldhäusl, P.:* Ergebnisse des Versuches Wien der OEEPE/C. – Presented Paper for Comm. IV, XIVth Congress of ISP, Hamburg 1980.
- *Timmerman, J.; Förstner, R.:* Kurzbericht über die Ergebnisse des Versuchs Dordrecht der Kommission C der OEEPE. – Presented Paper for Comm. IV, XIVth Congress of ISP, Hamburg 1980.

- *Bernhard, J.; Schmidt-Falkenberg, H.:* OEEPE – Die Arbeiten der Kommission E „Interpretation". – Presented Paper for Comm. IV, XIVth Congress of ISP, Hamburg 1980.
- *Bachmann, W. K.:* Elimination des valeurs erronées dans un ensemble de mesures controlées. – Papers written in honor of the 70th birthday of Professor *Luigi Solaini* – Richerche di Geodesia Topografia e Fotogrammetria, Milano 1979, pp. 27–39.
- *Visser, J.:* The European Organisation for Experimental Photogrammetric Research (OEEPE) – The Thompson Symposium 1982. – The Photogrammetric Record, London 1982, pp. 654–668.
- *Spiess, E.:* Revision of Topographic Maps: Photogrammetric and Cartographic Methods of the Fribourg Test. – The Photogrammetric Record, London 1983, pp. 29–42.
- *Jerie, H. G. and Holland, E. W.:* Cost model project for photogrammetric processes: a progress report. – ITC Journal, Enschede 1983, pp. 154–159.
- *Ackermann, F. E.* (Editor): Seminar – Mathematical Models of Geodetic/Photogrammetric Point Determination with Regard to Outliers and Systematic Errors – Working Group III/1 of ISP – Commission A of OEEPE. – Deutsche Geodätische Kommission bei der Bayerischen Akademie der Wissenschaften, Reihe A, Heft Nr. 98, München 1983.
- *Brindöpke, W., Jaakkola, M., Noukka, P., Kölbl, O.:* Optimal Emulsions for Large Scale Mapping – OEEPE–Commission C. – Presented Paper for Comm. I, XVth Congress of ISPRS, Rio de Janeiro 1984.
- *Ackermann, F.:* Report on the Activities of Working Group III/1 During 1980–84. – Comm. III, XVth Congress of ISPRS, Rio de Janeiro 1984.
- *Förstner, W.:* Results of Test 2 on Gross Error Detection of ISP WG III/1 and OEEPE. – Comm. III, XVth Congress of ISPRS, Rio de Janeiro 1984.
- *Gros, G.:* Modèles Numériques Altimétriques – Lignes Characteristiques – OEEPE Commission B. – Comm. III, XVth Congress of ISPRS, Rio de Janeiro 1984.
- *Ducher, G.:* Preparation d'un Essai sur les Ortho- et Stereo-Orthophotos. – Comm. IV, XVth Congress of ISPRS, Rio de Janeiro 1984.
- *van Zuylen, L.:* The influence of reproduction methods on the identification of details in orthophoto maps. – ITC Journal, Enschede 1984, pp. 219–226.
- *Visser, J.:* OEEPE- News – The European Organization for Experimental Photogrammetric Research. – ITC Journal, Enschede 1984, pp. 330–332.
- *Brindöpke, W., Jaakkola, M., Noukka, P., Kölbl, O.:* Optimale Emulsionen für großmaßstäbige Auswertungen. – Bildmess. u. Luftbildw. 53 (1985) 1, pp. 23–35.
- *Thompson, C. N.:* Some New Horizons for OEEPE. Presented Paper to the Symposium of Commission IV, ISPRS in Edinburgh, 8.–12. September 1986, pp. 299–306.

- *Dowman, I.:* The Restitution of Metric Photography Taken From Space – Comm. II, XVIth Congress of ISPRS, Kyoto 1988.
- *Kilpelä, E.:* Statistical Data on Aerial Triangulation – Comm. III, XVIth Congress of ISPRS, Kyoto 1988.
- *de Haan, A.:* An Analysis of the Precision of a DEM Obtained from SPOT Data – Comm. IV, XVIIth Congress of ISPRS, Washington 1992.
- *Ducher, G.:* OEEPE Test on Orthophoto and Stereo-Orthophoto Accuracy – Comm. IV, XVIIth Congress of ISPRS, Washington 1992.
- *Veillet, I.:* Accuracy of SPOT Triangulation With Very Few or no Ground Control Point – Comm. IV., XVIIth Congress of ISPRS, Washington 1992.

The official publications and the special publications issued in Frankfurt am Main are for sale at the

Institut für Angewandte Geodäsie
– Außenstelle Berlin –

Stauffenbergstraße 13, D-10785 Berlin

Organisation Européenne d'Etudes Photogrammétriques Expérimentales
Publications officielles

Content